Spring 5-15-2015

Human Ipsilateral Motor Physiology and Neuroprosthetic Applications in Chronic Stroke

David Thomas Bundy
Washington University in St. Louis

WASHINGTON UNIVERSITY IN ST. LOUIS

School of Engineering and Applied Science
Department of Biomedical Engineering

Dissertation Examination Committee:
Eric C. Leuthardt, Chair
Dennis L. Barbour
Maurizio Corbetta
Catherine E. Lang
Daniel W. Moran
Kurt A. Thoroughman

Human Ipsilateral Motor Physiology and Neuroprosthetic Applications in Chronic Stroke

by

David Thomas Bundy

A dissertation presented to the
Graduate School of Arts & Sciences
of Washington University in
partial fulfillment of the
requirements for the degree
of Doctor of Philosophy

May 2015
St. Louis, Missouri

Table of Contents

List of Figures

List of Tables

Acknowledgments

As I near the completion of my graduate work and reflect upon my time at Washington University, it is clear that it is only through the support of many others that it is possible to finish a PhD, so there are many people that deserve a great deal of thanks and appreciation for the role that they have played on this journey.

First and foremost, I would like to thank my advisor Dr. Eric Leuthardt. Throughout my time here, your enthusiasm and vision has truly been a driving force behind the lab. I am honored to have you both as a friend and mentor. Thanks also to my entire thesis committee who have provided valuable encouragement and feedback on this dissertation and also wonderful advice to help me navigate the next steps in my career. To Charlie, Mohit, Zac, Nick, Mrinal, Carl, and all of my other fellow lab members, thank you for the community and collaborative spirit you helped foster and especially for your friendship. Thank you to the patients who participated in these studies and the staff of the epilepsy monitoring units, without whom this work would not have been possible. Thank you also to Dr. Thoroughman for allowing us to use his Flock of Birds system for Chapter 3, to Erik Zellmer for performing the finite element modeling shown in Chapter 4, and Dr. Corbetta for helping us to recruit stroke patients and for providing their imaging data for Chapter 5. Additionally, I was fortunate to participate in the Cognitive, Computational, and Systems Neuroscience Program and the TL1 Predoctoral Clinical Research Training Program. The financial support that I received from the NSF and NIH enabled me to complete this work. Thank you also to the faculty and staff for making both of those programs wonderful research training and career development experiences.

Finally I owe a huge debt of gratitude to my family. Thank you to my parents, Tom and Caren and my sister Cathy for your support, the example that each of you has provided, and for encouraging me to and pursue science. Lastly, to my wife Elizabeth: thank you for your steadfast and unfailing love and for being willing to share and embark on this journey with me.

David Thomas Bundy

Washington University in St. Louis

May 2015

For my wife and family.

ABSTRACT OF THE DISSERTATION

Human Ipsilateral Motor Physiology and Neuroprosthetic Applications in Chronic Stroke

by

David Thomas Bundy

Doctor of Philosophy in Biomedical Engineering

Washington University in St. Louis, 2015

Professor Eric C. Leuthardt, Chair

Improving the recovery of lost motor function in hemiplegic chronic stroke survivors is a critical need to improve the lives of these patients. Over the last several decades, neuroprosthetic systems have emerged as novel tools with the potential to restore function in a variety of patient populations. While traditional neuroprosthetics have focused on using neural activity contralateral to a moving limb for device control, an alternative control signal may be necessary to develop brain-computer interface (BCI) systems in stroke survivors that suffer damage to the cortical hemisphere contralateral to the affected limb. While movement-related neural activity also occurs in the hemisphere ipsilateral to a moving limb, it is uncertain if these signals can be used within BCI systems. This dissertation examines the motor activity ipsilateral to a moving limb and the potential use of these signals for neuroprosthetic applications in chronic stroke survivors. Patients performed three-dimensional (3D) reaching movements with the arm ipsilateral to an electrocorticography (ECoG) array in order to assess the extent of kinematic information that can be decoded from the cortex ipsilateral to a moving limb. Additionally, patients performed the same task with the arm contralateral to the same ECoG arrays, allowing us to compare the neural representations of contralateral and ipsilateral limb movements. While

spectral power changes related to ipsilateral arm movements begin later and are lower in amplitude than power changes related to contralateral arm movements, 3D kinematics from both contralateral and ipsilateral arm trajectories can be decoded with similar accuracies. The ability to decode movement kinematics from the ipsilateral cortical hemisphere demonstrates the potential to use these signals within BCI applications for controlling multiple degrees of freedom. Next we examined the relationship between electrode invasiveness and signal quality. The ability to decode movement kinematics from neural activity was significantly decreased in simulated electroencephalography (EEG) signals relative to ECoG signals, indicating that invasive signals would be necessary to implement BCI systems with multiple degrees of freedom. For ECoG signals, the human dura also causes a significant decrease in signal quality when electrodes with small spatial sizes are used. This tradeoff between signal quality and electrode invasiveness should therefore be taken into account when designing ECoG BCI systems. Finally, chronic stroke survivors used activity associated with affected hand motor intentions, recorded from their unaffected hemisphere using EEG, to control simple BCI systems. This demonstrates that motor signals from the ipsilateral hemisphere are viable for BCI applications, not only in motor-intact patients, but also in chronic stroke survivors. Taken together, these experiments provide initial demonstrations that it is possible to develop BCI systems using the unaffected hemisphere in stroke survivors with multiple degrees of freedom. Further development of these BCI systems may eventually lead to improving function for a significant population of patients.

1 Introduction and Specific Aims

1.1 Introduction

A challenge in the treatment of stroke survivors is the restoration of chronically lost motor function. A large number of patients experience hemiparesis after stroke, and furthermore, motor recovery has been shown to plateau after approximately three months, leaving a significant number of stroke survivors chronically impaired (Duncan, Goldstein et al. 1992; Jorgensen, Nakayama et al. 1995; Go, Mozaffarian et al. 2014). Therefore, there is a critical need to develop methods to restore function after stroke that are independent of the location of the lesion and the level of residual motor function.

We propose that a brain-computer interface system, or BCI, which is a system that uses signals recorded from the brain to control a computer system or other external assistive device, can be used to restore function after stroke. A large and well-developed body of work has shown that neural activity contralateral to a moving limb contains relevant information about motor intent, and furthermore, that this neural activity can be used to control a BCI system with multiple degrees-of-freedom (Taylor, Tillery et al. 2002; Leuthardt, Schalk et al. 2004; Wolpaw and McFarland 2004; Schalk, Miller et al. 2008; Velliste, Perel et al. 2008; Rouse and Moran 2009). In patients with unilateral damage to their cortex or the underlying white matter caused by a hemispheric stroke, a different control signal would be necessary. In addition to motor signals from the contralateral hemisphere that are the focus of most motor-BCI systems, a large body of work demonstrates the presence of motor-related activity in the hemisphere ipsilateral to a moving limb, both in motor-intact human subjects (Kim, Ashe et al. 1993a; Crone, Miglioretti et

al. 1998b; Pfurtscheller and Lopes da Silva 1999; Shibasaki and Hallett 2006; Wisneski, Anderson et al. 2008), and after stroke (Weiller, Chollet et al. 1992; Weiller, Ramsay et al. 1993; Green, Bialy et al. 1999; Johansen-Berg, Rushworth et al. 2002). This activity in the ipsilateral cortical hemisphere has the potential to be used to develop BCI applications for stroke.

The central hypothesis for this work is that motor signals ipsilateral to the affected hand after stroke contain sufficient information to control a BCI system, and furthermore, that these signals can be used by stroke survivors to control a BCI system that will improve long-term function. If proven correct, BCI systems can be developed that may lead to multiple clinical end points as shown in Figure 1.1.

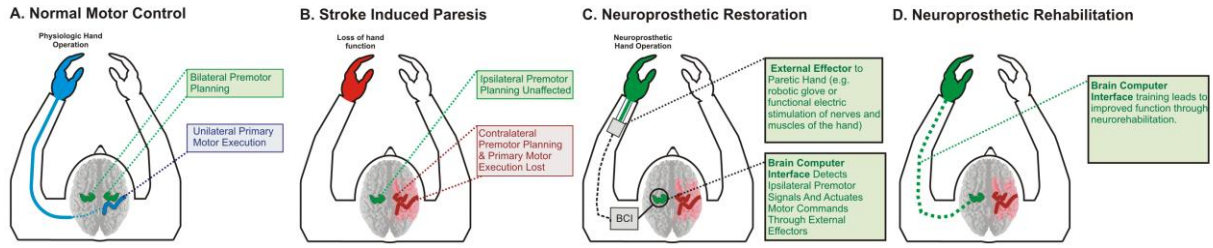

Figure 1.1 Ipsilateral BCI systems for stroke
A. In motor-intact humans, each hemisphere of the brain drives the opposite-sided limbs. **B.** After a stroke, hemiparesis can be caused either because of a broad cortical lesion or subcortical lesion. However, motor activity in the contralesional hemisphere that is related to the planning and execution of ipsilateral limb movements remains intact. **C.** This ipsilateral motor activity in the unaffected hemisphere may be able to drive a BCI system to restore function. **D.** In addition to chronic device control, a second clinical end-point may be to train with a BCI system that drives an external stimulator in order to strengthen contralesional motor pathways in the hopes of effecting functional rehabilitation.

First, BCI systems recording activity from the healthy hemisphere may allow for reanimation of the affected limb through the control of external assistive devices. If reliable control over a sufficient number of degrees-of-freedom can be developed, long-term control of an external assistive device would allow for increased function. Second, pairing BCI control with a relevant external stimulation may strengthen existing pathways and lead to improved rehabilitation after a stroke. The rationale for this research is that we will develop a greater understanding of the

nature of ipsilateral motor activity and its potential use for a BCI system with multiple degrees-of-freedom by defining the extent and type of information that can be decoded from the ipsilateral hemisphere. Furthermore, by both evaluating the ability to use less invasive recordings for BCI system development and determining if stroke survivors are able to control a BCI system with their motor intentions, we will further establish the technical requirements and the feasibility of BCI systems utilizing the unaffected hemisphere in stroke survivors.

1.2 Specific Aims

This dissertation will seek to test the central hypothesis and advance the development of neuroprosthetics in stroke survivors through the following specific aims:

Aim 1: Determine the extent of kinematic information related to movements of the ipsilateral arm that is present in motor-intact human subjects. The working hypothesis for this aim is that electrocorticography (ECoG) signals from motor-intact human subjects, recorded ipsilateral to a moving arm, will contain sufficient information to decode kinematics of three-dimensional (3D) arm movements.

Aim 2: Determine the extent of separability of the kinematic information encoded by neural activity during ipsilateral and contralateral arm movements in motor-intact patients. We hypothesize that electrocorticography recordings from a single hemisphere can be used to decode kinematics about arm movements of either the contralateral or the ipsilateral limb. Furthermore, we hypothesize that the features used to decode arm movements of the contralateral and ipsilateral limbs will be distinct in terms of their cortical topography and spectral frequency.

Aim 3: Evaluate the effect of reducing the invasiveness of electrophysiological recordings on the signal quality and extent of information that can be decoded for BCI systems. We hypothesize that as we decrease the invasiveness of recording methods, that there will also be a decrease in signal quality leading to a decrease in the ability to decode information. We will test this in two sub-hypotheses. First, that electroencephalography (EEG) signals recorded from the scalp contain significantly less information about motor intent than ECoG recordings from the cortical surface. And second, that the human dura will cause more subtle effects on signal quality that will be relevant to BCI implementation.

Aim 4: Determine if stroke survivors can utilize ipsilateral motor signals from unaffected cortex to control a BCI system. The working hypothesis is that ipsilateral motor signals (i.e. signals from the unaffected hemisphere which are distinct from brain signals associated with contralateral movement) will provide sufficient information to enable control of a cursor on a computer screen.

1.3 Dissertation Overview and Organization

This thesis is divided into six chapters. Chapter 2 places this dissertation into the context of the existing literature by providing the background and significance for this research. The motivation for developing BCI systems for stroke survivors is provided followed by a review of the role of ipsilateral motor physiology in controlling normal motor function and in controlling motor movements during recovery from stroke. The chapter concludes by describing existing neuroprosthetic systems and their applications in stroke

Chapter 3 describes the methods and results addressing the first two hypotheses: that ECoG recordings can be used to decode kinematics of ipsilateral limb movements, and second, that the

neural representations of contralateral and ipsilateral limb movements are separable. Chapter 3 also uses ECoG recordings to simulate of EEG signals in order to evaluate whether kinematics can be decoded non-invasively as described in aim 3.

Chapter 4 covers the second component of specific aim 3 by evaluating the effect of the human dura on the signal quality of ECoG recordings at different spatial scales. The results highlight the tradeoff between reducing the invasive nature of electrode implantations and decreased signal quality that should be taken into account when designing and implementing BCI systems. This chapter is based upon a previously published manuscript (Bundy, Zellmer et al. 2014).

Chapter 5 tests the final major hypothesis of the work by demonstrating the ability of chronic stroke survivors to control a BCI system using neural activity in their unaffected hemisphere. The results of this study demonstrate the feasibility for future BCI systems in stroke. This chapter is also based upon a previously published manuscript (Bundy, Wronkiewicz et al. 2012).

Chapter 6 concludes this work with a discussion of the collection of the results presented, the implications of these findings, and several potential avenues for further examination based upon the findings of these studies.

2 Background

2.1 Clinical Significance

Stroke is the most common neurological disorder and leading cause of serious long-term disability in the United States with an incidence of 795,000 strokes per year and a prevalence of 6.8 million adult Americans who have suffered a stroke (Go, Mozaffarian et al. 2014). Globally, approximately 15 million people suffer strokes annually leaving 5 million people per year disabled (Mackay, Mensah et al. 2004). Of survivors of stroke, 15-30% are left permanently disabled and 20% require institutional care (Go, Mozaffarian et al. 2014). These deficits are significant, as recovery from stroke has traditionally been thought to plateau after 3 months (Duncan, Goldstein et al. 1992; Jorgensen, Nakayama et al. 1995). While there are a number of therapies that have been shown to be effective in improving function after stroke such as constraint induced movement therapy (Wolf, Thompson et al. 2010), or electromyogram-triggered stimulation (Francisco, Chae et al. 1998; Takahashi, Der-Yeghiaian et al. 2008; der-Yeghiaian, Sharp et al. 2009), these therapies generally require a minimum level of volitional motor function, making them unsuitable for some patients. Because of this, the majority of patients with complete hemiparesis do not recover any level of function (Kwakkel, Kollen et al. 2003), and the most significant predictors of upper limb recovery are initial post-stroke measures of upper limb impairment (Coupar, Pollock et al. 2012). Therefore, there is a substantial patient population affected by stroke in which motor deficits cause significant impacts, not only on individual patients and their families, but also on society as a whole. Because of the lack of effective methods to encourage functional recovery, particularly in the most severely affected patients, there is a critical need to develop novel tools to restore function after stroke. One potential way to meet this need is to develop neuroprosthetic systems that can translate a patient's

neural activity from the unaffected hemisphere into commands to control an assistive device or rehabilitation system. This chapter motivates the use of neuroprosthetics in stroke survivors and places this dissertation in the context of the existing body of literature. We begin by providing an overview of normal motor neurophysiology with a focus on the role of neural activity in the hemisphere ipsilateral to a moving limb. We follow this by describing the changes in motor physiology, particularly within the unaffected hemisphere, that take place during recovery from stroke. Finally, this chapter concludes with a description of neuroprosthetic systems that have been developed and the gaps in knowledge that remain in order to develop neuroprosthetic applications for stroke survivors.

2.2 Motor Neurophysiology

The neurophysiology associated with the planning and execution of motor actions has a long history based upon a wide array of paradigms, recording modalities, and techniques. This section describes the neural correlates of normal motor control by focusing on evidence from individual recording modalities and techniques. As the hemisphere ipsilateral to the affected limb has been identified as a potential mechanism for recovery after stroke, this section will particularly focus on the similarities and differences between neural activity during movements of the contralateral and ipsilateral limbs.

2.2.1 Anatomical Pathways

There are a number of anatomical pathways that play a potential role in the production of movements. While the majority of descending fibers from motor areas cross to the opposite side of the spinal cord, approximately 15% of fibers descend uncrossed in the spinal cord ipsilateral to their cortical origin in both animals (Glees and Cole 1952; Nyberg-Hansen and Brodal 1963) and humans (Barnes 1901; Nyberg-Hansen and Rinvik 1963; Yakovlev and Rakic 1966).

Additionally, although primary motor areas make up the largest input to the corticospinal tract from a single region, a collectively larger number of descending fibers originate in non-primary motor areas, including the supplementary motor areas (SMA), cingulate motor areas (CMA), and premotor areas (Nyberg-Hansen and Rinvik 1963; Dum and Strick 1991). Furthermore, motor cortex is strongly interconnected with non-primary motor areas in the frontal lobe and parietal lobe (Dum and Strick 1991) as well as the opposite hemisphere via the corpus callosum (Kaas 1995). Therefore, it is important to keep in mind that both cortical hemispheres have the potential to play a role in planning and executing unilateral motor movements either through pathways that decusate and descend in the contralateral spinal cord, that descend directly in the ipsilateral spinal cord, or through interactions between motor areas within and across the cortical hemispheres.

2.2.2 Single-Unit Electrophysiology

In addition to the presence of anatomic pathways, functional measures of neural activity at different spatial and temporal scales can be used to investigate the relationship between neural activity and motor movements. The most direct measure of neural activity is to use implanted microelectrodes to record action potentials fired by individual neurons. Early studies investigating the activity of single units found individual neurons in the primary motor cortex of primates that either increase or decrease their firing during flexion or extension movements of the wrist (Evarts 1966). As the majority of cells were found to fire in relation to muscle force, it was postulated that neural activity in primary motor cortex was related to intrinsic muscle activation (Cheney and Fetz 1980). However, other studies that have utilized reaching movements to targets arranged around a two-dimensional (2D) plane have found that in the majority of motor cortical cells active during reaching movements, the rate of firing varies about

a preferred direction with a broadly tuned distribution that can be fit by a cosine function (Georgopoulos, Kalaska et al. 1982). Furthermore, by representing each of a population of tuned neurons as a vector making a weighted contribution to an overall population vector, movement directions in three-dimensional (3D) space could be determined from neural activity in motor areas (Georgopoulos, Schwartz et al. 1986). Additional work has built upon the population vector to show that population vectors are stable across 3D space (Caminiti, Johnson et al. 1991). Along with direction, motor cortical activity is also related to additional kinematic parameters including speed (Moran and Schwartz 1999b; Moran and Schwartz 1999a; Schwartz and Moran 1999), position (Georgopoulos, Caminiti et al. 1984; Wang, Chan et al. 2007), hand rotation (Wang, Chan et al. 2010), as well as the object to be grasped in a reach-to-grasp task (Rouse, Roussin et al. 2014). There is still some debate about whether motor cortical cells encode low-level muscle activations or higher-level kinematic parameters as neurons tuned to both types of parameters have been found in tasks designed to dissociate muscle contractions and extrinsic movement directions during movements of a single joint (Kakei, Hoffman et al. 1999).

While the majority of studies examining the relationship between single-unit neurophysiology and motor activity have focused on movements of the limb contralateral to the site of recording, a number of studies have examined the relationship between single-unit neural activity and movements of the ipsilateral arm. In particular, although the majority of primary motor cortex neurons alter their firing rate with movements of the contralateral limb, a subset of neurons change their firing rate during movements of the same-sided limb in both humans (Goldring and Ratcheson 1972) and non-human primates (Evarts 1966; Tanji, Okano et al. 1987; Tanji, Okano et al. 1988; Aizawa, Mushiake et al. 1990). Specifically approximately 8% of neurons in primary motor cortex respond to distal movements of the limb ipsilateral to the site of recording with no

change in firing during movements of the contralateral limb (Tanji, Okano et al. 1988). Ipsilateral and bilateral neurons have also been found in larger quantities in a transitional zone between the hand and face representations of primary motor cortex (Aizawa, Mushiake et al. 1990). When comparing neurons recorded from primary motor cortex to those recorded in non-primary motor areas (i.e. premotor cortex or SMA), a larger percentage of neurons in non-primary motor areas had context-dependent movement relationships, such as bilateral relationships (firing during either ipsilateral limb or contralateral limb movements), exclusive relationships (i.e. active during ipsilateral but not contralateral or bilateral movements, bilateral but not ipsilateral or contralateral limb movements, or unilateral movements but not bilateral movements) (Tanji, Okano et al. 1988). When focusing on bimanual synergies of movement, an equal number of neurons in primary motor cortex and SMA display activity during bimanual movements that cannot be accounted for by the activity during unimanual movements alone (Donchin, Gribova et al. 1998). Neurons with activity related to bimanual movements are also located in dorsal premotor cortex, CMA, and posterior parietal cortex (Kermadi, Liu et al. 2000).

Further examination shows that kinematic parameters are also represented within the relationships between neural activity and ipsilateral limb movements. Cells in dorsal premotor cortex are strongly tuned to movement direction independent of the arm that will be moving, particularly during a pre-movement delay. Cells in primary motor cortex, on the other hand, exhibit stronger directional tuning with the contralateral arm, although several cells in primary motor cortex also have directional tuning to ipsilateral or bilateral arm movements (Cisek, Crammond et al. 2003). Furthermore, population vectors for movements of both arms can be predicted simultaneously, even when the two arms move in opposite directions (Steinberg, Donchin et al. 2002). Therefore, neural activity is related not only to contralateral limb

movements, but also simple movements of the ipsilateral limb. Furthermore, during more natural and complex bimanual tasks, a more complicated relationship between neural activity and movements is apparent.

2.2.3 Field Potentials

Another useful tool in studying the relationship between neural activity and behavior is to examine the summed electrophysiological activity of a population of cortex. A variety of electrode sizes and locations can be used to measure field potentials with an inverse relationship between the invasiveness of the electrodes and the spatial specificity of the recorded signals.

Spectral Power Changes

With his invention of the electroencephalogram (EEG) and observation that the amplitude of occipital alpha oscillations increased when human subjects closed their eyes, Hans Berger first provided the ability to study the electrical activity of the brain non-invasively (Berger 1969). Changes in oscillatory activity related to behavior were extended to motor movements by Jasper and Andrews who observed decreases in the pre-central alpha rhythm during motor movements that was separable from Berger's occipital alpha rhythm (Jasper and Andrews 1938). Using an early electrocorticogram recorded at the surface of the brain, the amplitude of the higher frequency beta band was also observed to decrease during voluntary movements of the contralateral arm, and although weaker, during voluntary movements of the ispsilateral arm as well (Jasper and Penfield 1949).

Building upon the initial demonstrations, Pfurtscheller and colleagues characterized these low-frequency phenomena more fully and termed the decrease in spectral power during activity as event-related desynchrnonization (ERD) and the rebound of power afterwards as event-related synchronization (ERS) (Pfurtscheller and Aranibar 1979). EEG and magnetoencephalography

(MEG) recordings show that alpha (8-12Hz) and beta (12-25Hz) band ERD begins approximately 1.75 seconds before movement onset in the hemisphere contralateral to the moving arm and becomes bilateral immediately before the movement onset (Pfurtscheller and Aranibar 1979; Pfurtscheller and Berghold 1989; Pfurtscheller and Lopes da Silva 1999). By examining electrode sites covering the whole head, ERD and ERS can be observed simultaneously with locations displaying ERD involved in task-relevant processing and locations displaying ERS at rest (Pfurtscheller 1992). Additionally, the alpha band was found to contain both a lower (8-10Hz) component and a more topographically specific higher (10-12Hz) component (Manganotti, Gerloff et al. 1998; Pfurtscheller, Neuper et al. 2000). Furthermore, the beta band is separable from the alpha band as it contains both a harmonic of the greek letter μ-shaped alpha rhythm as well as an additional component (Pfurtscheller, Stancak et al. 1997) that is distinct from the alpha band both in the timing (Salmelin and Hari 1994) and topography (Pfurtscheller and Berghold 1989).

While EEG allows examination of spectral power changes in low frequencies (below 30 Hz), EEG has poor spatial and spectral resolution, limiting the ability to examine spectral changes at higher frequencies (Cooper, Winter et al. 1965; Pfurtscheller and Cooper 1975). Electrocorticography (ECoG) recordings made from the surface of the brain allow for examination of the electrophysiological correlates of neural activity with increased spatial and spectral resolution. Studies of low frequencies confirmed observations made using EEG, showing that alpha and beta ERD occurs during movements of both the contralateral and ipsilateral limbs over a broad area of cortex (Arroyo, Lesser et al. 1993; Crone, Miglioretti et al. 1998b). Additionally, ECoG allows for examination of electrophysiological activity in the gamma band (>30 Hz). Early studies of the gamma band activity using ECoG showed that

spectral power in two distinct gamma bands, a low gamma band (35-50 Hz) and a high gamma band (75-100 Hz), both increase during motor movements (Crone, Miglioretti et al. 1998a). Gamma band power changes are modulated in the opposite direction from alpha and beta band ERD, are more somatotopically specific than low frequency power changes, and were found only in the hemisphere contralateral to a moving limb (Crone, Miglioretti et al. 1998a). Several studies have also examined the relationship between high gamma band spectral power and movement kinematics and found tuning to contralateral arm kinematics in both LFP recordings (Heldman, Wang et al. 2006) and ECoG recordings (Schalk, Kubanek et al. 2007; Anderson, Blakely et al. 2012). While tuning also occurs between low frequency spectral power changes and arm kinematics, tuning between high frequency spectral power and arm kinematics occurs in a greater proportion of electrode sites (Heldman, Wang et al. 2006; Sharma, Gaona et al. 2009; Anderson, Blakely et al. 2012).

With regards to ipsilateral arm movements, alpha and beta band ERD are consistently observed in the hemisphere ipsilateral to a moving limb (Pfurtscheller and Lopes da Silva 1999). During ipsilateral ERD, There is an increased period of excitability to transcranial magnetic stimulation (TMS) pulses, indicating that ERD ipsilateral to a moving limb may play a role in facilitating movements (Rau, Plewnia et al. 2003). Prior work from our lab has focused on the difference between cortical physiology related to movements of the ipsilateral and contralateral limbs, demonstrating that ECoG activity during ipsilateral limb movements occurs earlier, occupies different frequency ranges (ipsilateral arm movements: 37.5 Hz, contralateral arm movements: <30 Hz and >70Hz), and is preferentially located in premotor cortices (Wisneski, Anderson et al. 2008). Additionally, ECoG spectral power is also tuned to kinematics of ipsilateral arm movements (Sharma, Gaona et al. 2009).

Movement-Related Cortical Potentials

Along with observing changes in frequency-specific spectral power, temporal changes in field potentials occur before and during voluntary motor movements. By storing EEG signals from a simple motor task on tape, playing them in reverse, and averaging across trials, Kornhuber and Deecke discovered the bereitschaft (readiness) potential, a slowly increasing negativity in the EEG signal over motor areas that begins bilaterally about 2s before movement onset with the maximal negativity located at the vertex (Kornhuber and Deecke 1965). In addition to the bereitschaft potential, there is an increase in the negative slope of the cortical potential approximately 400ms before movement onset that has been termed the late bereitschaft potential (also referred to as the movement potential or NS' component) with a maximal negativity over the contralateral hemisphere. Finally, a pre-motor positivity, a small positive potential that is bilaterally symmetric has also been found (Gilden, Vaughan et al. 1966; Deecke, Scheid et al. 1969; Shibasaki and Hallett 2006). While volume conduction from bilateral motor cortices is a possible explanation for the maximal component of the bereitschaft potential being located at the vertex, in bilateral parkinsonian patients, the lateral components of the bereitschaft potential are abolished, but the component at the vertex remains (Deecke and Kornhuber 1978). Therefore, part of the mechanism underlying the bereitschaft potential must be explained independent of primary motor cortex, potentially relying on the SMA. Furthermore, a potential real-time measure of the bereitschaft potential, the local motor potential (LMP), which is obtained by low-pass filtering EEG or ECoG signals, is tuned to movement direction (Schalk, Kubanek et al. 2007).

An important question is whether these movement-related cortical potentials originate from the same or different mechanisms as the spectral power changes described previously. There are

several pieces of evidence to suggest that movement-related cortical potentials are generated by separate mechanisms. First, the changes in topography of ERD and movement-related cortical potentials are opposite. Alpha and beta band ERD begin in the hemisphere contralateral to a moving limb and become bilateral immediately before movement onset while the early part of the bereitschaft potential is bilaterally symmetric and the late bereitschaft potential, occurring in the last 400ms before movement, is localized over the contralateral hemisphere. This finding has been confirmed using ECoG where it was found that movement-related cortical potentials start broadly and become focal in the contralateral hemisphere closer to movement onset, while alpha and beta band ERD starts in the contralateral hemisphere and becomes bilateral around movement onset (Toro, Deuschl et al. 1994). Additionally, in patients with primary lateral sclerosis, movement-related cortical potentials such as the bereitschaft potential are decreased, while beta band ERD is preserved, indicating that the physiological mechanisms responsible for movement-related cortical potentials and ERD are unique and separable. Therefore, field potentials contain multiple unique spectral and temporal components, which demonstrate relationships to motor movements of both the contralateral and ipsilateral limb.

2.2.4 Functional Imaging

Local increases in neural activity that are directly measured using electrophysiological methods are also correlated with increased blood flow and, to a lesser extent, increased oxygen consumption, providing a means to examine neural activity through positron emission tomography (PET) or functional Magnetic Resonance Imaging (fMRI) blood oxygen level dependent (BOLD) signals (Fox and Raichle 1986; Frostig, Lieke et al. 1990). While these functional imaging methods suffer from poor temporal resolution due to the slow time course of the hemodynamic response function, they allow for simultaneous investigation of whole-brain

activity with good spatial resolution. Early studies utilizing functional imaging methods to study voluntary motor movements found that during unilateral motor movements, the primary motor cortex is only active in the hemisphere opposite the moving limb, while SMA and premotor cortices are bilaterally active (Roland, Larsen et al. 1980; Roland, Meyer et al. 1982; Roland 1985).

Functional imaging has also shown a relationship between neural activity and ipsilateral limb movements. Early studies found that while the contralateral primary motor cortex and bilateral SMA and premotor cortices were active during both arm and hand movements, the ipsilateral primary motor cortex was only active during more proximal shoulder movements (Colebatch, Deiber et al. 1991). Later studies found that while activations of the primary motor cortex are stronger and occupy a greater cortical surface area during movements of the contralateral hand, the ipsilateral primary motor cortex is also active during distal hand movements (Yoshii, Ginsberg et al. 1989; Grafton, Mazziotta et al. 1992; Kawashima, Yamada et al. 1993; Kim, Ashe et al. 1993a; Kawashima, Roland et al. 1994). Taken together, SMA, premotor cortex, and primary motor cortex all demonstrate increased activity in relation to ipsilateral arm and hand movements. Activations during ipsilateral arm movements have been found to be stronger in the left hemisphere (Kim, Ashe et al. 1993b) and stronger during complex finger movement tasks as opposed to simple finger movement tasks (Rao, Binder et al. 1993). These task-specific effects on ipsilateral motor activity may indicate that activations of motor areas in the hemisphere ipsilateral to a moving limb are related to the increased planning load required from the dominant hemisphere in executing movements of either arm or the increased planning load necessary to execute more complex sequences of movements. Given the callosal connections between primary motor cortices (Kaas 1995), an alternative explanation for the activity in the

ipsilateral hemisphere is that it represents cross-callosal inhibition. Furthermore, the presence of interhemispheric inhibition has been directly demonstrated through paired pulse TMS experiments (Ferbert, Priori et al. 1992; Di Lazzaro, Oliviero et al. 1999). Several studies, however, have shown that activations in the ipsilateral hemisphere are shifted ventral, lateral, and anterior to the simultaneous activations in the contralateral hemisphere, showing that the observed activity in the ipsilateral hemisphere cannot be accounted for solely by homotopic cross-callosal inhibition (Cramer, Finklestein et al. 1999; Verstynen and Ivry 2011). While not homotopic cross-callosal inhibition, one function of ipsilateral motor activity may be to inhibit the production of mirror movements, as inhibition of the premotor cortex causes increased correlation between fMRI activity in the left and right motor cortices (Verstynen and Ivry 2011). Furthermore, during cued unimanual finger movements of individual digits, while the activity in the SMA and premotor cortices increase bilaterally, activity in primary motor cortex increases contralateral to the moving limb and decreases ipsilateral to the moving limb (Diedrichsen, Wiestler et al. 2013).

While the functional imaging studies described above used simple movements and sequences of movements, more complex motor tasks give a more detailed view of motor-system activations. In addition to primary motor cortex, a large network of cortical areas in the parietal lobe and the frontal lobe are involved in visually guided reaching movements (Filimon 2010; Gallivan, McLean et al. 2013). During bimanual movements, while the fMRI activations in the primary motor cortex related to ipsilateral finger movements disappear, there are regions in the boundary between primary motor cortex and premotor cortex in which fMRI activity encodes both ipsilateral and contralateral finger movements (Diedrichsen, Wiestler et al. 2013). This broad network of motor areas is also highlighted by differences in the ability to decode limb-specific

action choices and action-specific limb choices with fMRI activity. In particular, the superior parieto-occipital cortex, the anterior intraparietal sulcus, SMA, and the primary motor cortex can be used to decode the action of the contralateral limb, the ventral premotor cortex and dorsolateral prefrontal cortex can be used to predict the action of either limb but not which limb is used, and the posterior intraparietal sulcus, the middle intraparietal sulcus, the dorsal premotor cortex, the pre-SMA, and movement planning activity from the primary motor cortex can be used to predict both the limb and action used (Gallivan, McLean et al. 2013). While the ability to predict the movement type from an area of cortex is not sufficient to determine if that region is actively involved in the planning and execution of movements, it is likely a necessary condition for its involvement. Taken together, the planning and execution of motor actions involves a broad and complex network of regions with activity in the ipsilateral hemisphere potentially involved both to inhibit mirror movements as well as contribute to the planning and execution of movements.

2.2.5 Lesion Studies

While measures of functional activity show that cortex ipsilateral to a moving limb may be involved in the planning and execution of motor movements, changes that occur after cortical lesions provide evidence for a direct role of the ipsilateral hemisphere in executing motor movements. First, after inducing a unilateral lesion in the primary motor cortex of non-human primates, a decrease in hand strength ipsilateral to the lesion occurs with a modest but statistically significant affect on function (Glees and Cole 1952; Bashir, Kaeser et al. 2012). These findings have been confirmed in human stroke survivors who have been found to have ipsilesional motor deficits both acutely (Baskett, Marshall et al. 1996; Yelnik, Bonan et al. 1996) and chronically (Sunderland 2000; Cramer, Mark et al. 2002; Haaland, Prestopnik et al. 2004).

These deficits were found not only in movements involving the whole arm, but also in aimed movements of a single distal joint (Yarosh, Hoffman et al. 2004).

By comparing studies of ipsilesional motor deficits, it was observed that right hemisphere lesions impact tasks requiring sensorimotor integration (Baskett, Marshall et al. 1996), while lesions to the left hemisphere preferentially affect the initial component of movements (Haaland, Prestopnik et al. 2004). A potential explanation for the difference in ipsilesional deficits caused by right and left hemisphere lesions can be found in the dynamic dominance hypothesis for handedness (Sainburg and Kalakanis 2000; Sainburg and Schaefer 2004; Goble and Brown 2007; Goble and Brown 2008). The dynamic dominance hypothesis postulates that the non-dominant hemisphere is specialized for proprioceptive matching and final positioning, while the dominant hemisphere is specialized for planning dynamic components of movements, such as the trajectory, initial acceleration, or interaction torques. The dynamic dominance hypothesis also allows several predictions to be made about the types of ipsilesional deficits that will be associated with each hemisphere. These predictions have led to studies showing that when compared to normal controls and patients with right hemisphere damage, patients with left hemisphere damage had poorer scaling of acceleration amplitude with movement distance, a decreased ability to adapt initial movement trajectories to visuomotor rotations, and poor intersegmental coordination during corrective movements (Schaefer, Haaland et al. 2007; Schaefer, Haaland et al. 2009a; Schaefer, Mutha et al. 2012). On the other hand, patients with right hemisphere damage had decreases in the ability to scale acceleration duration leading to decreased accuracy, a decreased ability to correct their movement trajectory online after a visuomotor rotation, and performed corrective movements later and towards the wrong location in a task requiring corrective movements (Schaefer, Haaland et al. 2007; Schaefer, Haaland et al.

2009a; Schaefer, Mutha et al. 2012). These differences were specific to patients with contralesional hemiparesis (Haaland, Schaefer et al. 2009). Therefore the results of multiple studies demonstrate dissociable ipsilesional deficits, indicating that each hemisphere contributes to the planning and execution of ipsilateral limb movements.

While the presence of ipsilesional motor deficits demonstrates that each hemisphere plays a role in the execution of same-sided limb movements, it is uncertain whether these deficits are caused by a disruption of activity descending in the ipsilateral spinal cord, or by a disruption of the balance of inter-hemispheric inhibition. Several examples showing that the ability to produce voluntary movements is maintained after large and significant lesions demonstrate the potential for generating ipsilateral limb movements in isolation from the contralateral hemisphere. In early descriptions of right hemispherectomies, several surgeons noted that patients could perform movements of the left (contralesional) limbs (Dandy 1928; Gardner 1933). Additionally, non-human primates could perform movements with all four limbs even after removal of both premotor cortices and one primary motor cortex or after removal of one premotor cortex and bilateral primary motor cortices (Bucy 1933; Bucy and Fulton 1933). Therefore, each cortical hemisphere not only plays a role in the production of ipsilateral limb movements, but each hemisphere is also sufficient to execute movements of the ipsilateral limbs after contralateral lesions.

2.2.6 Stimulation Studies

A final piece of evidence for the role of individual motor areas in producing voluntary movements comes from electrical stimulation of the brain. As illustrated by the famous cartoons displaying the motor homunculus, stimulation of the human motor cortex produces movements of the opposite side of the body in a broadly overlapping representation of body parts (Penfield

and Boldrey 1937; Penfield and Rasmussen 1950). Motor and sensory representations are found not only with stimulation of the primary sensorimotor cortex, but sensory percepts are also generated with stimulation of secondary sensory areas and a representation of motor movements caused by stimulation is also found in the SMA (Penfield and Jasper 1954). While stimulation of the primary motor cortex produces movements of body parts contralateral to the site of stimulation, multiple studies have also shown that stimulation of an area in the premotor cortex on the superior lip of the precentral sulcus of non-human primates produces movements of the ipsilateral extremities (Bucy and Fulton 1933; Wyss 1938; Aizawa, Mushiake et al. 1990). The ability to elicit movements of the ipsilateral limbs through cortical stimulation persists after a spinal hemisection and after sectioning of the corpus callosum with subsequent removal of the contralateral premotor cortex, demonstrating that the movements ipsilateral to the site of stimulation are not caused by a spinal circuit or pathways that have crossed to the contralateral hemisphere via the corpus callosum prior to descending (Bucy and Fulton 1933). In contrast to premotor cortex, ipsilateral limb movements elicited from stimulation of primary motor cortex are normally dependent upon an intact contralateral motor system, but can still be produced independent of the contralateral motor system when the efficacy of the descending ipsilateral corticospinal system is augmented (Brus-Ramer, Carmel et al. 2009).

2.2.7 Ipsilateral Motor Physiology Summary

Taken together, studies utilizing a variety of recording modalities and methods demonstrate the existence of neural activity related to movements of the ipsilateral limbs with varied timing and cortical topography, indicating that a variety of cortical mechanisms are represented. Additionally, this neural activity has been found to contain specific information about ipsilateral limb movements such as the direction or movement type, indicating both that ipsilateral motor

activations may be necessary for the execution of ipsilateral limb movements and that these activations may be useful in developing neuroprosthetic systems. While the presence of dissociable ipsilesional deficits does not exclude the possibility that some of the motor-related activity in the ipsilateral hemisphere is used to inhibit mirrored activity from the contralateral hemisphere, it demonstrates that there is also an active role of each hemisphere in the execution of ipsilateral limb movements. Finally, the presence of ipsilesional movements after broad lesions and the fact that ipsilateral movements can be produced through cortical stimulation in isolation from the contralateral hemisphere indicates that descending pathways in the ipsilateral spinal cord can play a role in the execution of motor movements. Therefore, these same ipsilateral pathways may be useful for the recovery of motor function after a hemispheric lesion.

2.3 Motor Physiology After Stroke

In addition to playing a role in the planning and execution of motor movements in motor-intact subjects, the ipsilateral hemisphere may also play a role in the recovery of an impaired limb after stroke. Functional imaging has shown that ipsilateral activity from the unaffected hemisphere is increased when compared to normal controls after recovery from stroke (Weiller, Chollet et al. 1992; Weiller, Ramsay et al. 1993; Cramer, Nelles et al. 1997; Nelles, Spiekramann et al. 1999). Similarly, ipsilateral activity in the unaffected hemisphere increases not only after normal recovery but is also increased after training with constraint induced movement therapy (Levy, Nichols et al. 2001; Schaechter, Kraft et al. 2002). Additionally, increases in neural activity in the unaffected hemisphere related to affected hand movements are not isolated to measures of cerebral blood flow. Studies utilizing EEG after recovery from stroke found that movement-related cortical potentials are shifted towards the unaffected hemisphere during affected hand movements when compared to unaffected hand movements (Honda, Nagamine et al. 1997;

Green, Bialy et al. 1999). One possibility is that these increases in neural activity ipsilateral to the affected hand facilitate recovered motor function. Evidence for this possibility comes from the fact that TMS applied to disrupt the contralesional premotor cortex of stroke survivors slowed reaction times associated with affected hand movements (Johansen-Berg, Rushworth et al. 2002). Additionally, inhibitory repetitive TMS to the dorsal premotor cortex, the primary motor cortex, or the superior parietal lobe in the unaffected hemisphere of recovered stroke survivors led to decreases in recovered hand motor performance (Lotze, Markert et al. 2006).

An alternative possibility is that increased ipsilateral motor activity in the contralesional hemisphere hinders motor recovery. In animal models of stroke, remapping of the perilesional motor representations occurs during motor recovery (Nudo, Wise et al. 1996). In human patients, decreases in ipsilateral motor activity from the unaffected hemisphere correlate with recovery in both longitudinal and cross-sectional studies of recovery from stroke (Ward, Brown et al. 2003a; Ward, Brown et al. 2003b). Similarly, while in the acute period after a stroke, ipsilateral motor activity is increased in the unaffected hemisphere, after recovery, motor activity becomes more lateralized due to increases in ipsilesional activity (Marshall, Perera et al. 2000). Along with measures of neural activity from functional imaging, decreases in the difference in TMS thresholds necessary to elicit affected limb movements from the contralesional hemisphere relative to the ipsilesional hemisphere are associated with poor motor recovery after stroke (Turton, Wroe et al. 1996; Netz, Lammers et al. 1997). Furthermore, training with CIMT has also been shown to lead to increases in contralateral motor representations in the ipsilesional hemisphere (Liepert, Miltner et al. 1998; Liepert, Bauder et al. 2000). As the contralesional primary motor cortex maintains increased inhibition of the ipsilesional primary motor cortex

during affected hand movements, ipsilesional hemisphere activity may limit recovery due to altered interhemispheric interactions (Murase, Duque et al. 2004).

There are several important considerations to take into account when considering evidence for the potential mechanisms responsible for rehabilitation. First, a variety of different measures for rehabilitation have been used in studies. Therefore, patients with similar functional recovery may fall into the recovered group of one study and the impaired group of another study depending upon the measure used (Cramer 2004). Additionally, as increases in task complexity, subject attention, and perceived effort are associated with increased neural activity during voluntary motor movements (Manganotti, Kitamura 1993a, 1993b, Jankelowitz, Slobounov), changes in neural activity after recovery from stroke may represent alterations in the level of attention and effort needed for movement planning and execution.

Although the previous evidence is conflicting, it may be possible to integrate these findings into a single view describing the role of the unaffected hemisphere after stroke. First, several of the studies described above have found increases in neural activity in both the affected and unaffected hemispheres during affected hand movements after recovery from stroke (Green, Bialy et al. 1999; Levy, Nichols et al. 2001). Additionally, cortico-muscular coherence between cortex and the affected hand is found in a wider area in stroke survivors than in normal controls, including in regions of the contralesional hemisphere (Rossiter, Eaves et al. 2012). This indicates that in some patients, the contralesional hemisphere can drive affected hand muscles after stroke. Furthermore, in a study using MEG to measure motor potentials after recovery from stroke, while patients who recovered completely showed normal lateralization of their neural activity during motor movements, patients who recovered incompletely had better recovery with

increased ipsilateral motor activity in the unaffected hemisphere (Tecchio, Zappasodi et al. 2006). This difference in recovery makes sense when we consider that recovery after stroke is correlated with corticospinal tract integrity (Fries, Danek et al. 1993; Carter, Patel et al. 2012). Taken together, optimal recovery may be mediated by traditional contralateral motor pathways, however, in patients with extensive cortical or subcortical lesions, while function may not be completely restored, restoration of motor function may be mediated by ipsilateral motor activity from the contralesional hemisphere.

2.4 Neuroprosthetic Applications

Because of the relationships that have been observed between neural activity and movements of the ipsilateral limbs, these signals represent a potential control signal for brain-computer interface applications. A brain-computer interface (BCI) system or brain-machine interface (BMI) system is a system that records neural activity, translates that activity into a machine command, and uses that command to control an external assistive device based upon the intentions of the user. While the idea of using neural activity related to motor intentions to control a prosthetic system has existed for several decades (Brindley and Craggs 1972; Craggs 1975), the past several years has seen significant developments in the ability to design and implement BCI systems using a variety of recording modalities. The ideal experiments studying BCI control involve closed-loop tasks in which the subject attempts to control the BCI system using only their brain signals. In addition to closed-loop experiments, many studies use machine learning algorithms to demonstrate the potential for open-loop prediction of behavioral parameters such as movement kinematics. While these open-loop studies do not model the affect of learning and adaptation that occurs with closed-loop BCI control, they enable investigators to

study the feasibility of BCI applications using various recording methods and decoding algorithms on a limited data set.

2.4.1 Invasive BCI Systems

To date, chronically implanted invasive microarrays have been used in animal and early human trials to produce BCI systems with the greatest number of degrees-of-freedom. These systems utilize either changes in the rate of single neuron or multi-neuron spiking or changes in local field potential activity to control prosthetic systems. Estimates for the number of neurons needed to simultaneously decode arm movements range between 150 neurons with serial single unit recordings and 600 units from multielectrode arrays (Georgopoulos, Kettner et al. 1988; Wessberg, Stambaugh et al. 2000). While a large number of neurons would be necessary to achieve optimal kinematic decoding, it is possible to decode kinematics in an open-loop setting using multielectrode arrays with 40-200 electrodes (Wessberg, Stambaugh et al. 2000; Taylor, Tillery et al. 2002; Wu, Black et al. 2003; Ganguly, Secundo et al. 2009). One study also demonstrated that it is possible to use multielectrode arrays to decode kinematics of ipsilateral arm movements in non-human primates (Ganguly, Secundo et al. 2009).

Along with off-line decoding of movement kinematics, implanted multielectrode arrays can be used for closed-loop BCI control. In non-human primate models, these systems have been used to control a cursor in 3D space (Wessberg, Stambaugh et al. 2000; Serruya, Hatsopoulos et al. 2002; Taylor, Tillery et al. 2002) as well as to control a robotic arm for collecting and eating food (Carmena, Lebedev et al. 2003; Velliste, Perel et al. 2008). Additionally, microelectrode arrays have been implanted in human patients with tetraplegia to control an artificial cursor and robotic arm (Kennedy and Bakay 1998; Hochberg, Serruya et al. 2006; Kim, Simeral et al. 2008). Importantly, because of the ability of subjects to adapt their neural activity to BCI control

algorithms during closed-loop feedback, on-line BCI control can be achieved with fewer recorded units than needed for off-line movement decoding (Taylor, Tillery et al. 2002).

While invasive microelectrode arrays can be used to implement BCI systems with several degrees of freedom, there are several limitations. Implanting microelectrode arrays entails very invasive surgical procedures with a risk of damage to the cortex around the implant site (Bjornsson, Oh et al. 2006) as well as significant clinical risks such as infection. Additionally, over several months, the brain's immune response causes the implanted microelectrodes to become encapsulated, leading to increased impedance and a significant decrease in signal quality that causes decreases in BCI performance (Williams, Hippensteel et al. 2007).

2.4.2 Non-invasive BCI Systems

At the opposite end of the spectrum from invasive microelectrode arrays are non-invasive recording methods such as EEG. Because EEG is applied to the scalp, electrodes can be easily applied and can be easily utilized in patient populations. While a variety of signals have been used for EEG BCI systems (Pfurtscheller, Neuper et al. 2003) ERD-based BCI systems have particular relevance for motor-impaired populations, including stroke survivors, due to the fact that ERD occurs normally during motor execution (see section 2.1.3). Additionally, ERD has been shown to occur with imagined motor movements, indicating that it would be applicable to patient populations that are unable to execute motor movements (Pfurtscheller and Neuper 1997). Furthermore, EEG ERD-based BCI systems have been used in normal controls and patient populations (Wolpaw, McFarland et al. 1991; Pfurtscheller, Muller et al. 2003; Pfurtscheller, Neuper et al. 2003; Wolpaw and McFarland 2004; McFarland, Sarnacki et al. 2010).

While EEG is a powerful tool for BCI systems due to its ease of use and non-invasiveness, it suffers from poor signal quality and susceptibility to noise. To date the best performance of an EEG BCI system is 3 degrees-of-freedom (McFarland, Sarnacki et al. 2010), which was only achieved after months of intensive training. Additionally, EEG recordings have decreased spatial and spectral resolution when compared to invasive recordings (Cooper, Winter et al. 1965; Pfurtscheller and Cooper 1975), limiting the total number of degrees-of-freedom that can be simultaneously controlled. Furthermore, because of its location on the scalp, EEG recordings are very susceptible to artifacts such as EMG or eye blinks that can corrupt recordings and decrease BCI performance (Cooper, Winter et al. 1965; Wolpaw, McFarland et al. 2003).

2.4.3 ECoG BCI Systems

A third alternative that has been proposed for BCI systems as a compromise between the extremes of microelectrode arrays and EEG are ECoG recordings made from the surface of the brain. In humans, most studies investigating the use of ECoG as a control signal for BCI systems have generally used clinical electrodes implanted in epilepsy patients for localization of the epileptic foci with an electrode size on the order of a few millimeters and an interelectrode distance of approximately 1 cm.

Spectral power changes in ECoG signals occur not only during overt motor movements, but also during imagined movements (Leuthardt, Schalk et al. 2004). Because of this, they may be useful in motor-impaired patients who are unable to perform overt motor movements. Furthermore, motor-intact human subjects can modulate the spectral power of ECoG signals to control a computer cursor (Leuthardt, Schalk et al. 2004; Wilson, Felton et al. 2006; Felton, Wilson et al. 2007; Schalk, Miller et al. 2008). Additionally, ECoG has been utilized in a quadriplegic patient to generate a BCI system with 3 degrees-of-freedom based upon motor imagery of movements at

multiple independent joints with good signal quality for durations up to one month (Wang, Collinger et al. 2013). Micro-ECoG arrays with sub millimeter electrode sizes have also been proposed as a means to obtain signals with increased spatial specificity. These arrays have been utilized for online BCI control in experiments in non-human primates (Rouse and Moran 2009; Rouse, Williams et al. 2013) with stable signal quality demonstrated for up to four years (Moran, 2015, *Personal Communication*).

While closed-loop ECoG BCI systems have generally used either changes in spectral power associated with imagined movements of a single joint in humans or high gamma power in arbitrary electrodes in primates, a more natural format for device control may be to develop a biomimetic BCI that uses signals decoded from natural kinematic parameters of movements. By examining the ability to predict behavioral performance using ECoG activity, it is possible to begin to determine whether biomimetic device control is feasible. Additionally, off-line prediction of movement parameters allows investigation of a variety of potential BCI control strategies from a single data set, which is advantageous because of the short duration of electrode implantation in the human epilepsy patients studied with ECoG.

Using invasive LFP recordings, it is possible to decode movement direction of 2D forelimb movements in rat motor cortex (Slutzky, Jordan et al. 2011) and 2D arm movements in non-human primates (Rickert, Oliveira et al. 2005; Ince, Gupta et al. 2010; Flint, Lindberg et al. 2012). In addition to LFPs derived from microelectrode arrays implanted into the parenchyma, ECoG signals recorded either subdurally or epidurally have also been utilized to decode 2D movement directions in rats (Slutzky, Jordan et al. 2011) and non-human primates (Flint, Lindberg et al. 2012) as well as to perform continuous decoding of movement kinematics from

2D (Flint, Lindberg et al. 2012; Marathe and Taylor 2013) and 3D arm movements in primates (Chao, Nagasaka et al. 2010; Chen, Shin et al. 2013). While most studies using LFP and ECoG recordings to decode movements have used recordings contralateral to the limb decoded, one study also demonstrated that LFP recordings in the hemisphere ipsilateral to a moving arm could be use to predict 2D arm movements in primates (Ganguly, Secundo et al. 2009).

Along with decoding kinematics of motor movements in animal models, ECoG recordings from human epilepsy patients have been used to decode information about voluntary motor movements. Classification of movement direction of both arm and hand movements has been achieved using recordings from periods before and during movement execution (Reddy, Reddy et al. 2009; Wang, Gunduz et al. 2012; Chestek, Gilja et al. 2013). Additionally, ECoG signals can be used to decode continuous movement trajectories of finger flexion/extension movements (Chestek, Gilja et al. 2013) and 2D arm movements (Schalk, Kubanek et al. 2007; Pistohl, Ball et al. 2008; Sanchez, Gunduz et al. 2008). While a few studies have used ECoG recordings to predict trajectories of 3D movements, the behavioral tasks used had correlations between speed and movement direction, reducing the true dimensionality of the information decoded (Hotson, Fifer et al. 2012; Nakanishi, Yanagisawa et al. 2013). Therefore, to date, the extent of information about movement kinematics that can be decoded from human ECoG recordings is uncertain. A few studies have also demonstrated the ability to decode continuous kinematic trajectories of the arm ipsilateral to ECoG arrays implanted in motor-intact human patients (Ganguly, Secundo et al. 2009; Hotson, Fifer et al. 2014). While these studies demonstrate the ability to decode kinematics of ipsilateral limb movements from ECoG signals, it is unclear how the ability to decode kinematics of the ipsilateral and contralateral arm is related.

The ability to decode continuous kinematics of voluntary motor movements from ECoG recordings illustrates the potential use of ECoG signals in designing BCI systems that balance the need for generating accurate control signals representing multiple degrees-of-freedom with the need to limit the invasiveness of implant procedures and maximize signal stability. The previous studies demonstrate that linear decoding methods are often sufficient for decoding continuous trajectories of arm movements in primates and humans. While the potential feature space includes a large number of temporal and spectral features, slow temporal fluctuations of the local motor potential (LMP) and changes in high gamma band power have generally been the most important features in previous off-line decoding models (Schalk, Kubanek et al. 2007; Hotson, Fifer et al. 2014).

2.4.4 BCIs for Stroke

While the majority of work towards developing BCI systems has focused on patients with an intact cortex who suffer from conditions such as spinal cord injury or amyotrophic lateral sclerosis, BCIs may also be useful in patients suffering from hemispheric strokes. BCI systems for stroke survivors could be used to either control an assistive device such as a robotic arm or exoskeleton or as a tool to encourage rehabilitation. Several simple BCI systems have been implemented in hemispheric stroke survivors using EEG or MEG signals (Buch, Weber et al. 2008; Daly, Cheng et al. 2009; Soekadar, Witkowski et al. 2011; Ramos-Murguialday, Broetz et al. 2013; Tung, Guan et al. 2013; Ang, Chua et al. 2014; Mukaino, Ono et al. 2014; Soekadar, Silvoni et al. 2015). Early results indicate that training with a BCI-based rehabilitation system can lead to functional gains after stroke (Ramos-Murguialday, Broetz et al. 2013), although additional studies will be needed to further develop our understanding of the role of lesion location, functional impairment, BCI-system design, and training dose in maximizing functional

improvement. While these studies have used activity in the ipsilesional hemisphere, because of the role of the contralesional hemisphere in recovery from stroke (see section 2.3) as well as the fact that the ability to modulate cortical activity decreases with increased cortical damage (Buch, Modir Shanechi et al. 2012), the contralesional hemisphere may be relevant for BCI applications after stroke.

2.5 Summary

Developing new methods to improve function after stroke represents an urgent clinical need. One possible mechanism for recovery is the remapping and strengthening of connections from the unaffected hemisphere. In normal motor control, the ipsilateral hemisphere plays a role in the execution of lateralized limb movements as exemplified by modulation of functional activity during movements of the ipsilateral limb. After stroke, while optimal recovery is generally associated with the involvement of the ipsilesional hemisphere, the contralesional hemisphere may facilitate recovery in some patients. Additionally, BCI systems have the potential to restore function after stroke either through the control of artificial assistive devices or through its use as a rehabilitation tool. While previous BCI systems for stroke have focused on the ipsilesional hemisphere, because of the potential role of the contralesional hemisphere in recovery from stroke and changes to neural activity after stroke, contralesional BCI systems may be beneficial for some patients.

Based upon this rationale, there are several avenues of research that we will explore. First, while electrophysiological activity has been found in the hemisphere ipsilateral to a moving limb, the extent of information that can be decoded and used in a BCI system is uncertain. Furthermore, BCI systems in the ipsilateral hemisphere will require separable control of both limbs, therefore,

determining the similarities and differences between the encoding of ipsilateral and contralateral limb movements will be vital. Finally, to begin the process of implementing contralesional BCI systems in stroke survivors, it will be necessary to determine the level of information that can be decoded from invasive and non-invasive recordings, to better understand the technical requirements for invasive BCI implementation, and to determine if stroke survivors can intentionally modulate activity in their unaffected hemisphere to control a BCI system.

3 Electrocorticographic Decoding of Contralateral and Ipsilateral Reaches

3.1 Introduction

Brain-computer interface (BCI) systems have the potential to restore function in stroke survivors by using neural activity to control an external device. In healthy human subjects, movement-related changes in neural activity occur in the hemisphere ipsilateral to a moving limb with cortical physiology that is distinct from the contralateral hemisphere (Wisneski, Anderson et al. 2008). Furthermore, after recovery from stroke, affected hand movements are associated with increased activity in the ipsilateral hemisphere in some patients (Weiller, Chollet et al. 1992; Weiller, Ramsay et al. 1993; Cramer, Nelles et al. 1997; Honda, Nagamine et al. 1997; Green, Bialy et al. 1999; Nelles, Spiekramann et al. 1999; Levy, Nichols et al. 2001; Schaechter, Kraft et al. 2002). Taken together, contralesional hemisphere movement-related neural activity may be useful in BCI systems for stroke survivors.

One method to establish the feasibility of BCI systems is to determine if neural activity can be used to decode behavioral intentions. In animal models, Electrocorticography (ECoG) signals have been used to decode kinematic trajectories of two-dimensional (2D) and three-dimensional (3D) movements of the upper limb (Chao, Nagasaka et al. 2010; Slutzky, Jordan et al. 2011; Flint, Lindberg et al. 2012; Chen, Shin et al. 2013; Marathe and Taylor 2013). In humans, ECoG signals have also been used to decode trajectories of 2D movements (Schalk, Kubanek et al. 2007; Pistohl, Ball et al. 2008; Sanchez, Gunduz et al. 2008). While several studies have used ECoG to decode movement trajectories not constrained to two dimensions, speed and movement direction were correlated in at least one dimension, thereby reducing the dimensionality of

information decoded (Hotson, Fifer et al. 2012; Nakanishi, Yanagisawa et al. 2013; Hotson, Fifer et al. 2014). Therefore, the extent of kinematic information that can be decoded from human ECoG recordings is uncertain.

While the majority of studies examining the ability to decode trajectories of reaching movements have used neural activity contralateral to the moving arm, the ipsilateral hemisphere may be useful for BCI systems in stroke survivors. Additionally, although human ECoG recordings have been used to decode time courses of ipsilateral limb kinematics in one or two dimensions (Ganguly, Secundo et al. 2009; Hotson, Fifer et al. 2012; Hotson, Fifer et al. 2014), the extent of information that is encoded in the hemisphere ipsilateral to a moving limb is unknown. Furthermore, the similarities and differences in the neural representations of contralateral and ipsilateral limb kinematics within a single hemisphere are also unknown. Understanding these differences will be important to ensure that BCI systems using neural activity from the ipsilateral cortex can be controlled independent of contralateral limb movements.

This study sought to determine whether ECoG signals recorded from human patients could be used to decode 3D kinematics of contralateral and ipsilateral arm movements. This study is unique in that by having the same patients perform movements of both arms, we sought to define the differences in the accuracy and features used to decode kinematics of both limbs from a single hemisphere. Finally, by simulating EEG signals, we gained an understanding of the reduction in decoding accuracy with non-invasive recording methods.

3.2 Methods

3.2.1 Patient Characteristics

The participants in this study were patients with intractable epilepsy who underwent temporary placement of subdural ECoG electrode arrays for localization of their epileptic foci and mapping of eloquent cortices for pre-surgical planning. ECoG electrodes were implanted for a period of approximately one week (5 days – 14 days), during which time the recordings utilized in this study were collected. The Institutional Review Board of the Washington University School of Medicine approved the study protocol, and all patients provided written informed consent prior to participating in the study. Table 3.1 contains patient characteristics for all 5 patients. Of the patients, 4 were right-handed, and all electrode arrays were located in the hemisphere contralateral to the dominant hand. Notably, one participant (Patient 2) had weakness of the arm contralateral to the site of electrode implantation due to mass effects from the implant.

Table 3.1 Patient characteristics and electrode locations

	Electrode Locations	Epileptic Focus Location	Handedness	Age at Data Collection	Contralateral Trials	Ipsilateral Trials
Patient 1	Right temporal / frontal strips	Right Mesial Temporal	Left	40	288	128
Patient 2	Left frontotemporal grid and strips	Left Anterior/Mesial Temporal	Right	27	104	240
Patient 3	Left frontotemporal grid and strips	Left Anterior Temporal	Right	53	140	0
Patient 4	Left frontotemporal grid and strips	Left Frontal/Central	Right	18	256	256
Patient 5	Left Frontotemporal grid and strips	Left Anterior Sub-Temporal	Right	56	256	256

3.2.2 Data Acquisition

Clinical ECoG arrays (PMT Corporation, Chanhassen, MN or Ad-Tech, Racine, WI) were utilized for this study. Electrodes were platinum-iridium disks surrounded in silastic sheets.

Electrodes had a diameter of 4 mm (2.3 mm diameter exposed) and an inter-electrode distance of 1 cm. Electrode arrays were configured in 8x8 grids, 1x4 strips, 1x6 strips, or 1x8 strips as shown in Figure 3.1A. In addition to the cortically facing recording electrodes, a 1x4 or 1x6 strip of electrodes was implanted facing the skull for use as ground and reference signals. Recordings were made using g.USBamp biosignal amplifiers (g.tec, Graz, Austria), which utilized 24-bit resolution analog-to-digital converters, an internal sampling rate of 38.4 kHz, and an internal anti-aliasing filter at 5 kHz. The BCI2000 software package (Schalk, McFarland et al. 2004a) was used to record ECoG signals with a sampling rate of 1200 Hz and no additional external filtering.

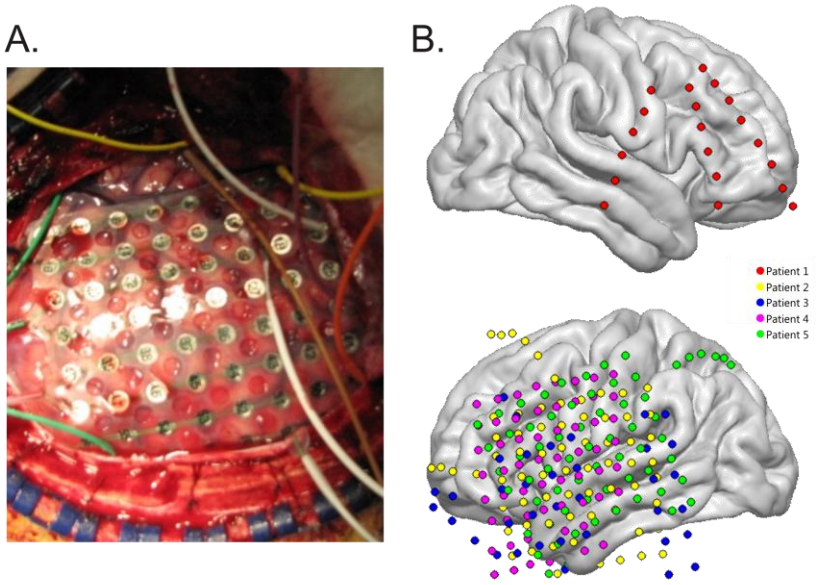

Figure 3.1 Electrocorticography implants and electrode localization
A. A photograph of a typical ECoG implant is shown. The electrodes were implanted beneath the dura as part of an 8x8 grid, 1x4 strips, 1x6 strips, or 1x8 strips. Electrodes had an exposed diameter of 2.3mm and an inter-electrode spacing of 1 cm. **B**. Electrode locations for each patient were mapped onto an atlas brain, allowing for comparison of ECoG activity by cortical locations across patients. Electrode locations were based solely upon each patient's clinical needs.

3.2.3 Electrode Localization

Electrode locations were solely dependent upon the clinical needs of each patient. Electrode coordinates in atlas space were estimated from lateral radiographs collected after electrode

implantation. The getLOC package (Miller, Makeig et al. 2007) was used to approximate electrode coordinates with an accuracy of approximately 1 cm. Figure 3.1B displays the electrode locations for each of the 5 patients, showing that areas within the frontal and parietal lobe were well sampled across patients. To display the results of the analyses described in the following sections, we mapped quantitative results onto an atlas brain using a weighted spherical Gaussian kernel centered at each electrode location. Gaussian kernels from all electrodes were linearly superimposed onto the atlas brain and the contribution from each electrode was normalized based upon the number of nearby electrodes. Quantitative results were compared for all patients across cortical locations.

3.2.4 Behavioral Task

To examine the relationship between ECoG signals and reaching movements, a 3D center-out reaching task was used. Hand positions for the moving limb were collected using a Flock of Birds six degree-of-freedom motion capture system (Ascension Technology, Shelburne, VT). A single sensor was fixed to the index and middle fingers of the moving arm to track hand position. Hand positions in 3D space were sampled at 37.5 Hz. Kinematic data was recorded and synchronized with ECoG signals using a custom-programmed Flock of Birds filter that was integrated into the BCI2000 system.

The center-out reaching task consisted of cued reaches to 8 targets positioned at the corners of a physical cube with 50 cm long sides that was set in front of the patient. All reaches began from a target at the center of the cube and progressed to one of the 8 corners of the cube. LED lights that were placed at the center target and each of the external targets provided patients with stimulus cues and reward feedback that was synchronized to the ECoG and kinematic recordings through a custom-built microcontroller circuit that interfaced with the BCI2000 system via a USB

interface and custom-programmed BCI2000 application module. During performance of the task, patients were seated in their hospital bed in a semi-recumbent position with the center target placed at the patient's midline approximately 40 cm away from their chest. Figure 3.2A shows the physical apparatus used for the reaching task. To compare contralateral and ipsilateral arm movements, in four of the five patients, the task was performed using the arm contralateral to the electrode array in one session and with the arm ipsilateral to the electrode array in a second recording session.

Prior to beginning task performance, the task was calibrated to determine the location of the target positions and to account for any limitations in patient-specific range-of-motion. Figure 3.2B shows the time-course for a correct trial. Each trial began with a visual cue for patients to move their hand to the center hold position at which time a hold-A period began, lasting for 500 ms for Patient 1 and 1000 ms for Patients 2-5. During the hold-A period no other stimuli about the target for the current trial was provided. After completion of the hold-A period, a 2 second plan period began, during which time one of the external targets was illuminated and patients were instructed to plan a reaching movement to the target indicated. Patients were instructed to plan but not initiate the reaching movement and to maintain holding their hand at the center target. At the conclusion of the plan period, the indicated external target changed colors, cueing the patient to initiate a reaching movement to the external target. Upon reaching the external target, the LED at the specific target turned to green, indicating that the patient had correctly reached the target and cueing the beginning of a 500 ms hold-B period. At the conclusion of the hold-B period, the center target and each of the 8 external targets were illuminated in green to indicate a successful trial completion. If patients reached to an incorrect target or did not reach the correct target within the 4 second time period allowed for the movement, the trial was

aborted and all LED lights were illuminated in red to indicate an unsuccessful trial. In Patients 4 and 5, a trial was also aborted if the patient moved before the end of the hold-A, plan, or hold-B periods. The 8 targets were presented in a random order and patients completed multiple runs with 2-4 trials to each target for a total of 16-32 total trials per run. Ideal task performance consisted of 8 runs of 32 trials, for a total of 256 trials. The total number of trials collected and duration of each run were adjusted based upon each patient's stamina and comfort. Table 3.1 contains the total number of trials performed by each patient with the contralateral and ipsilateral limbs.

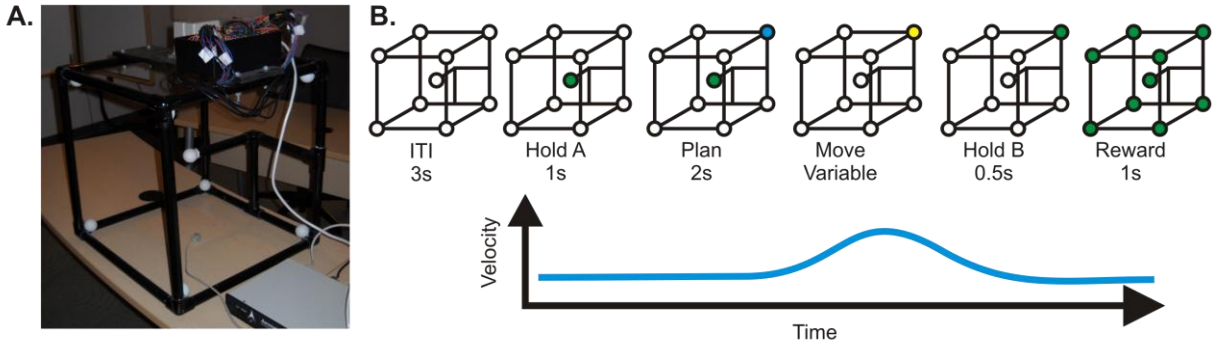

Figure 3.2 Behavioral task apparatus and trial timing
A. The photograph displays the apparatus used for the center-out reaching task. A cube with 50 cm sides was placed in front of the patient. Target locations and reward feedback were provided with LED lights placed at the 8 corner targets and center target. **B.** Each trial began with a 1 second hold-A period in which the subject held their hand at the central target. A 2 second planning delay was used during which time the subject was cued to the target of the reach and instructed to plan but not initiate a reaching movement to the appropriate target. After the movement "go" cue, subjects initiated a reach to the target. A successful trial ended with completion of a hold-B period in which subjects held their hand at the exterior target location.

3.2.5 Data Processing

Data Preprocessing

After data collection, a number of preprocessing steps were carried out. Initially, ECoG signals were visually inspected in both the spectral and temporal domain. Any channels that displayed non-physiologic activity or epileptic activity were excluded from all further analyses (Patient 1: 7 electrodes, Patient 2: 7 electrodes, Patient 3: 10 electrodes, Patient 4: 4 electrodes, Patient 5: 19 electrodes). Next, the spectral and temporal domain signals for each trial were examined. Trials

containing non-physiologic spikes or interictal epileptic activity were rejected. The hand position data collected for each trial were also visually examined and trials in which the hand position left the sampling range of the Flock of Birds receiver and trials in which patients initiated a reach to an incorrect target were also rejected. After this screening process, the total number of trials analyzed was: Patient 1: 245 contralateral, 119 ipsilateral; Patient 2: 76 contralateral, 187 ipsilateral; Patient 3: 104 contralateral; Patient 4: 221 contralateral, 177 ipsilateral; Patient 5: 202 contralateral, 208 ipsilateral. ECoG signals were then re-referenced to the common average. For 8x8 channel ECoG grids spanning multiple amplifiers, individual common averages were calculated for each recording amplifier. For 1x4, 1x6, and 1x8 channel strips, individual common averages were calculated for each strip of electrodes. Finally, signals were band-pass filtered between 0.1 Hz and 260 Hz using a 3rd order butterworth filter. Additionally, all noise harmonics below 260 Hz were removed from the data, including harmonics of the 60 Hz line frequency as well as harmonics of a 100 Hz artifact signal commonly observed in the system, using a 3rd order butterworth notch filter with a 5 Hz bandwidth. Both the band-pass and notch filters were run forwards and backwards to avoid inserting phase distortions into the signals.

Spectral Analysis Methods

Next, ECoG signals were segmented into 300 ms time windows with shifts of 50 ms between windows. Spectral power was estimated in 2 Hz bins with center frequencies from 3 Hz to 253 Hz using an autoregressive model with a model order of 75 (Marple 1987b). As ECoG power spectra are not normally distributed, power spectra were normalized using a log transform. Finally, power spectra were converted to z-score values, using the mean and standard deviation of spectral power from 200 ms after the beginning of the hold-A period until the end of the hold-A period. The z-score operation accounts for the 1/f fall-off in spectral power by ensuring that

the mean and variance of spectral power is the same at each frequency. Additionally, positive and negative z-scores indicate respective increases and decreases in spectral power relative to the hold-A period. The hold-A period was chosen as the baseline period for the task as patients had not received any target information, were not moving, and were maintaining their hand in a similar position in all trials. Exemplar spectral power changes were examined by aligning the spectral power during each trial to the onset of movement. Frequency bins and time windows with significant power changes were identified by using a one-sample t-test comparing the mean of z-score values for a given frequency bin and time window to zero.

For all later analysis procedures, spectral power was averaged into 7 canonical frequency bands: theta (4-8 Hz), mu (8-12 Hz), beta 1 (12-24 Hz), beta 2 (24-34 Hz), gamma 1 (34-55 Hz), gamma 2 (65-95 Hz), and gamma 3 (130-175 Hz). These 7 frequency bands were chosen to ensure inclusion of relevant frequency bands while avoiding all noise harmonics. Finally, the band-averaged spectral power was again z-scored relative to the hold-A period. The two z-score calculations were used to ensure first, that each frequency contributed equally to the band-averaged power estimates, and second, that the variance was similar across frequency bands, irrespective of the number of frequencies contained within a single frequency band.

Temporal Analysis Methods

In addition to the spectral features described above, the local motor potential (LMP), which is obtained by filtering time domain signals with a smoothing filter, has been shown to contain information related to movement kinematics (Schalk, Kubanek et al. 2007; Pistohl, Ball et al. 2008; Hotson, Fifer et al. 2014). To calculate the LMP, signals were segmented into 300 ms time windows with shifts of 50 ms between windows. A 2nd order Savitzky-Golay smoothing filter was calculated for each 300 ms window. Finally, the LMP time series were z-scored relative to

the hold-A period. Therefore, the variance of the LMP was equalized to the variance of the spectral power in each of the canonical frequencies with positive and negative values indicating respective increases and decreases in the LMP amplitude relative to the baseline hold-A period.

Kinematic Processing

Kinematic data was recorded as 3D positions with the positive x-axis oriented towards the patient in the anterior-posterior direction, the positive y-axis oriented laterally to the left, and the positive z-axis oriented inferiorly. The hand position data recorded in 3D space was differentiated to determine the components of velocity in the three cardinal directions. Non-directional hand speed was calculated by normalizing the velocity at each time point. The onset of movement for each trial was determined as the time point at which hand speed crossed 20% of the maximum hand speed for the trial. To align kinematic information with ECoG spectral and temporal features, kinematic information was segmented into 300 ms windows with shifts of 50 ms between windows and was averaged within each window.

To evaluate whether behavioral performance differed between the contralateral and ipsilateral arms, we calculated the reaction time and peak hand speed for each trial. Reaction times were calculated as the time from the movement cue until the onset of movement. Median reaction times were calculated after excluding reaction times that differed from the mean by more than 2 standard deviations. We were unable to evaluate the reaction times for Patient 1 as they consistently initiating reaching movements before the movement cue. Patient 1 was included in all remaining analyses as these analyses focused on the execution of movement and not the planning of motor movements in isolation from execution. To examine the dimensionality of the kinematic dataset, we performed principle components analysis (PCA) on hand speed, velocity in the three cardinal directions, and position along the three cardinal axes after normalizing each of

the 7 kinematic parameters between 0 and 1. The percent of information explained by each principle component was compared.

3.2.6 Electrophysiological Activity During Arm Reaches

Several analyses were performed to investigate the changes in electrophysiological activity that occurred before and during the execution of contralateral and ipsilateral arm reaches. Additionally, we examined the relationship between these changes and specific characteristics of movements.

Movement-Related Electrophysiological Activations

To examine the timing, sign, and amplitude of changes in ECoG activity related to reaches of the contralateral and ipsilateral arms, time courses of z-scored ECoG features (spectral power in the 7 canonical frequency bands outlined above and LMP amplitude) were aligned from 1 second before movement onset to 2 seconds after movement onset. Average z-scores were calculated for each electrode and feature. A one-sample t-test was used to determine if the mean z-score value for a specific electrode, feature, and time window was significantly different from zero. As a z-score value of zero represents the average activity for the hold-A period, this measure was used to determine changes in electrophysiological activity from baseline. Multiple comparison correction was performed using the Benjamini-Hochberg-Yekutieli method (Benjamini and Hochberg 1995; Benjamini and Yekutieli 2001) of False Discovery Rate (FDR) correction to account for the correlated p-values caused by the overlapping time windows. The locations and timing of significant power changes were compared between contralateral and ipsilateral arm reaches.

Electrophysiological Tuning to Movement Speed and Movement Target

In addition to the presence or absence of significant changes in ECoG activity related to reaching

movements, the relationship between ECoG activity and kinematic parameters of contralateral and ipsilateral arm reaches was analyzed. To examine the correlation between ECoG activity and movement speed, z-scored values of ECoG features were concatenated across trials for time windows from 2 seconds before movement onset until the end of each trial. A linear correlation coefficient was calculated between the time course of movement speed and the time course of each ECoG feature. To account for differences in the timing of individual features, correlation coefficients were calculated for all lags between 0 seconds and 1 second in 50 ms steps, and the maximum absolute correlation coefficient for each channel and feature was stored. The relationship between the activity for each of the 8 features and movement speed was combined across patients and mapped onto an atlas brain as described above. The relationship between ECoG activity and movement speed of each arm was examined for each feature by calculating the correlation between the topography of speed tuning for the contralateral arm and the topography of tuning for the ipsilateral arm.

To examine the directional tuning across features and cortical locations, we regressed the contribution of hand speed from the z-scored ECoG activity separately for each channel and feature. Next the average of the speed-regressed z-scores from movement onset until target acquisition was calculated for each feature, channel, and trial, and were grouped into 8 classes for each channel and feature based upon the movement target. Finally a one-way ANOVA was calculated to determine if there was a significant relationship between ECoG activity and target direction for each channel and feature. Each combination of electrode and feature was then classified as having contralateral tuning, ipsilateral tuning, bilateral tuning, or no directional tuning based upon whether significant ($p<0.05$) tuning was found after correcting for multiple

comparisons using FDR correction based upon the total number of electrodes, features, and hand conditions tested (Benjamini and Hochberg 1995).

3.2.7 Prediction of Arm Movement Kinematics

Beyond examining the relationship between changes in neural activity and reaching movements of each arm, if ECoG signals can also be used to decode kinematics, then this decoded information could be the basis for controlling a BCI system. Therefore, we examined the ability to decode kinematics from ECoG signals. Furthermore we compared the prediction accuracies and prediction models for the contralateral and ipsilateral arms.

General Machine Learning Methods

To examine the ability to decode reaching movement kinematics using ECoG signals, the datasets for the contralateral and ipsilateral arm movement conditions were each divided into training and testing sets. We generated a training set by randomly sampling 7/8th of the trials and the remaining trials were held out as a test set. The full training and testing sets were constructed by concatenating each trial from 2 seconds before the onset of movement until the end of the trial.

Machine Learning Strategy

While the eventual goal was to develop a decoding model to predict time courses of speed, velocity, and position, because of the planning delay incorporated in the center-out task, the behavioral data consisted of two active conditions. First, the task had active rest periods, during which time patients held their hands in the center of the workspace, and second, the patients made active reaching movements to the external target. As previous studies have demonstrated improvements in kinematic decoding through the use of a hierarchical regression model

(Flamary and Rakotomamonjy 2012), we chose to implement a two-step hierarchical decoding model to decode kinematics of reaching movements as shown in Figure 3.3.

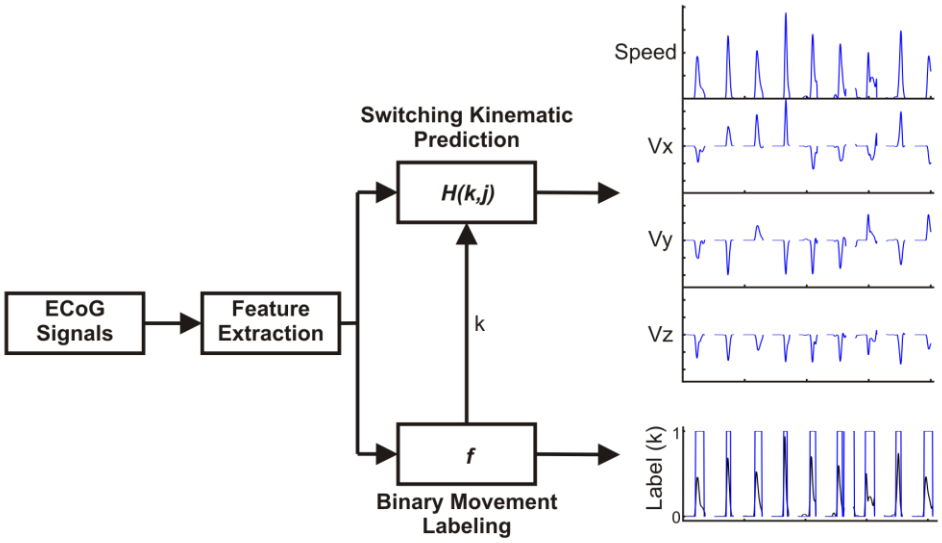

Figure 3.3 General machine learning strategy
To predict 3D kinematics, a hierarchical PLS regression model was used. After feature extraction, a logistic regression model classified time windows as either movement or rest. Two PLS regression models were trained, one relating ECoG features and kinematics during movement periods, and a second PLS model relating ECoG features and kinematics during non-movement periods. The final model output was generated from the outputs of the two PLS models by using the logistic regression output to switch between them.

The first component of our hierarchical prediction method was to classify whether the patient was moving or not with a logistic regression model. A threshold of 10% of the maximum movement speed was applied to generate the movement and rest labels. The features used to train the model consisted of the z-scores of each of the 8 features (7 frequency bands and LMP). To account for potential differences in the optimal time lag between kinematics and neural activity for different channels and features, the correlation coefficient between training set hand speed and neural activity was calculated with time lags between 0 seconds and 1 second in 50 ms steps. For each channel and feature, the lag producing the maximum absolute correlation coefficient with movement speed was used in the logistic regression model. To train the logistic regression model, we minimized the loss function shown in Equation 3.1, where X is an n x d input feature

matrix of ECoG data, w is a d x 1 weight vector, y is an n x 1 vector of class labels (1 movement, -1 rest), and the λ_1 and λ_2 are the hyperparameter weights associated with the l1 and l2 norms respectively.

$$L(w) = \frac{1}{n}\sum_{n} \log\left(1 + e^{X(n)*w*y}\right) + \lambda_1\|w\|_1 + \lambda_2\|w\|_2 \tag{3.1}$$

After finding the set of weights that minimize the loss function above, the output of the model was calculated as shown in Equation 3.2.

$$p(y == 1) = \frac{1}{e^{-X*w}} \tag{3.2}$$

The output of the logistic regression model can be considered as a probability that the current time window is from a movement period. Time windows with output probabilities above 0.5 were classified as movement periods and time windows with output probabilities below 0.5 were classified as rest periods. Within the training set, 7 fold cross-validation was used to determine the optimal values for the regularization hyperparameters. After determining the hyperparameters, the entire training set was used to train the model and the testing set was used to evaluate the accuracy of the model.

The output from this classification step was used to switch between two regression models, one to predict each kinematic parameter while patients were at rest and a second model to predict each kinematic parameter during movement periods. We used a similar method to a prior study that demonstrated the ability to use a partial-least squares (PLS) regression model to decode continuous traces of kinematic data from ECoG signals in primates (Chao, Nagasaka et al. 2010). The PLS model estimates a lower dimensional latent structure within the input data and uses this latent structure to fit a regression in order to avoid over-fitting (Wold, Ruhe et al. 1984). For our

model, the inputs consisted of the z-scored activity for each of the 7 canonical frequency bands and the LMP at each channel. Individual feature vectors were produced for all time lags between -500 ms and 1000 ms in 50 ms steps, with positive lags indicating neural activity leading kinematics and negative lags indicating neural activity lagging after kinematics. As the filters used during the preprocessing steps were run both forwards and backwards to avoid phase distortion, the neural activity in each time-window was not necessarily causal relative to the kinematic data, therefore we chose to use neural activity both leading and lagging the kinematic time courses to be predicted. Because of this, the results should be interpreted as representative of the entire sensorimotor system and not necessarily as causal activity related to motor planning alone. The outputs for the model consisted of non-directional movement speed, 3D movement velocity, and 3D hand position. The relationship between ECoG activity and kinematics is described by Equation 3.3, with M(t) representing a kinematic parameter and w representing a prediction weight for a specific channel, feature, and time lag.

$$M(t) = \sum_{Channels} \sum_{Features} \sum_{\tau=-500ms}^{1000ms} w(ch, feat, \tau) * Zscore(ch, feat, t - \tau) \tag{3.3}$$

Within the training set, 7 fold cross validation was used to determine the optimal number of latent features that minimized the mean squared prediction error. The final prediction model was generated from the full training set and the testing set was used to evaluate the accuracy.

Evaluation of Prediction Accuracy

To evaluate the accuracy of movement prediction, we generated 100 randomly sampled training and testing sets. Accuracy of the classification between movement and rest was calculated as the percent of the total test set windows that were correctly classified. Accuracy of the PLS regression model was evaluated by computing the correlation coefficient and root mean squared

error (rMSE) between the actual values and predicted values for each of the 7 kinematic parameters (speed, velocity: V_x, V_y, V_z, and position: X, Y, Z). To evaluate the accuracy of the PLS model in isolation from the performance of the logistic regression model, we used the true movement and rest labels to switch between the PLS regression model predictions for movement and rest.

We evaluated the statistical significance of the models from chance using two surrogate predictions to ensure that the predictions were not affected by any systematic bias. To evaluate the significance of the temporal features within the model, we generated a surrogate kinematic dataset by randomly reordering the trials within the training set, randomly selecting a new trial onset from within each training set trial, and generating a new time course by wrapping data from the beginning of the trial to the end of the trial. This procedure ensured that the temporal relationship between the ECoG signals and kinematics was random, while maintaining the autocorrelation structure of the kinematics. Information regarding the construction of the temporal surrogates, exemplar surrogate time courses, and a comparison of the autocorrelation structures of the original and surrogate kinematics is contained in the supplementary information in the appendix. For each training and testing set, we trained one model using the original kinematic data and a second model using the surrogate kinematics. Both models were tested using the original testing set. A second surrogate method that was similar to one used in other studies of kinematic prediction (Chao, Nagasaka et al. 2010; Hotson, Fifer et al. 2014) was used to evaluate the significance of ECoG features and channel assignments. For each training set, we reshuffled the channel and frequency assignments of the prediction weights 100 times and generated test accuracies using both the original and reshuffled weights. The statistical significance of both the movement classification and kinematic prediction models was evaluated

using a Wilcoxon rank sum test to compare the median actual accuracy with the median surrogate accuracy. Bonferroni correction was used to correct for the total number of predictions tested.

Evaluation of Feature Importance

Because we equalized the variance of each ECoG feature prior to generating prediction models, the weights for each channel and feature could be compared to evaluate the importance of each feature type and cortical location between hand conditions. To examine the importance of features in the classification of movement and rest conditions, logistic regression prediction weights were averaged across each of the 100 training sets. For each frequency band, the magnitude and location of average model weights was mapped onto an atlas brain as described previously. For the PLS regression model predicting kinematics, the relative importance of cortical locations during the movement model was evaluated by normalizing the sum of the absolute value of the prediction weights for a given channel or feature with the sum of the absolute value of all prediction weights as shown in Equation 3.4.

$$Wnorm(ch) = \frac{\sum_{Features}\sum_{Lags}|w(ch, feat, lag)|}{\sum_{Features}\sum_{Lags}\sum_{Chans}|w(ch, feat, lag)|}$$
$$Wnorm(feat) = \frac{\sum_{Chans}\sum_{Lags}|w(ch, feat, lag)|}{\sum_{Features}\sum_{Lags}\sum_{Chans}|w(ch, feat, lag)|} \quad (3.4)$$

Normalized feature weights were calculated for each channel, feature, and hand. Normalized weights for each channel were mapped onto a single atlas brain to combine weights across patients.

3.2.8 Simulation of Non-Invasive Recordings

We used ECoG recordings to simulate non-invasive electrophysiological recordings and used these simulated signals to evaluate the tradeoff in reduced decoding accuracy with reduced

invasiveness. The difference between ECoG and electroencephalography (EEG) recordings has been characterized as the result of a low-pass frequency filter and an additional spatial filter (Cooper, Winter et al. 1965; Pfurtscheller and Cooper 1975). Our EEG simulation method, shown in Figure 3.4, was based upon a method previously published (Freudenburg, Gaona et al. 2014). Briefly, we low-pass filtered each ECoG signal with a 3rd order butterworth filter with a cut-off frequency of 45 Hz. Next, the simulated EEG signals were derived by spatially filtering the low-pass filtered ECoG channels. Finally, as described in Section 3.2.5, we computed the LMP amplitude and the spectral power in 5 canonical frequency bands (theta: 4-8 Hz, mu: 8-12 Hz, beta 1: 12-24 Hz, beta 2: 24-34 Hz, and gamma: 35-55 Hz). These 6 features were then used in a hierarchical regression model to predict speed and movement velocity as described in Section 3.2.7. Finally, the kinematic prediction accuracy for the original ECoG signals and simulated EEG signals were compared. This analysis was performed on three of the 5 patients (Patients 2, 4, and 5) as these patients had 8 x 8 electrode grids allowing for use of the 4 x 4 spatial filter to generate EEG simulations.

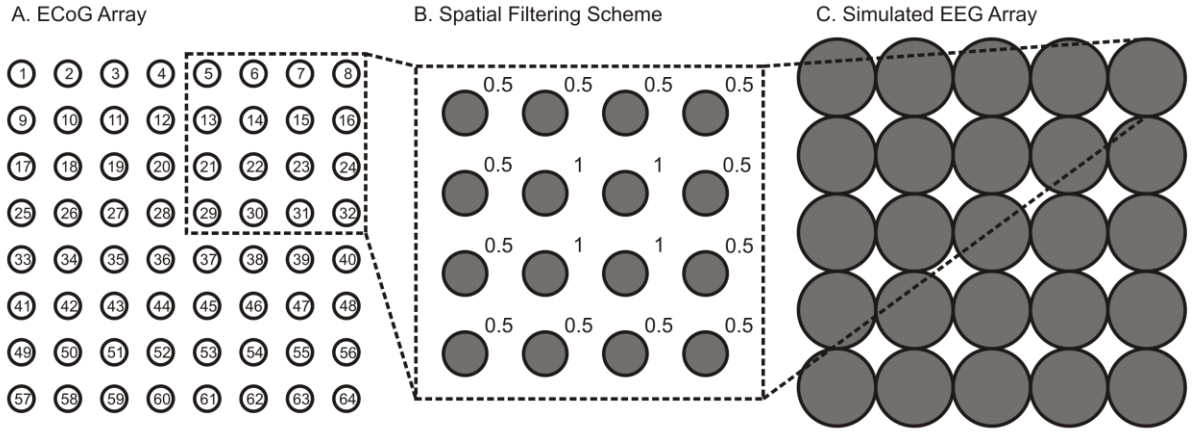

Figure 3.4 EEG simulation spatial methodology
A. To simulate EEG signals from ECoG signals, a low-pass filter was applied to the entire 8x8 ECoG grid. **B**. A 4x4 spatial filter with the weights shown was applied to the low-pass filtered ECoG signals. **C**. The spatial filter was shifted along each row and column to generate a 25-channel array of simulated EEG signals from the original 8x8 channel ECoG array.

3.3 Results

3.3.1 Behavioral Performance

All patients were able to consistently and accurately perform reaching movements to the target locations. Table 3.2 contains behavioral data comparing contralateral and ipsilateral reaching movements. After excluding trials with reaction times greater than 2 standard deviations from the mean, median reaction times for contralateral and ipsilateral arms differed by less than 100 ms for Patient 2 and less than 50ms in Patients 4 and 5. Additionally, in all patients, median peak movement speed was also similar between the contralateral and ipsilateral arms, differing by at most 3 cm/s. To evaluate the true dimensionality of the reaching movements performed, we calculated the percent of variance explained by the principle components of the seven component kinematic parameters used: speed, velocity (V_x, V_y, V_z), and position (X, Y, Z). As shown in Table 3.2, the first principle component explained at most 35% of the variance. Additionally each of the first four principle components explained at least 11% of the variance in all patients and arm conditions, indicating that multiple independent degrees of freedom were truly controlled in the task.

Table 3.2 Patient-specific behavioral performance

Patient	Hand	Median Reaction Time (ms)	Median Peak Speed (cm/s)	Principal Component Variance				
				PCA 1	PCA 2	PCA 3	PCA 4	PCA 5-7
1	Contra	N/A	20.65	22%	19%	17%	14%	27%
	Ipsi	N/A	22.16	23%	20%	18%	12%	27%
2	Contra	904	16.65	26%	22%	19%	13%	20%
	Ipsi	820	16.35	26%	23%	20%	13%	19%
3	Contra	814	17.44	35%	21%	18%	11%	15%
	Ipsi	-	-	-	-	-	-	-
4	Contra	417	19.78	24%	23%	16%	13%	23%
	Ipsi	408	21.8	27%	21%	19%	13%	21%
5	Contra	625	28.62	24%	22%	20%	14%	21%
	Ipsi	579	31.62	23%	21%	20%	14%	21%

3.3.2 Movement Related Cortical Activity

Each of the 5 patients had electrodes that demonstrated significant changes in spectral power and LMP amplitude immediately prior to and during the performance of reaching movements. Time-frequency plots demonstrating changes in spectral power relative to baseline (hold-A) periods in exemplar electrodes are shown for contralateral and ipsilateral arm movements in Figure 3.5. In general, significant power changes around movement onset consisted of decreases in spectral power before and during movement execution in frequencies below 40 Hz, and increases in spectral power in high gamma band frequencies above 60 Hz. In the patient shown on the left, electrodes in premotor regions and primary sensorimotor cortices can be found that demonstrate either similar or different patterns of spectral power changes between contralateral and ipsilateral arm movements. For this patient in particular, in primary sensorimotor cortices, high gamma band power increases during contralateral but not ipsilateral arm movements. For electrodes in premotor regions, however, high gamma band power increases are associated with both contralateral and ipsilateral arm movements. One exemplar electrode even shows a larger amplitude increase in high gamma band power during ipsilateral arm movements when compared to the contralateral arm. In contrast in a second patient, very similar spectral power changes are observed in contralateral and ipsilateral arm movements, even in primary sensorimotor regions. Additionally, in this patient, a finer-scale temporal relationship between high gamma band power and movement onset at different locations can be observed. Significant increases in high gamma band power occur first in the posterior parietal cortex, begin a few hundred milliseconds before movement onset in primary motor cortex, and have a peak after the onset of movement in sensory areas.

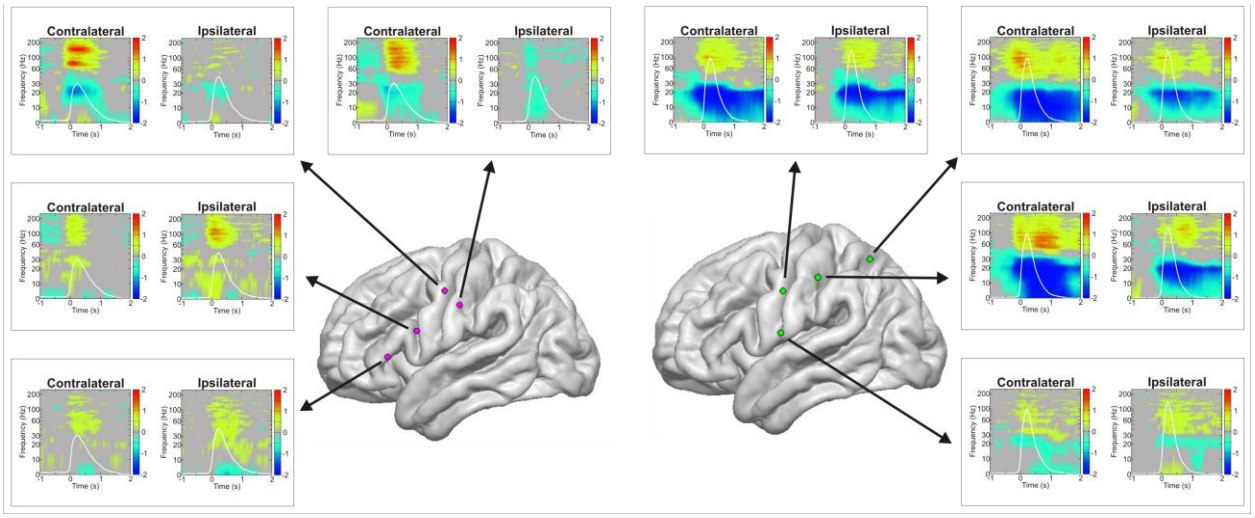

Figure 3.5 Exempar movement-related spectral power changes

Exemplar significant (p<0.05 uncorrected) movement-related spectral power changes during movements of the contralateral and ipsilateral arms for selected electrodes from 2 patients. Time-frequency plots display significant spectral power changes. Color scales show z-scores of spectral power relative to the hold-A period. White traces show the average movement speed. In the patient shown on the left, significant high gamma (>60 Hz) power increases and mu and beta band ERD occur for contralateral arm movements, while for ipsilateral arm movements, no high gamma power increases occur (top plots). In non-primary motor areas, significant high gamma power increases are observed during both contralateral and ipsilateral arm movements (left plots). In the patient shown on the right, both low frequency ERD and high gamma power increases occur in every electrode shown. Posterior parietal cortex demonstrates the earliest onset of high gamma band power increases (top right), followed by primary motor cortex (top), followed by sensory areas where the peak high gamma band power increase follows movement onset (right).

Figure 3.6 displays changes in the LMP signal averaged across trials in several exemplar electrodes from a single patient. Particularly in primary sensorimotor regions, a negative shift in LMP amplitude can be seen around the onset of movements of both the contralateral and ipsilateral limbs that follows the time course of the movement speed.

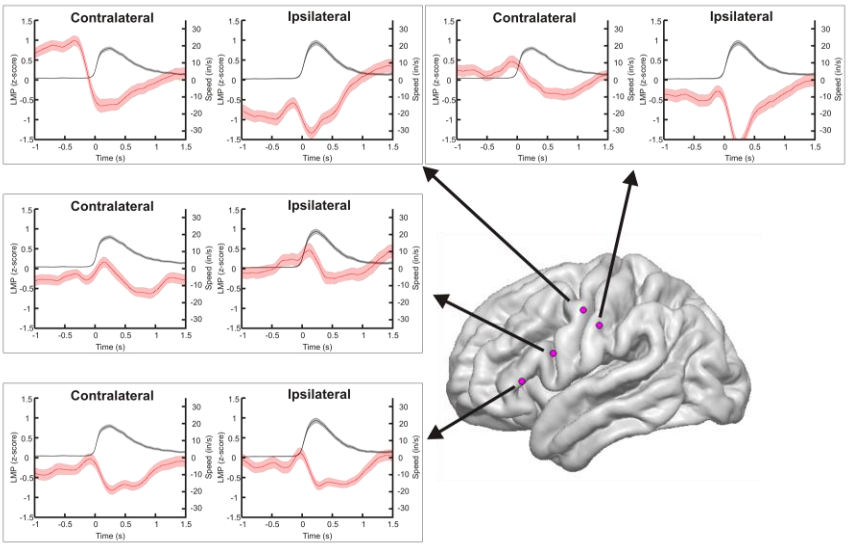

Figure 3.6 Exemplar movement-related local motor potential amplitude
Exemplar LMP amplitude changes during contralateral and ipsilateral arm movements. Red traces show the uncorrected 95% confidence intervals of z-scored LMP amplitude, black traces show the 95% confidence interval for movement speed. In primary sensorimotor regions (top plots), a negative shift in LMP amplitude is observed around the onset of movement. In non-primary motor areas, a brief positive deflection in LMP amplitude is observed around the time of movement onset (left plots).

Across patients, movement-related changes occur in multiple ECoG features. Changes to individual features occur with distinct amplitudes and timing relative to the onset of movements of the contralateral and ipsilateral arm. Figure 3.7 shows statistically significant changes of selected features occurring at selected time windows relative to movement onset. All features displayed are z-scores relative to the hold-A period.

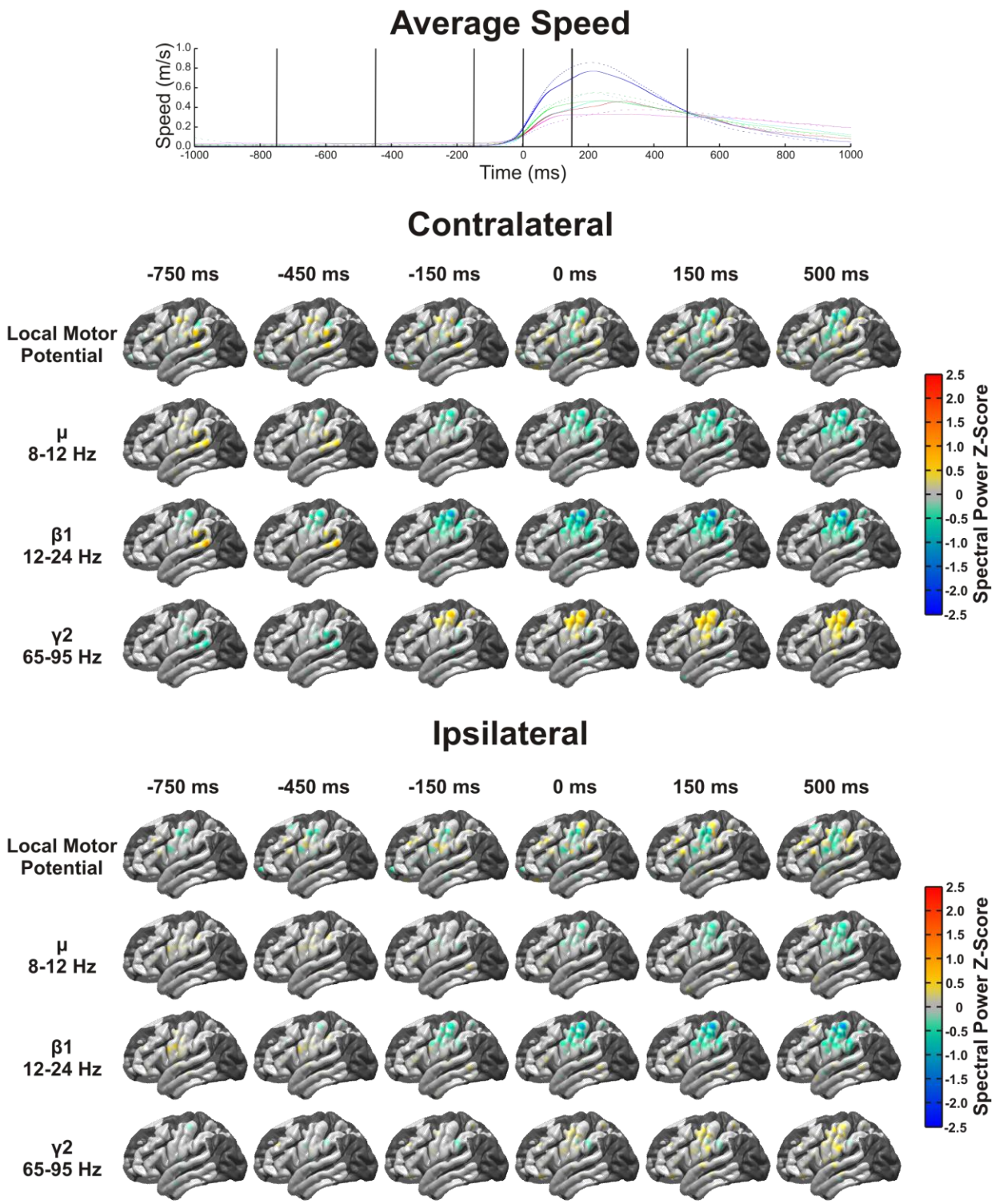

Figure 3.7 Group averaged movement-related ECoG activations

Movement-related ECoG activations, averaged across patients, show differences in ECoG activations during contralateral and ipsilateral limb movements. Top: Average movement speed for contralateral arm movements (solid lines) and ipsilateral arm movements (dashed lines). After aligning each trial to the onset of movement, the average time course of movements is similar across patients and hand conditions. Vertical lines indicate time points selected for the brain plots shown below. Middle: Average

ECoG activations during contralateral arm movements. Color scales represent averaged z-scores relative to the hold-A period. Dark grey areas on the atlas brain show areas without electrode coverage. Data were thresholded for significant ($p<0.05$) activations after FDR correction. Beta ERD occurs first, becoming broader around the onset of movement, followed by mu ERD. Next, high gamma band power increases occur over primary sensorimotor areas. Finally, focal decreases in LMP amplitude occur in primary sensorimotor cortices immediately before movement onset. Bottom: Average ECoG activations during ipsilateral arm movements. Beta and mu band ERD have similar amplitudes, but begin later than contralateral arm movements. High gamma band power increases occur later and are lower in amplitude in ipsilateral compared to contralateral arm movements.

Across patients, beta and mu band event-related desynchronization (ERD) is observed broadly over sensorimotor regions before and during movement execution. For the contralateral arm, significant beta band ERD begins at least 1 second before movement onset followed by mu ERD, which begins 650 ms before movement onset. High gamma band power significantly increases beginning approximately 300 ms before movement onset. Finally, decreases in LMP amplitude are localized to the primary sensorimotor cortices with increases in LMP amplitude anterior and posterior. LMP amplitude changes begin immediately before movement onset. When compared to the contralateral arm, movement-related ECoG spectral power changes occur later relative to ipsilateral arm movements. Beta band ERD begins 500 ms before movement onset, mu band ERD begins 200 ms prior to movement onset, and high gamma band power increases occur immediately before movement onset. Furthermore, while mu and beta band ERD is similar in amplitude during contralateral and ipsilateral reaches, high gamma band power increases are lower in amplitude during ipsilateral arm movements. Significant decreases of LMP amplitude related to ipsilateral arm movements begin earlier for ipsilateral than contralateral movements, but similar to contralateral arm movements, become broader throughout primary sensorimotor cortex immediately before movement onset.

3.3.3 ECoG Encoding of Movement Kinematics

Along with examining the changes in ECoG activity during reaching movements of the contralateral and ipsilateral limbs, we also investigated the similarities and differences in the relationship of these ECoG features to kinematics of contralateral and ipsilateral reaching

movements. Initially, we examined the relationship between ECoG features and the speed of movements in any direction. Figure 3.8 shows the relationship between ECoG activity and movement speed across patients in the form of topographies of statistically significant ($p<0.05$) correlation coefficients. Mu and beta band power are negatively correlated with movement speed in a broad region centered over primary sensorimotor cortices. A negative correlation also occurs between movement speed and LMP amplitude within a more focal region centered over primary sensorimotor cortices. In contrast, sensorimotor cortex high gamma band power is positively correlated with speed. Furthermore, each of these ECoG features displays very similar statistical tuning to both contralateral and ipsilateral arm movements. This similarity in the topography of tuning of ECoG activity to movement speed is shown by the strong correlation between the topographies of speed tuning especially in the mu, beta, and high gamma bands. Specifically, the correlation between the topographies of contralateral and ipsilateral speed tuning for each feature is LMP: 0.4541, theta: 0.4760, mu: 0.8541, beta 1: 0.8907, beta 2: 0.7326, gamma 1: 0.1767, gamma 2: 0.7201, and gamma 3: 0.6995.

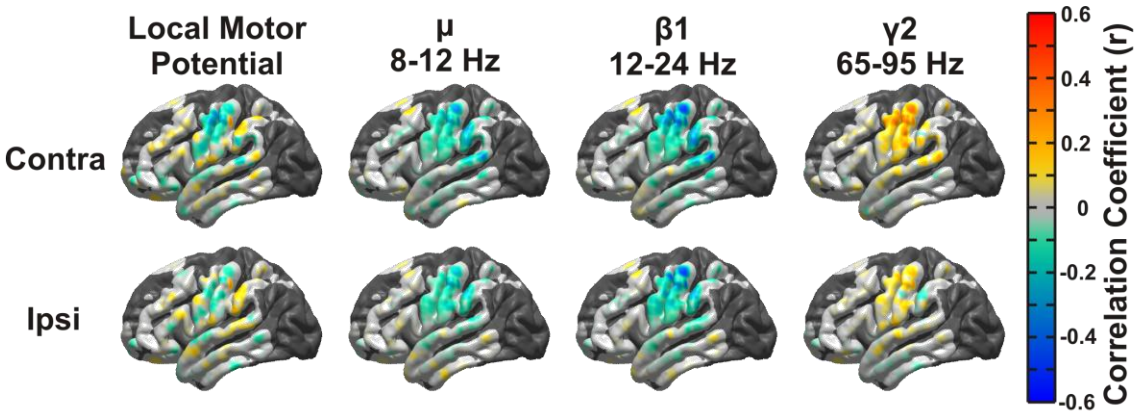

Figure 3.8 ECoG tuning to movement speed
Individual brain plots show the relationship between movement speed and z-scores of ECoG activity averaged for individual cortical locations across patients. The color scale shows the correlation coefficient between movement speed and ECoG activity. Dark grey regions represent regions with no electrode coverage. There is a similar focal negative relationship between LMP amplitude and movement speed centered on the central sulcus for both contralateral and ipsilateral arms. Additionally, there is a similar negative relationship between mu and beta band power and movement speed in a broad area centered on primary motor

cortex for both contralateral and ipsilateral arms. For high gamma band power, while tuning for the ipsilateral arm is weaker than the contralateral arm, both display a relatively broad positive tuning between spectral power and movement speed.

In addition to movement speed, we also found that ECoG activity is tuned to movement direction. For each patient in which both contralateral and ipsilateral arms were used, we determined if a significant ($p<0.05$) relationship existed between ECoG activity and target direction. Electrodes with significant tuning were classified as contralateral if directional tuning was found for contralateral arm movements only, ipsilateral if directional tuning was found for ipsilateral arm movements only, or bilateral if tuning was found with both contralateral and ipsilateral arm movements. The locations of electrodes from each class are displayed in Figure 3.9 and are tabulated by ECoG feature in Table 3.3. Electrodes displaying directional tuning are found for each of the features studied. In particular, electrodes displaying beta band and high gamma band directional tuning were focused in motor cortical areas. Additionally LMP amplitude was tuned to movement direction in the largest number of electrodes with cortical locations covering large regions of the primary motor cortex, parietal lobe, and frontal lobe.

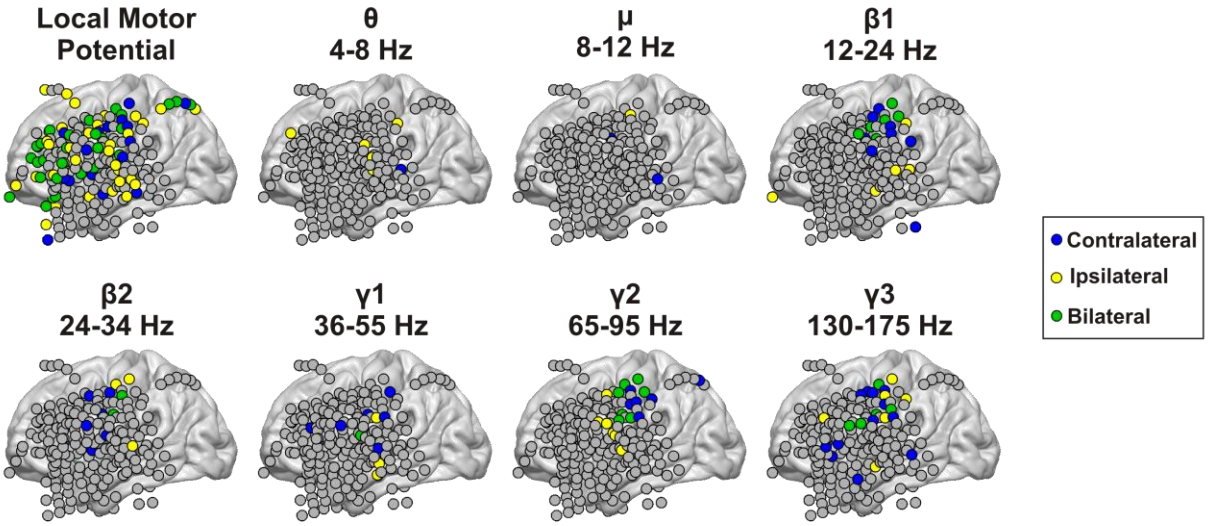

Figure 3.9 ECoG tuning to movement direction
Individual brain plots show electrodes that have significant ($p<0.05$) tuning to movement direction for contralateral (blue), ipsilateral (yellow), and bilateral (green) movements. For beta and high gamma frequency bands, several electrodes show tuning in each of the three categories. For LMP amplitude, a very broad area located in primary sensorimotor cortices, parietal cortex,

and frontal cortex demonstrates significant tuning to movement direction of one or both arms. FDR correction was used to correct for the total number of comparisons made across electrodes, features, and limb sides.

Table 3.3 Directionally tuned electrodes

	Contralateral (n (%))	Ipsilateral (n (%))	Bilateral (n (%))	Any Tuning (n (%))
LMP	16 (8.0%)	36 (18.1%)	29 (14.6%)	81 (40.7%)
Theta (4-8 Hz)	1 (0.5%)	5 (2.5%)	0 (0.0%)	6 (3.0%)
Mu (8-12 Hz)	2 (1.0%)	1 (0.5%)	0 (0.0%)	3 (1.5%)
Beta 1 (12-24 Hz)	8 (4.0%)	5 (2.5%)	6 (3.0%)	19 (9.6%)
Beta 2 (24-34 Hz)	6 (3.0%)	3 (1.5%)	2 (1.0%)	11 (5.5%)
Gamma 1 (35-55 Hz)	6 (3.0%)	3 (1.5%)	1 (0.5%)	10 (5%)
Gamma 2 (65-95 Hz)	6 (3.0%)	6 (3.0%)	7 (3.5%)	19 (9.6%)
Gamma 3 (130-175 Hz)	12 (6.0%)	6 (3.0%)	5 (2.5%)	23 (11.6%)

3.3.4 ECoG Prediction of Movement Kinematics

The features of ECoG signals related to the execution of motor movements were then used to decode continuous traces of kinematic information (speed, velocity, and position) of both arms.

Classification of Movement and Rest

The initial component of the decoding model involved training a logistic regression to classify each time point as either movement or rest. Exemplar binary predictions of movement and rest are shown for test sets from ipsilateral and contralateral arm movements of a single patient in Figure 3.10. The predicted movement states match the actual labels closely during both contralateral and ipsilateral arm movements, showing a good ability to predict whether a patient is moving or not using ECoG.

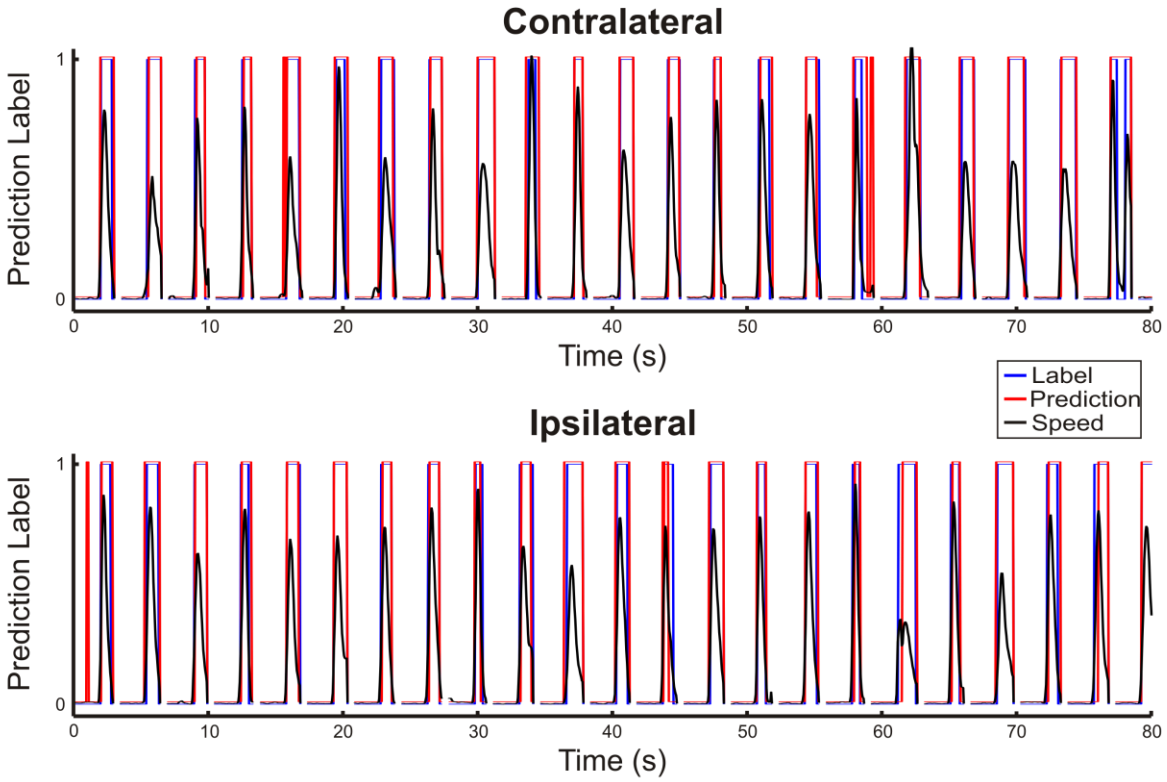

Figure 3.10 Exemplar classification of movement and rest periods
Exemplar predictions of movement classes were generated using contiguous trials within held-out testing sets. Black traces show the actual hand speed that was used to generate true movement class labels shown in blue. Predicted movement class labels are shown in red and correspond well with the actual labels.

Accuracies of predictions of movement and rest, which were calculated as the percent of individual time windows that were predicted correctly, are shown for contralateral and ipsilateral reaches in Table 3.4. Final prediction accuracies were compared to chance prediction levels produced with two surrogate datasets derived by shuffling the temporal relationship between movement class labels and ECoG data, or by shuffling the channel and feature assignments of the model weights. The true prediction accuracy is significantly higher than accuracy produced by either of the surrogate datasets in all patients after Bonferroni correction for the total number of comparisons. Furthermore, prediction accuracies produced by the surrogate methods were similar to the overall proportion of movement and rest classes in the dataset, demonstrating that the reshuffling strategies used were a good approximation for chance prediction. Exemplar

surrogate prediction traces are shown in the supplementary figures within the appendix.

Table 3.4 Logistic regression prediction accuracies

Patient	Hand	Original Accuracy	Shuffled Time Accuracy	p	Shuffled Feature Accuracy	p
1	Contra	67.78% (2.02)	53.28% (1.97)	**<0.000001**	50.92% (3.40)	**<0.000001**
	Ipsi	69.76% (2.44)	57.64% (2.29)	**<0.000001**	53.62% (3.53)	**<0.000001**
2	Contra	73.43% (3.93)	48.91% (5.59)	**<0.000001**	50.08% (4.96)	**<0.000001**
	Ipsi	77.72% (2.90)	54.61% (2.78)	**<0.000001**	53.37% (4.26)	**<0.000001**
3	Contra	81.97% (3.23)	63.42% (2.28)	**<0.000001**	60.82% (3.75)	**<0.000001**
	Ipsi	-	-	-	-	-
4	Contra	85.08% (2.40)	60.22% (2.64)	**<0.000001**	56.06% (4.40)	**<0.000001**
	Ipsi	84.08% (2.19)	63.065 (2.24)	**<0.000001**	57.57% (3.49)	**<0.000001**
5	Contra	90.10% (1.36)	70.97% (1.42)	**<0.000001**	69.57% (2.18)	**<0.000001**
	Ipsi	90.93% (1.39)	72.44% (1.29)	**<0.000001**	71.55% (1.66)	**<0.000001**

Continuous Prediction of Kinematic Traces

The second component of our machine learning model was composed of 2 PLS regression models, one to describe the relationship between ECoG features and seven kinematic parameters (speed, velocity: V_x, V_y, V_z, and position: X, Y, Z) during non-movement periods, and a second model to characterize the relationship between ECoG signals and the same kinematic parameters during movement periods. To examine the ability of this hierarchical PLS regression model to predict the time courses of kinematics during novel time periods, we trained each of the PLS regression models on a training set and used a separate test set to examine the accuracy of predictions. To evaluate the ideal performance of the PLS regression models in isolation from the ability to classify movement and rest periods, the actual movement and rest labels were used as the switch between the movement and rest PLS regression models.

For non-directional movement speed, model predictions were significantly more correlated to actual hand speed than predictions generated with either of the surrogate method for both contralateral and ipsilateral arm movements in all patients as shown in Figure 3.11. Additionally model predictions of movement speed had significantly lower rMSE values than either of the surrogate models for both the contralateral and ipsilateral arm movements in all patients.

Because the true movement class labels were used to evaluate the accuracy of the PLS models alone, the surrogate models for speed had positive correlations with the actual hand speed, but these correlations were significantly lower than the actual model predictions in all patients. This is because the actual predictions fit the time course of movements much more closely than the surrogate predictions. Exemplar surrogate predictions using both surrogate methods are shown in the appendix.

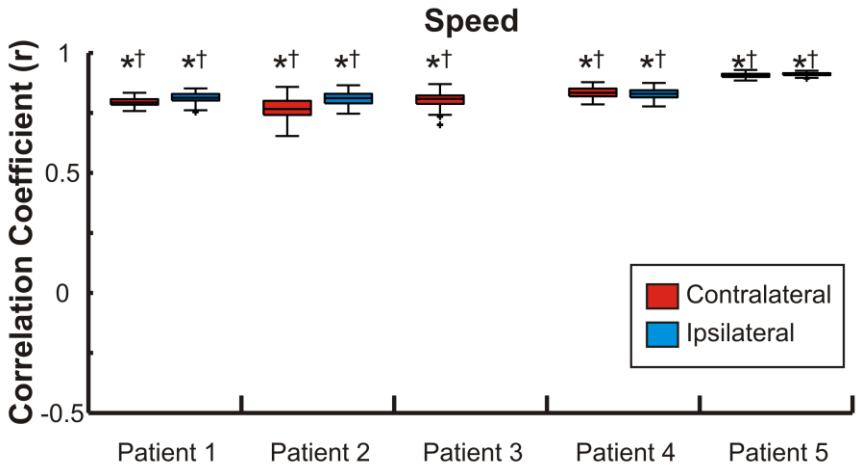

Figure 3.11 PLS speed prediction accuracy
Distributions show the correlation coefficients between predicted and actual movement speed. Distributions were generated from test sets using the actual movement class labels to switch between PLS regression models. Prediction accuracies are similar in contralateral and ipsilateral arm movements for all patients. Distributions marked with a * symbol are significantly different from surrogate models generated by shuffling the temporal relationship between ECoG and kinematics. Distributions marked with a † are significantly different from surrogate models generated by shuffling feature and channel weights. All predictions are significantly better than both surrogate models.

Ideal test accuracies across patients and hand conditions are shown in Figure 3.12 for directional kinematics (velocity and position). The PLS model accuracy for both directional and non-directional kinematic variables are summarized in Table 3.5. Predictions of velocity had significantly greater correlations and significantly lower rMSE values than both surrogate models for 12 of the 15 velocity components (3 directions, 5 patients) and in 10 of 12 (3 directions, 4 patients) velocity components of ipsilateral arm movements tested. Contralateral arm position predictions had significantly greater correlation coefficients and significantly lower

rMSE from both surrogate models in 10 of 15 (3 directions, 5 patients) position components tested and in 10 of 12 (3 directions, 4 patients) position components tested for ipsilateral arm movements. Therefore, components of 3D kinematics were predicted by our hierarchical PLS model with accuracies better than chance in multiple patients and for both contralateral and ipsilateral arm movements. In one patient in particular, prediction of kinematic time courses was highly significant for each of the seven kinematic components and for both the contralateral and ipsilateral arm movements.

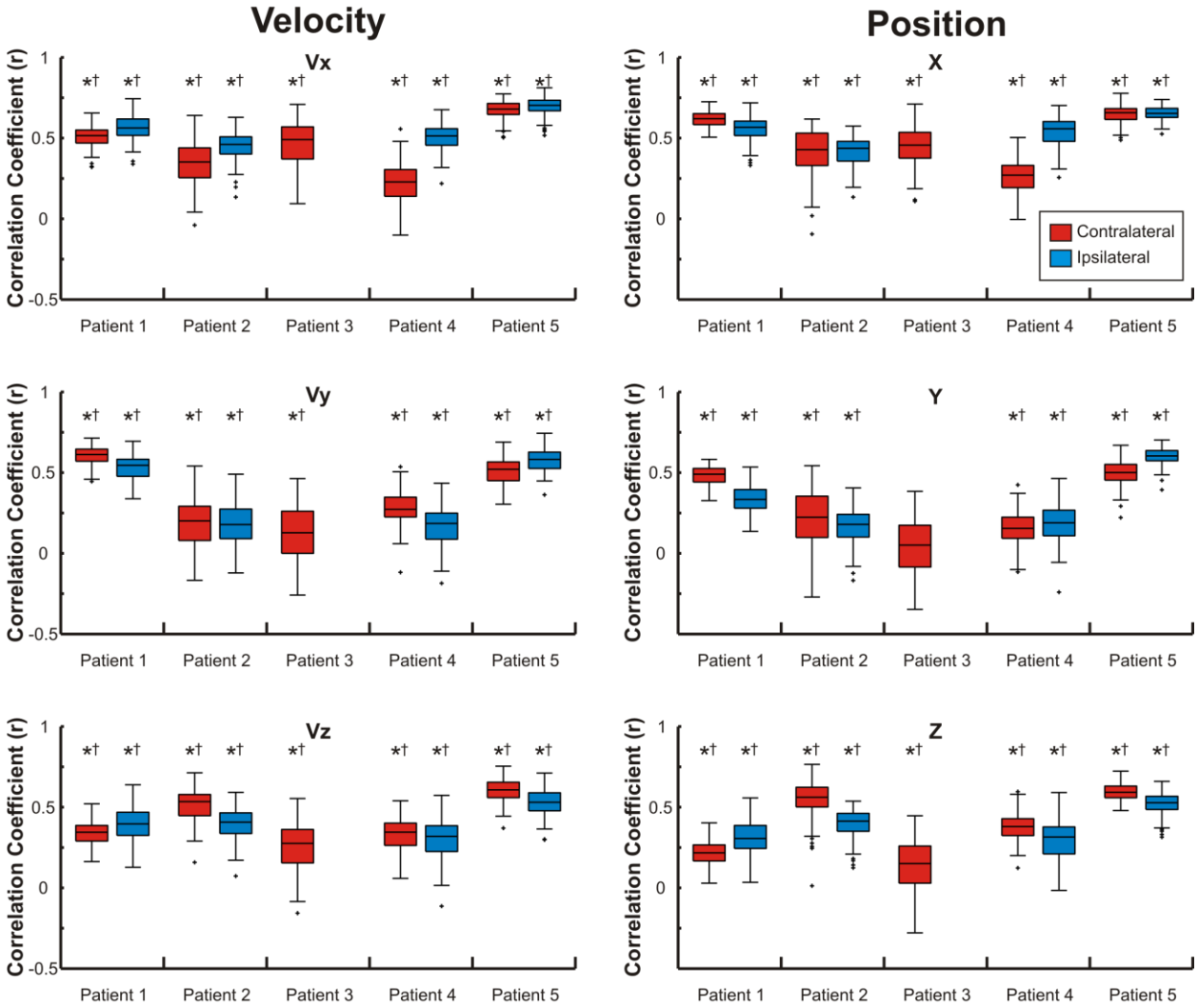

Figure 3.12 PLS directional kinematic prediction accuracy
Distributions show the correlation coefficients between predicted and actual velocity (left column) and position (right column). Distributions were generated from test sets using the actual movement class labels to switch between PLS regression models.

Prediction accuracies are similar for contralateral and ipsilateral arm movements within each patient. Distributions marked with a * symbol are significantly better than chance based upon surrogate models generated by shuffling the temporal relationship between ECoG and kinematics. Distributions marked with a † are significantly better than chance based upon surrogate models generated by shuffling feature and channel weights. A number of velocity and position components are significant for both contralateral and ipsilateral arm movements.

Table 3.5 PLS model prediction accuracies

Correlation								
Patient	Hand	Speed	Velocity			Position		
			Vx	Vy	Vz	X	Y	Z
1	Contra	0.7936*†	0.5156*†	0.6125*†	0.345*†	0.6201*†	0.4906*†	0.2171*†
	Ipsi	0.8133*†	0.5629*†	0.5452*†	0.3962*†	0.5669*†	0.3340*†	0.3059*†
2	Contra	0.7664*†	0.3521*†	0.2015*†	0.5349*†	0.4285*†	0.2238*†	0.5620*†
	Ipsi	0.8117*†	0.4607*†	0.1786*†	0.407*†	0.4366*†	0.1795*†	0.4135*†
3	Contra	0.8084*†	0.4908*†	0.1273*†	0.2756*†	0.4564*†	0.0507	0.1509*†
	Ipsi	-	-	-	-	-	-	-
4	Contra	0.8341*†	0.2285*†	0.2725*†	0.3451*†	0.2702*†	0.1544*†	0.3800*†
	Ipsi	0.8299*†	0.5133*†	0.1854*†	0.3193*†	0.5581*†	0.1890*†	0.3151*†
5	Contra	0.9072*†	0.6796*†	0.5207*†	0.6076*†	0.6575*†	0.5004*†	0.5928*†
	Ipsi	0.9119*†	0.7033*†	0.5823*†	0.5304*†	0.6532*†	0.6037*†	0.5275*†
Root Mean Square Error								
Patient	Hand	Speed (cm/s)	Velocity			Position		
			Vx (cm/s)	Vy (cm/s)	Vz (cm/s)	X (cm)	Y (cm)	Z (cm)
1	Contra	10.26*†	11.39*†	9.52*†	11.25*†	7.11*†	7.9*†	8.42†
	Ipsi	10.53*†	12.7*†	10.05*†	10.92*†	8.14*†	9.99*†	8.75*†
2	Contra	8.6*†	8.19*†	10.35*	9.39*†	7.03*†	9.66†	7.43*†
	Ipsi	8.32*†	8.15*†	10.6†	9.61*†	6.4*†	8.52†	7.42*†
3	Contra	8.86*†	8.47*†	11.05	9.31*†	5.86*†	8.52	6.89
	Ipsi	-	-	-	-	-	-	-
4	Contra	8.81*†	10.87†	10.99*†	10.32*†	7.35*†	8.48	8.43*†
	Ipsi	9.61*†	9.37*†	11.41†	11.04*†	6.29*†	8.69	8.18*†
5	Contra	9.22*†	10.59*†	12.43*†	11.04*†	6.59*†	7.84*†	6.68*†
	Ipsi	9.83*†	11.12*†	12.47*†	12.71*†	6.42*†	7.14*†	7.25*†

* - Siginificantly different from a surrogate model created using temporally reshuffled training data.
† - Significantly different from a surrogate distribution created by reshuffling channel and feature weights.

Finally, the full model prediction accuracies were calculated on testing sets through utilizing the combination of the predicted logistic regression output to predict movement classes and switch between predictions from the two PLS regression models in order to generate predicted kinematic time courses. Average correlations between actual and predicted kinematics are shown in Table 3.6. Accuracies for the full model prediction are lower than the best-case scenario in which actual movement labels are used to switch between PLS regression models (Table 3.5). Additionally, velocity and position accuracies are highest along the x (anterior-posterior) axis and lowest along the y (lateral) axis. When using the predicted movement classes to switch

between PLS regression models for generating predicted kinematic traces, predictions of speed were significantly more correlated to the actual movement speed and had significantly lower rMSE values than both surrogate methods for both contralateral and ipsilateral arm movements in 4 of the 5 patients. Additionally, predictions of velocity components had significantly greater correlations and significantly lower rMSE than both surrogate models in 11 of 15 velocity components tested for contralateral arm movements and in 9 of 12 velocity components tested for ipsilateral arm movements. Contralateral arm position predictions had significantly greater correlations and significantly lower rMSE than both surrogate models in 9 of 15 position components tested. Position predictions were better than chance for 10 of 12 position components tested for ipsilateral arm movements. In one patient in particular, predictions were highly significant for each kinematic parameter tested for both contralateral and ipsilateral reaches. Exemplar time courses of actual and predicted kinematics using the full hierarchical PLS regression model are shown for this patient in Figure 3.13. As can be seen, time courses of predicted kinematics align well with the time courses of actual kinematics for both contralateral and ipsilateral arm reaches.

Table 3.6 Full model prediction accuracies

Correlation								
Patient	Hand	Speed	Velocity			Position		
			Vx	Vy	Vz	X	Y	Z
1	Contra	0.3144	0.3692*†	0.4455*†	0.1679*†	0.5605*†	0.4497*†	0.1624*†
	Ipsi	0.3772	0.3725*†	0.3447*†	0.2798*†	0.5172*†	0.2848*†	0.2964*†
2	Contra	0.5881*†	0.3009*†	0.2002*†	0.4686*†	0.3934*†	0.204*†	0.5588*†
	Ipsi	0.6355*†	0.4198*†	0.1571*†	0.3573*†	0.3918*†	0.1637*†	0.3891*†
3	Contra	0.6564*†	0.4267*†	0.1481*†	0.2397*†	0.4171*†	0.0696	0.1764*†
	Ipsi	-	-	-	-	-	-	-
4	Contra	0.749*†	0.2181*†	0.2518*†	0.3346*†	0.2543*†	0.1504*†	0.3685*†
	Ipsi	0.7336*†	0.4739*†	0.1743*†	0.293*†	0.5284*†	0.1567*†	0.3022*†
5	Contra	0.7961*†	0.6302*†	0.4437*†	0.55*†	0.6579*†	0.5128*†	0.5486*†
	Ipsi	0.8103*†	0.664*†	0.5339*†	0.4738*†	0.6691*†	0.6221*†	0.4891*†
Root Mean Square Error								
Patient	Hand	Speed	Velocity			Position		
			Vx (cm/s)	Vy (cm/s)	Vz (cm/s)	X (cm)	Y (cm)	Z (cm)
1	Contra	18.16	12.62*†	10.99*†	12.13†	7.50*†	8.07*†	8.62†
	Ipsi	18.85	14.54*†	11.57*†	11.48†	8.50*†	10.17*†	8.83*†
2	Contra	11.20*†	8.44*†	10.44	9.85*†	7.27*†	9.64†	7.48*†
	Ipsi	11.34*†	8.31*†	10.71†	9.80*†	6.54*†	8.50†	7.56*†
3	Contra	11.32*†	8.70*†	10.91	9.51*†	5.96†	8.34	6.81
	Ipsi	-	-	-	-	-	-	-
4	Contra	10.64*†	10.92†	11.09*†	10.26*†	7.41*†	8.45	8.45*†
	Ipsi	11.79*†	9.54*†	11.38†	11.15*†	6.44*†	8.76	8.18*†
5	Contra	13.30*†	11.19*†	12.97*†	11.52*†	6.55*†	7.74*†	6.96*†
	Ipsi	14.07*†	11.68*†	12.89*†	13.17*†	6.32*†	7.05*†	7.50*†

* - Siginificantly different from a surrogate model created using temporally reshuffled training data.

† - Significantly different from a surrogate distribution created by reshuffling channel and feature weights.

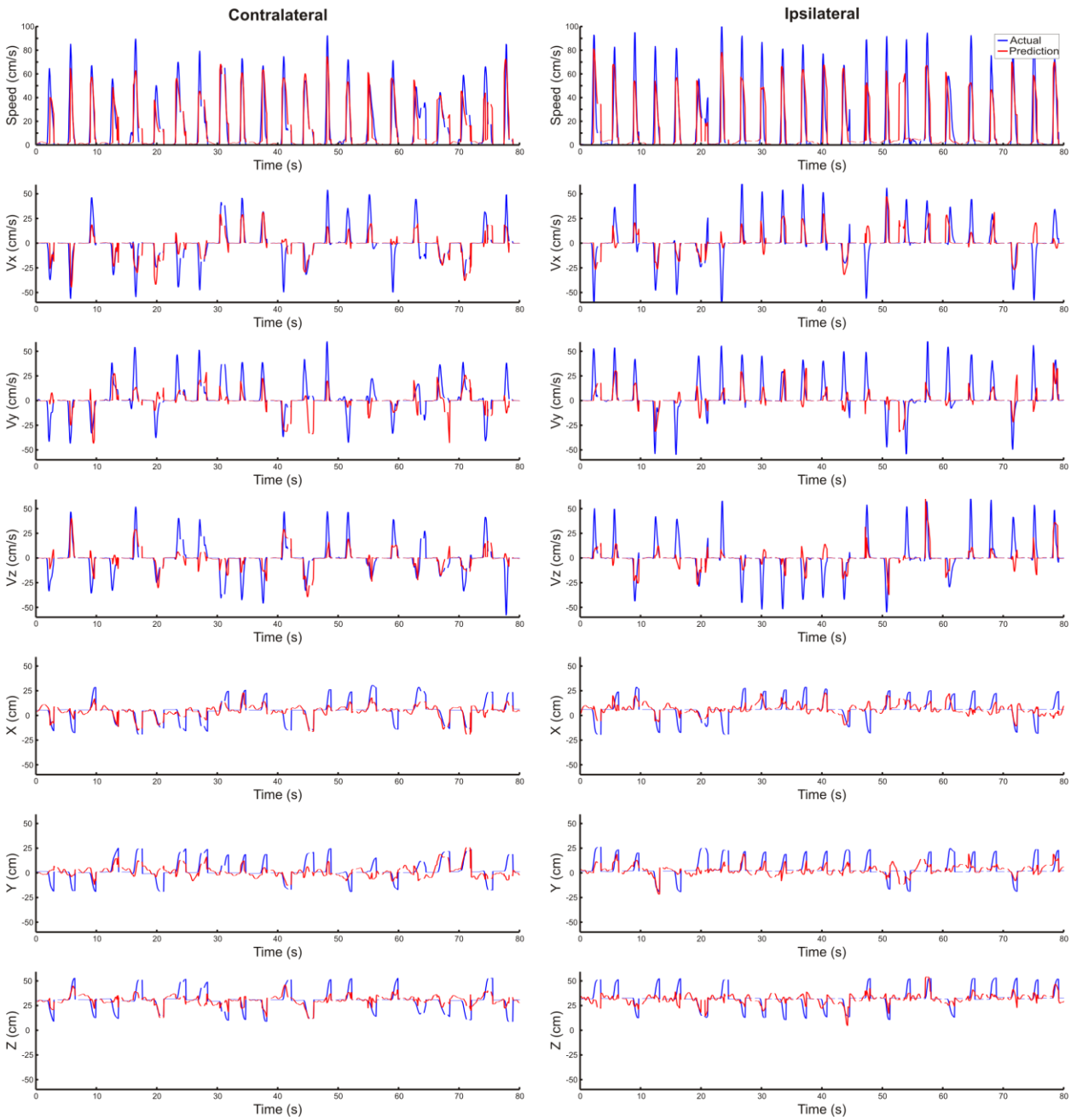

Figure 3.13 Exemplar kinematic predictions

Full model predictions were generated using the predicted movement classes from the logistic regression to switch between predicted PLS model outputs. Actual kinematic traces are shown in blue and predicted traces are shown in red for the contralateral (left column) and ipsilateral (right column) arm movements. Predictions were generated from contiguous trials of a single test set for the contralateral and ipsilateral arms. Kinematic predictions match the directions and time courses of actual kinematics very well.

Feature Importance

To evaluate the differences between prediction models trained for contralateral and ipsilateral arm movements, we examined the importance of individual ECoG feature types and cortical

locations. Average model weights that were used to classify movement and rest periods across patients are shown for selected features in Figure 3.14. The location and strength of feature weights are similar between models trained for contralateral arm movements and ipsilateral arm movements. Beta band and LMP features, in particular, demonstrate the largest amplitude prediction weights with negative weights centered in primary sensorimotor areas, indicating that decreases in sensorimotor cortex beta band power and LMP amplitude are associated with movement periods.

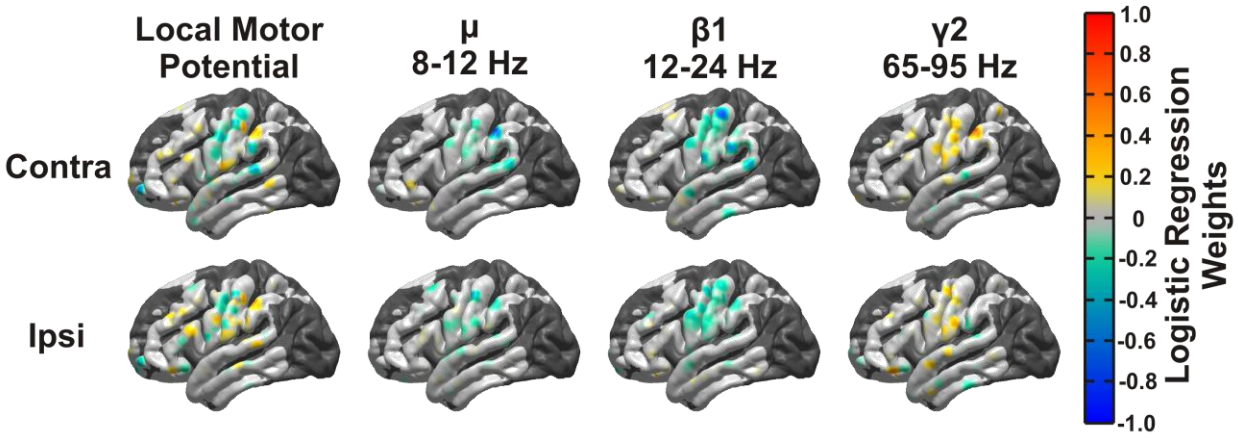

Figure 3.14 Logistic regression model weights
Average logistic regression model weights are shown for selected features for contralateral and ipsilateral arm movements. Beta band power and LMP amplitude in primary sensorimotor cortices have the strongest prediction weights across patients with decreases in beta band power and LMP amplitude used to predict movement periods. Regions shown in dark grey represent regions with no electrode coverage.

To evaluate the importance of individual features and cortical regions for the prediction of continuous kinematic parameters, we examined the movement period PLS regression models. As shown in Figure 3.15, prediction model weights were distributed in a broader area for directional kinematics as compared to speed and for contralateral as compared to ipsilateral arm movements. The location of the most important weights for models predicting contralateral and ipsilateral arm kinematics were both similarly located over primary sensorimotor regions.

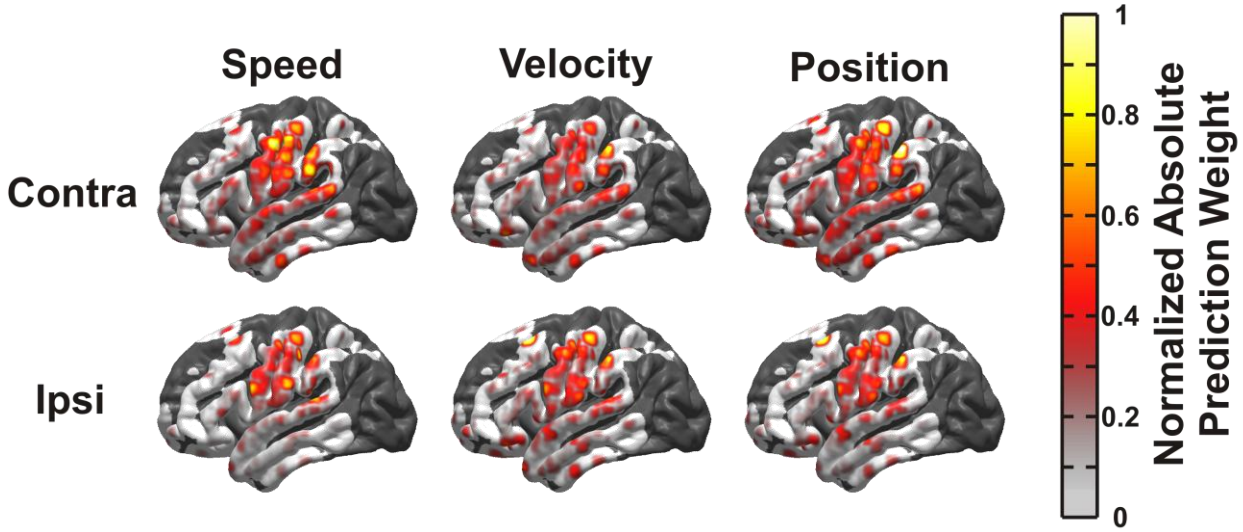

Figure 3.15 Topography of PLS prediction weights
Absolute values for movement-class PLS regression weights compared across cortical locations for all patients. The color scale represents the normalized absolute value of prediction weights by cortical location. Prediction of directional kinematics involves a broader area of cortex than needed to predict speed. Prediction of contralateral arm kinematics also involves prediction weights covering a broader topographic area than for ipsilateral arm kinematics. The most important cortical locations for all kinematic parameters are centered over primary sensorimotor areas for both contralateral and ipsilateral arm movements.

Across temporal and spectral features, the LMP amplitude consistently had the largest prediction weights for predicting kinematics of both contralateral and ipsilateral arm movements. Within spectral power features, the largest absolute model weights were found for high gamma band features in the 65-95 Hz and 130-175 Hz ranges. The relative importance of temporal and spectral ECoG features is shown in Figure 3.16.

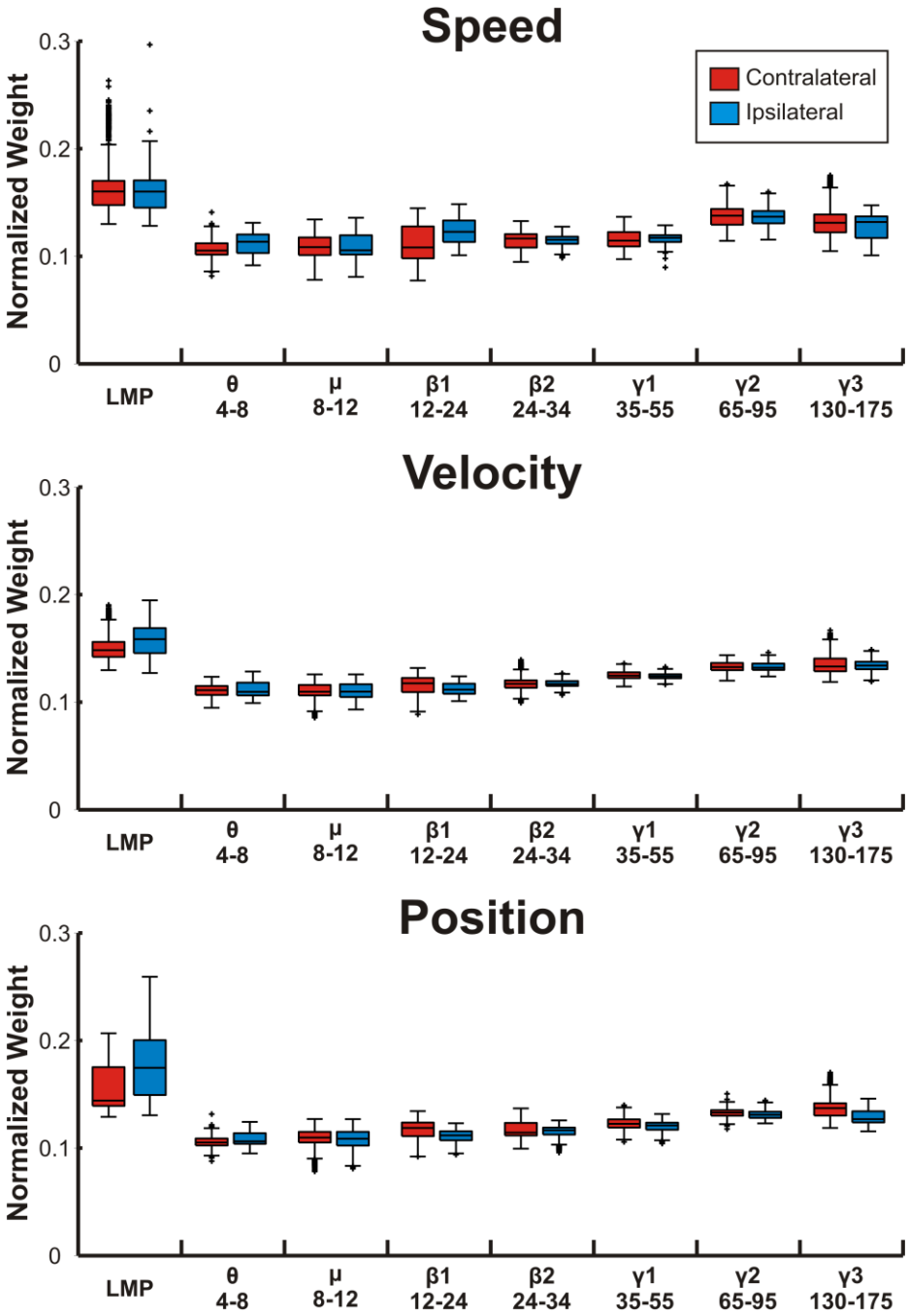

Figure 3.16 Importance of ECoG feature types for kinematic prediction
Distributions represent the normalized absolute movement-class PLS prediction weights across patients and electrodes for each feature type. For speed, velocity, and position LMP amplitude has the greatest absolute prediction weights for both contralateral and ipsilateral arm movements. Of spectral power features, high gamma band features have the highest absolute prediction weights.

3.3.5 Prediction of Movement Kinematics with Simulated EEG

Finally, the ability to predict kinematic parameters using non-invasive recording modalities was evaluated by using ECoG recordings to generate simulated EEG signals, which were then used to

train our hierarchical PLS regression model and generate test accuracies. Figure 3.17 compares average speed and velocity prediction accuracies of ECoG and simulated EEG signals. For each of the patients, arms, and kinematic types, correlations between actual and predicted kinematics were significantly lower for simulated EEG signals when compared to ECoG signals. The accuracy of movement classification was also significantly worse when using simulated EEG signals than when using ECoG signals. This decrease in prediction accuracy with simulated EEG signals is shown in Figure 3.18, which displays actual and predicted kinematics for a single test fold from a single patient using both ECoG signals and simulated EEG signals. For movement speed, while the step-like increases seen in predicted speed indicate that movement periods are classified well from rest, using actual ECoG signals to prediction speed produces time courses that follow the actual kinematic time courses much more closely. For velocity, predictions using simulated EEG signals are lower in amplitude and are often in the incorrect direction.

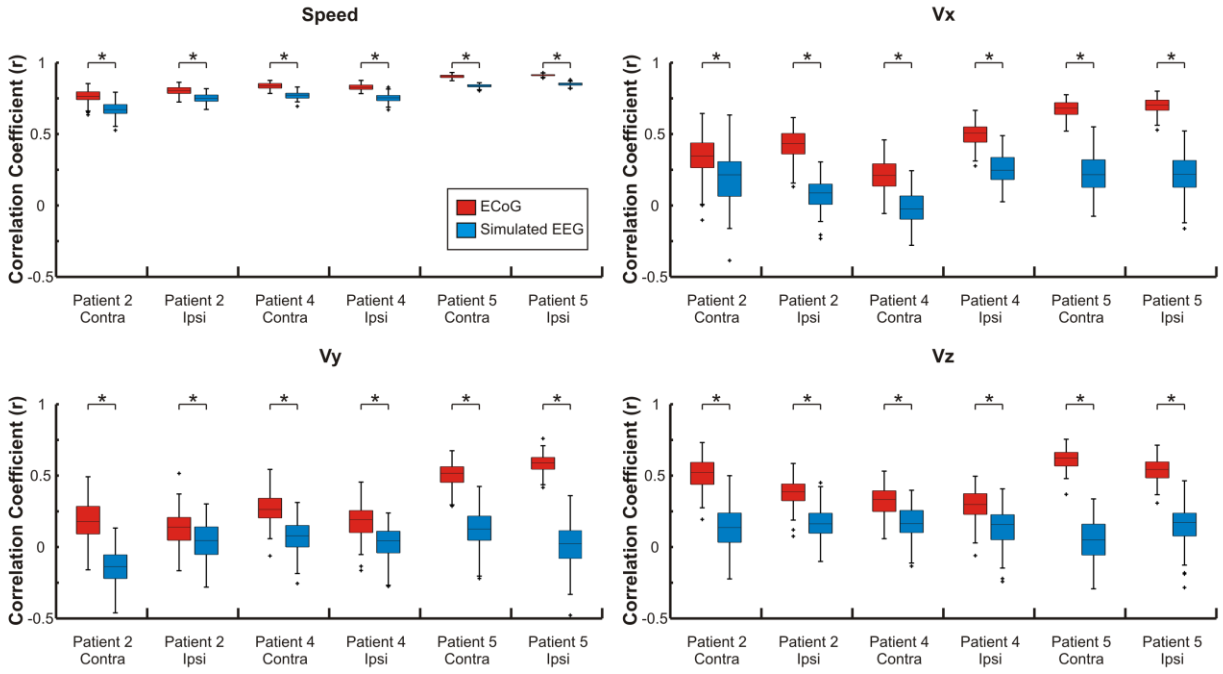

Figure 3.17 Comparison of ECoG and simulated EEG prediction accuracies
Distributions of prediction accuracies were generated using original ECoG signals and simulated EEG signals. For both speed and velocity, kinematic predictions made using ECoG signals were significantly better than predictions made using simulated

EEG signals. Distributions were generated using the full model with the logistic regression prediction used to switch between PLS regression models in order to produce the final kinematic predictions.

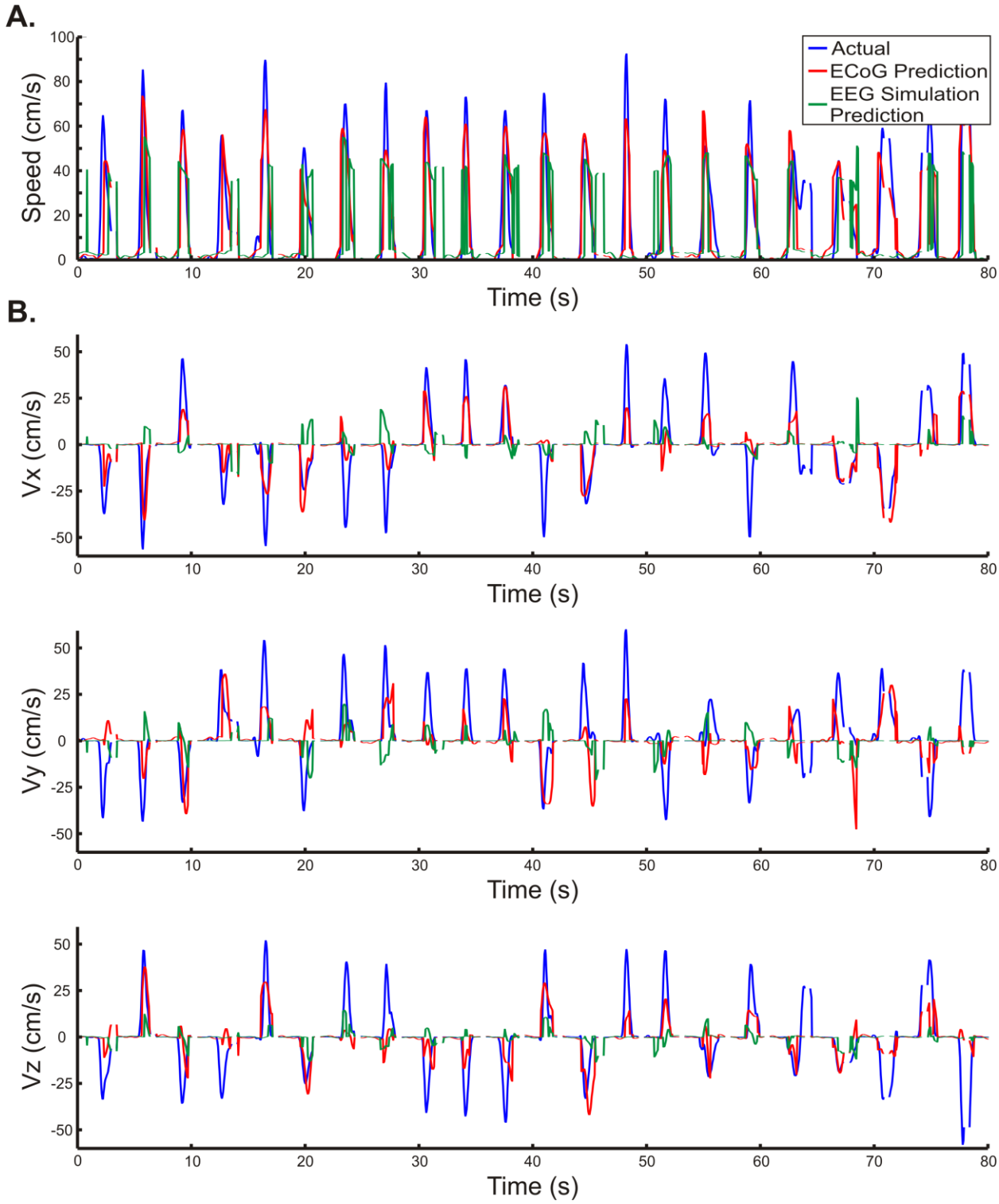

Figure 3.18 Exemplar kinematic prediction from simulated EEG signals

Exemplar predictions were generated for speed and velocity using the original ECoG signals (red traces) and simulated EEG signals (green traces). Prediction traces were generated from contiguous trials from a single test fold. While movement class can

be predicted well for simulated EEG data as indicated by the correlation between speed and the EEG simulation prediction, the profile of speed predictions match the actual speed profiles better when using ECoG signals as compared to simulated EEG signals. For velocity, the predictions made using simulated EEG signals are lower in amplitude and oriented in the incorrect direction more frequently than when predicting kinematics from actual ECoG signals.

3.4 Discussion

This study demonstrates that kinematics of 3D reaching movements can be decoded from ECoG signals in human patients. In particular, while the amplitude of movement-related power changes during contralateral and ipsilateral arm movements are different, the relationship between ECoG activity and movement kinematics of the contralateral and ipsilateral arms are very similar. Furthermore, ECoG signals not only maintain a statistical relationship to movement kinematics, but recordings from a single hemisphere can be used to decode kinematics of reaching movements of either hand with accuracies greater than chance. The prediction models used show that the representations of contralateral and ipsilateral arm kinematics within ECoG signals are similar, both in the importance of cortical locations and the importance of ECoG feature types. The ability to use ECoG recordings to decode kinematics of the same-sided hand underscores the possibility for a stroke survivor to use signals recorded from their unaffected hemisphere to control a BCI system.

While previous studies have shown that ECoG recordings in human patients can be used to decode 2D movement kinematics (Schalk, Kubanek et al. 2007; Pistohl, Ball et al. 2008; Sanchez, Gunduz et al. 2008), the extent of movement-related information that can be reliably decoded has been uncertain. Although previous studies have decoded movement trajectories of movements that were not constrained to two dimensions, these tasks had inherent correlations between movement directions and speed, reducing the true dimensionality of decoding (Hotson, Fifer et al. 2012; Nakanishi, Yanagisawa et al. 2013; Hotson, Fifer et al. 2014). In the task used in this study, the first kinematic principle component explained at most 35% of the variance in

any patient and the first 4 principle components each explained at least 11% of the variance in all patients, indicating that the movements performed truly included three independent directional dimensions and movement speed. Therefore, we believe that this study provides the first true demonstration of the ability to use ECoG recordings from human patients to decode 3D kinematics. While 3D kinematic decoding has also been demonstrated from ECoG recordings in non-human primates (Chao, Nagasaka et al. 2010; Shimoda, Nagasaka et al. 2012), the demonstration of kinematic decoding in humans is not trivial. Non-human primates typically require extensive periods of behavioral training prior to the recording of neural activity, leading to more consistent motor movements than would be expected in real-world behavior. Additionally, as long-term practice of a motor task leads to an increase in the size of the cortical area activated during task performance (Karni, Meyer et al. 1995), decoding of behavioral intentions during a trained motor task may not generalize to more typical novel behaviors.

Importantly, time courses of 3D kinematics were decoded with similar levels of accuracy for both contralateral and ipsilateral arm reaches. When compared to contralateral arm movements, mu and beta band ERD occurs in similar cortical locations during ipsilateral arm movements, but begins later relative to the movement onset time. Additionally, increases in high gamma band power also occur later and are lower in amplitude during ipsilateral arm movements than during contralateral arm movements. These differences in the timing and strength of spectral power changes correspond well with the majority of previous studies of movement-related spectral power changes from both non-invasive and invasive recording methods (Pfurtscheller and Aranibar 1979; Crone, Miglioretti et al. 1998a; Crone, Miglioretti et al. 1998b; Pfurtscheller and Lopes da Silva 1999). Although these findings contrast with a previous study from our lab demonstrating a unique physiology associated with ipsilateral hand movements (Wisneski,

Anderson et al. 2008), potential explanations for this difference are the increased complexity and attention necessary to perform visually guided reaches as opposed to simple hand movements and the random order of hand side in the previous study. While we found that the amplitude and timing of spectral power changes related to contralateral and ipsilateral arm movements were distinct, the speed and directional tuning of ECoG spectral power features were similar for contralateral and ipsilateral movements in both the strength and topography of tuning.

In addition to spectral power changes, the LMP signal was striking in the strength of its PLS prediction model weights and the broad distribution of directionally tuned electrodes. As the LMP is derived from low-pass filtering ECoG signals, it is likely that there is a correspondence between movement-related cortical potentials such as the bereitschaft potential and the LMP signal. Movement-related cortical potentials are characterized by a negative shift in signal amplitude with an increasing negativity immediately before the movement onset (Kornhuber and Deecke 1965; Deecke, Scheid et al. 1969; Shibasaki and Hallett 2006). Similarly, in this study, the LMP signal is negatively correlated with movement speed in electrodes located in primary sensorimotor areas. A number of previous studies have shown that LMP amplitude can be used to decode movement kinematics of the contralateral and ipsilateral arms (Schalk, Kubanek et al. 2007; Pistohl, Ball et al. 2008; Ganguly, Secundo et al. 2009; Hotson, Fifer et al. 2014), therefore the large amplitude of prediction weights and the broad region of directional tuning found for LMP signals in this study are unsurprising. It should be noted that the use of time-domain signals in on-line BCI control has been limited (Kennedy, Andreasen et al. 2004; Kennedy, Kirby et al. 2004), so it is uncertain if the significance of LMP signals for open-loop movement decoding will generalize to closed-loop BCI control where on-line adaption is necessary.

Because of the similarity between the neural representations of contralateral and ipsilateral limb movements, it is uncertain if kinematic decoding of contralateral and ipsilateral arm movements is separable. During each session, patients performed reaching movements with a single arm. As previous studies have shown that neural activity during bimanual movements is not simply a linear combination of neural activity observed during unimanual movements (Tanji, Okano et al. 1988; Donchin, Gribova et al. 1998; Kermadi, Liu et al. 2000; Diedrichsen, Wiestler et al. 2013; Gallivan, McLean et al. 2013), additional studies would be necessary to determine the differences in ipsilateral motor representations during unimanual and bimanual motor movements. It may be possible to incorporate additional levels of hierarchy to decode whether a movement is a unimanual contralateral arm movement, a unimanual ipsilateral arm movement, or a bimanual movement. This additional level of hierarchy could be used after determining that a movement is occurring but prior to decoding kinematics.

To implement a BCI system in stroke survivors, it would be ideal to avoid an invasive surgery if possible. Therefore, it is necessary to understand the decrease in signal quality that comes with non-invasive recording methods. While LMP signals from EEG recordings have been used to decode 3D movements with accuracies better than chance (Bradberry, Gentili et al. 2010), our predictions of kinematics using simulated EEG signals were significantly worse than predictions using actual ECoG signals. Although the simulated EEG signals used here did not cover the entire cortex as true EEG electrodes would, the ECoG signals were drawn from the same limited spatial locations. Furthermore, this decrease in decoding accuracy is expected because of the decreased spatial and spectral resolution of EEG signals relative to ECoG (Cooper, Winter et al. 1965; Pfurtscheller and Cooper 1975). Additionally, while artifacts such as eye blinks can be controlled for in a laboratory setting, it is much harder to control for artifacts during on-line BCI

control in real-world settings. Therefore, to implement a BCI system with multiple degrees of freedom in stroke survivors, an invasive recording method such as ECoG would be necessary. The ability to classify movement from rest, however, indicates that a simple BCI system, such as one designed for rehabilitation after stroke, can be implemented with non-invasive recording methods.

This study shows that the kinematics of ipsilateral and contralateral arm movements have similar representations in a single cortical hemisphere. There are several potential alternative considerations that should be noted. All of the recordings were made in patients with chronic epilepsy. Although care was taken to ensure that all seizures occurred at least 2 hours before or after recordings were made, and that trials with interictal activity were removed prior to analysis, it is difficult to determine if the results of this study were affected by the patient population used. As 4 of the 5 patients had epileptic foci located in the temporal lobe and the majority of effects were located in frontal and parietal areas, we believe that the results were not significantly affected by focal epileptic activity. Electrophysiological correlates of movements are also affected by a number of factors that may have been involved in this study. First, increased task complexity and effort increase movement-related cortical activations (Kitamura, Shibasaki et al. 1993a; Kitamura, Shibasaki et al. 1993b; Manganotti, Gerloff et al. 1998; Slobounov, Hallett et al. 2004). While reaction time and movement speed were similar between the two arms, all ECoG electrodes were located contralateral to the dominant hand. Therefore, the strong ipsilateral signals may have been related to increased effort for non-dominant hand movements relative to dominant hand movements. Similarly, the dominant hemisphere has been associated with dynamics, including trajectory control of both arms (Sainburg and Kalakanis 2000; Sainburg and Schaefer 2004; Schaefer, Haaland et al. 2007; Schaefer, Haaland et al. 2009a;

Schaefer, Haaland et al. 2009b; Schaefer, Mutha et al. 2012). As all electrodes were contralateral to the dominant limb, further work would be necessary to isolate any differences in these results that may occur with non-dominant hemisphere recordings. Additionally, ipsilateral motor activity has been posited to preferentially relate to proximal muscle movements (Colebatch, Deiber et al. 1991; Jankelowitz and Colebatch 2002). As the reaches used involved the entire arm, it is uncertain if these results will generalize to isolated directed movements of more distal body parts. Finally, postural movements of the hemibody contralateral to the moving arm represent a potential confound. Because of this, the results of this study must be interpreted within the context of the activity of the entire motor system and not of any individual musculature. Regardless of the role of stabilizing movements in the neural activity observed, the fact that we can decode information with multiple degrees of freedom still demonstrates the potential for BCI system development.

Overall, we have shown that ECoG signals from human patients can be used to decode kinematics of 3D reaches. Additionally, ECoG signals from a single cortical hemisphere can be used to decode kinematics not only of contralateral arm movements but also of the same-sided arm. Taken together, these results demonstrate that ECoG may be used to develop BCI systems with multiple degrees of freedom and that the unaffected hemisphere after stroke represents a potentially useful control signal for BCI applications.

4 Characterization of the Effects of the Human Dura on Macro- and Micro-Electrocorticographic Recordings

The results of the previous chapter show that there is a significant decrease in the accuracy of decoded kinematics when we use simulated non-invasive signals. Therefore, a neuroprosthetic system requiring control of multiple degrees of freedom will require implanted electrodes. A potential way to reduce the invasiveness of an electrocorticography (ECoG) implant would be to implant electrodes above the dura, however, it is important to understand the effect that the dura would have on signal quality. The body of this chapter is drawn from our previously published manuscript (Bundy, Zellmer et al. 2014)[1].

4.1 Introduction

In recent years, ECoG recordings, made from either epidural or subdural electrode contacts on the surface of the cortex, have emerged both as an important means to study human cortical electrophysiology (Fried, Ojemann et al. 1981; Allison, McCarthy et al. 1994; Crone, Miglioretti et al. 1998a; Crone, Miglioretti et al. 1998b; Jerbi, Ossandon et al. 2009; Miller, Zanos et al. 2009; Gaona, Sharma et al. 2011), as well as a signal platform for brain-computer interface (BCI) experiments when implanted beneath the dura acutely in humans (Leuthardt, Schalk et al. 2004; Leuthardt, Miller et al. 2006; Wilson, Felton et al. 2006; Felton, Wilson et al. 2007; Schalk, Miller et al. 2008; Schalk and Leuthardt 2011) and epidurally for chronic experiments in non-human primates (Rouse, Stanslaski et al. 2011; Rouse, Williams et al. 2013) due to its

[1] As the first author of this manuscript I participated in ECoG data collection, designed and performed the ECoG data analysis, and led the writing of the manuscript. Acknowledgement should be given to Erik Zellmer who performed the Finite Element Modeling described. Thanks should be given to Jeff Ojemann who allowed us to use the macro-scale ECoG data.

balance of invasiveness and signal quality. The initial work investigating the use of ECoG for BCI systems in humans was done using patients temporarily implanted with subdural ECoG grids as part of the clinical treatment for intractable epilepsy. These clinical electrode arrays typically have a diameter of a few millimeters and an inter-electrode spacing on the order of 1 cm (Engel 1996). Recent work has also investigated the use of subdural micro-ECoG arrays with smaller electrode sizes (on the order of hundreds of microns or smaller) and denser spacing in human patients (Leuthardt, Freudenberg et al. 2009; Wang, Degenhart et al. 2009; Kellis, Miller et al. 2010). The increased spatial resolution and smaller size of micro-ECoG arrays are an important technical step towards developing a chronic BCI system for clinical use. An important factor to consider in the development of micro-ECoG arrays is the impact of the human dura mater on the electrophysiological signals. While an epidural electrode array may reduce the risks of infection due to isolating the implant from the intracranial space as well as removing the increased risk for infection caused by a cerebrospinal fluid (CSF) leak (Tenney, Vlahov et al. 1985; Mollman and Haines 1986; Korinek 1997), it is important to understand the tradeoff in decreasing signal quality that would be experienced by moving the electrode arrays from a subdural to an epidural implantation.

There have been a number of previous studies based upon animal models that have evaluated the effect of the dura mater on ECoG signals. Perhaps the first measure of the signal quality of epidural ECoG is the usefulness in controlling a BCI system. To this end, studies in non-human primates have shown that epidural ECoG can be used for on-line control (Rouse and Moran 2009; Rouse, Stanslaski et al. 2011; Rouse, Williams et al. 2013) and that similar degrees of BCI performance are achieved using both local field potentials and epidural field potentials (Flint, Lindberg et al. 2012). Similarly, in offline analysis, epidural signals were used to effectively

decode forelimb movements in rats (Slutzky, Jordan et al. 2011). Furthermore, macro-scale epidural ECoG signals have been used off-line to decode continuous three-dimensional hand trajectories in non-human primates over the course of several months (Shimoda, Nagasaka et al. 2012). Additionally, the optimal spacing of subdural and epidural electrode arrays was similar when comparing electrophysiological recordings made utilizing ECoG arrays with 125 μm electrode contacts in rats with a finite element model of the rat brain (Slutzky, Jordan et al. 2010). While these studies indicate that epidural recordings may be similar to subdural recordings with regards to BCI applications in non-human models, there is a limited ability to generalize these studies to humans because of the different physiologic characteristics of the cortex and dura mater between humans and non-human animals (Shoshani, Kupsky et al. 2006; Treuting, Dintzis et al. 2012).

To date, there are a limited number of studies that have sought to characterize the effect of the dura on electrophysiological recordings in humans (Slutzky, Jordan et al. 2010; Torres Valderrama, Oostenveld et al. 2010). Based on the rat model described above, a finite element model of human cortex was constructed and the authors concluded that the optimal electrode spacing was similar between epidural and subdural recordings (Slutzky, Jordan et al. 2010). There were, however, no electrophysiological recordings in humans to confirm this, and the analysis examined only the spacing of electrodes and not the effect of the dura on the amplitude of ECoG signals (Slutzky, Jordan et al. 2010). In another study, epidural BCI performance was simulated by acquiring epidural and subdural signals intraoperatively, and then applying a transfer function to BCI control derived from subsequent subdural signals acquired extraoperatively (Torres Valderrama, Oostenveld et al. 2010). Here again, the authors concluded that the dura had little effect. While the study found that the transformed signals would still

allow for adequate BCI performance, the study is limited for several reasons. First, the intraoperative condition in which the transfer function of the dura was evaluated is different from the alert brain state during BCI control. In particular, the consistent decreases in gamma band power caused by anesthesia (Breshears, Roland et al. 2010) means that while the transfer function may be accurate for low frequency rhythms, it may not extrapolate to the higher frequency gamma band. It is this high gamma range in particular, that is often used for ECoG BCI control (Rickert, Oliveira et al. 2005; Heldman, Wang et al. 2006; Leuthardt, Schalk et al. 2009; Schalk and Leuthardt 2011). Second, the study only evaluated the effects of the dura on clinical electrode arrays, which are much larger and more spatially diffuse than the arrays that would likely be used for a chronically implanted BCI system. The different signal characteristics of micro-scale arrays, due to both sampling a smaller area of cortex and recording from electrodes with higher electrical impedances should be considered in evaluating the effects of the dura on ECoG signals.

To address the question of how the dura affects electrophysiological recordings in humans, this study investigated the effects of the human dura on ECoG signals from humans during awake, resting periods at both the macro- and micro-scale. We use both simultaneous electrophysiological recordings of macro- and micro-scale ECoG arrays as well as a finite element model of human cortex. The results of both techniques show that while there is little difference in macro-scale ECoG signals from above or below the dura, that micro-scale ECoG signals have very different amplitudes, spectral resolution, and spatial resolution.

4.2 Methods

4.2.1 Micro-ECoG Experiments

Patients

The patients that participated in this study underwent temporary placement of intracranial electrode grids to identify epileptic seizure foci. Four patients provided informed consent for the placement of two microelectrode arrays for research purposes (Figure 4.1A). In each subject, one microelectrode array was placed beneath the dura, in between or peripheral to the macro-scale contacts of a clinical ECoG grid. A second microelectrode array was slid below the skull superficial to the dura outside of the boundary of the craniotomy (Figure 4.1B). Electrode arrays were localized using radiographs and the "get location on cortex" technique (Figure 4.1C and 4.1D) (Miller, Makeig et al. 2007). Additionally, all micro-ECoG grid locations were compared to the cortical areas identified by the epileptologists as seizure foci or propagation regions to confirm that they did not overlap. All patients provided informed consent for the study, which were reviewed and approved by the Institutional Review Board of Washington University School of Medicine.

Electrocorticography Specifications

A special research microelectrode array was designed and utilized (PMT Corporation, Chanhassen, MN). Each electrode array consisted of 16 platinum iridium micro-wires with a diameter of 75 μm and an interelectrode spacing of 1 mm. Figure 4.1A shows a schematic of the array and photographs of the microelectrode array alone and placed relative to a standard clinical electrode array. Of the 16 contacts on the research micro-array, 12 micro-wire contacts were cortically facing and the 4 contacts at the corners of the array (spaced 3 mm apart) were facing the skull. The skull-facing contacts were designed so that two of the 4 non-cortical, impedance-matched contacts with good quality signals could be used as ground and reference contacts for

the recordings. Additionally, shielded cables were used to connect the micro-ECoG arrays to the amplifiers in order to increase the signal-to-noise ratio (SNR).

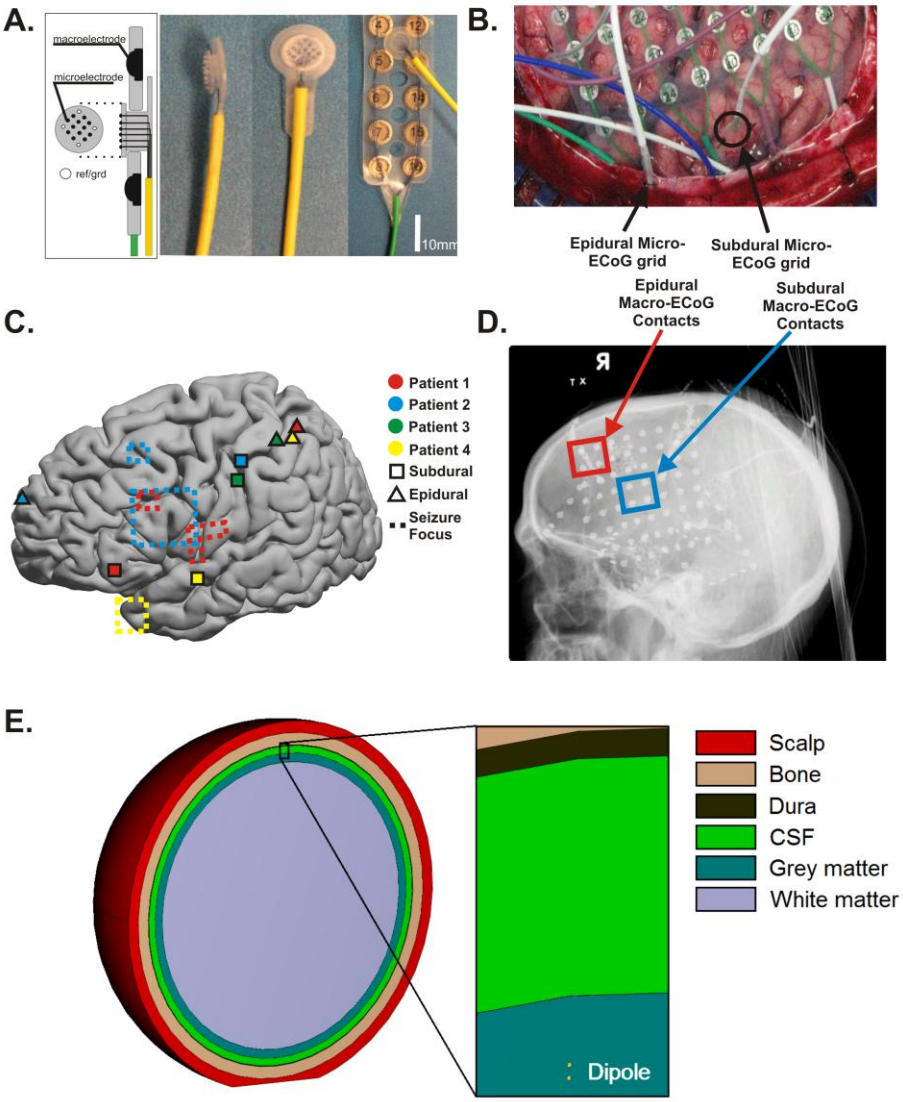

Figure 4.1 Electrocorticography and finite element modeling methods
A. A novel microelectrode with 70 µm electrode diameter and 1 mm inter-electrode spacing was implanted both epidurally and subdurally in 4 patients. The grids contained 12 cortically facing channels and 4 impedance-matched, skull-facing contacts to choose from for a ground and a reference contact. **B**. Subdural microgrids were implanted either in between or to the outside of clinical ECoG contacts. Epidural microgrids were slid between the dura and skull beyond the boundaries of the craniotomy. **C**. Locations of subdural and epidural microgrids across patients and cortical areas identified as epileptic foci or propagation regions. The seizure focus of Patient 3 is not visible as it was located sub-temporally. **D**. In an additional patient, due to an adherent dura during the implant surgery, a corner of the clinical ECoG grid was superior to the dura, allowing for comparison of epidural and subdural macro-ECoG signals in identical geometric configurations, allowing for comparison of the effect of the dura across electrode geometry. **E.** A schematic shows the geometric organization of the FE model. The model consisted of spherical subdomains with a radially oriented dipole placed within the gray matter layer. Electrodes of various diameters were simulated on the superior surface of the dura (epidural) or on the surface of the gray matter (subdural).

Electrocorticography Recordings and Preprocessing

Electrocorticography signals were acquired using biosignal amplifiers manufactured by g.tec (Graz, Austria). The combination of two out of the four upward facing contacts producing the cleanest signals was selected for use as ground and reference channels. Signals were sampled with 24-bit resolution with an internal sampling rate of 38.4 kHz and an internal 5 kHz antialiasing filter. Data were recorded with a sampling rate of 2.4 kHz. No additional filters were used.

The BCI2000 software package was utilized to record ECoG signals while patients were resting (Schalk, McFarland et al. 2004b). During the recordings, patients were positioned in their hospital bed in the semi-recumbent position. Patients were instructed to rest quietly and to remain as still as possible for the duration of the recordings. In Patients 2, 3, and 4, the epidural and subdural contacts were recorded simultaneously for a period of 5-10 consecutive minutes. In the final patient, Patient 1, the subdural and epidural contacts were recorded for distinct epochs of approximately 5 minutes each within a total time window of approximately 25 minutes.

After initial data collection, a number of steps were taken to preprocess the data. First, the data was high-pass filtered at 0.5 Hz. Next, the data was notch filtered to remove all 60 Hz harmonics below the Nyquist frequency from the data. The signals were then manually inspected to determine noisy channels, which were then removed from further analysis. All remaining channels were then averaged and regressed from the signal by calculating a regression coefficient of the common average to each channel and removing the weighted common average signal from each channel. Finally, the data was manually inspected to determine time intervals in which artifacts were present and the remaining time periods were segmented into 10 second windows with 5 second overlaps between windows for use in the analyses described below.

Figure 4.2 (upper plots) shows an exemplar 10 second time window from the subdural and epidural micro-ECoG grids from a single patient.

Power Spectral Density Analysis

An initial analysis was performed to examine the characteristics of the power spectrum in epidural and subdural recordings. The power spectral density (P(f,c,w) where f is the frequency bin, c is the channel, and w is the temporal window) was calculated as the square of the fast Fourier transform of each channel for each 10 second time window with a frequency resolution of 1 Hz. The power spectral densities for both epidural and subdural contacts were then converted to normalized spectra, $P_{N,}$ by dividing the spectra by the 99th percentile of power from any epidural or subdural contact (P_{99}) from the respective patient, as described in Equation 4.1. This allowed the power spectra (in decibels) of both epidural and subdural recordings to be compared on the same scale.

$$P_N(f,c,w) = \frac{P(f,c,w)}{P_{99}} \tag{4.1}$$

As ECoG power spectra are not normally distributed, they were normalized with a log transform. The log-transformed normalized spectra were concatenated across channels and time windows. Prior to comparing the epidural and subdural contacts, the normality of the distributions of log-transformed amplitudes at each frequency band was verified through visual inspection of a subset of frequencies and by the Kolmogorov-Smirnov test. Finally, the average log-transformed power spectra across time windows and channels of the epidural and subdural recordings were compared through an independent samples t-test. Multiple comparison correction was performed using the Benjamini-Hochberg-Yekutieli method of False Discovery Rate (FDR) correction

(Benjamini and Hochberg 1995; Benjamini and Yekutieli 2001) to correct for the number of frequency bands compared while accounting for the correlated nature of the test statistics.

Calculation of Noise Floor

In addition to comparing the normalized amplitudes of epidural and subdural recordings, it was hypothesized that a more meaningful measure of signal quality would be the spectral noise floor of recordings. Spectral analyses of ECoG recordings are characterized by a 1/f decrease in amplitude at frequencies below the noise floor and a flat power spectrum at frequencies above the noise floor (Miller, Sorensen et al. 2009). To examine the noise floor in epidural and subdural recordings the noise floor of each micro-ECoG grid was estimated using the power spectrum from each channel and temporal window between 550 Hz and 597 Hz. This frequency band was chosen because the power spectra had plateaued, it is located below the Nyquist frequency, and is located between any 60 Hz harmonics. Next, the average log-transformed power spectra from the epidural and subdural recordings were compared to their respective noise floors using an independent samples t-test. Multiple comparison correction was performed using the Benjamini-Hochberg-Yekutieli method of False Discovery Rate (FDR) correction (Benjamini and Hochberg 1995; Benjamini and Yekutieli 2001).

4.2.2 Macro-ECoG Experiment

As a secondary analysis to evaluate the effect of the dura on human clinical macro-ECoG electrodes, we identified a single patient who performed BCI experiments described previously (Leuthardt, Miller et al. 2006). During the implantation surgery, the dura was found to be adherent to the brain, therefore a corner of the clinical ECoG grid was superior to the dura while the remainder of the grid was inferior to the dura, allowing for evaluation of the effects of the human dura on macro-ECoG signals with an exposed electrode diameter of 2 mm and an

interelectrode distance of 1 cm (Ad-Tech Corporation, Racine, WI) (Figure 4.1D). Signals were recorded with Synamps2 amplifiers (Neuroscan, El Paso, TX). Signals were bandpass filtered (0.1-220 Hz) and digitized at 1000 Hz. As in the micro-ECoG experiments described above, recordings were made while the patients rested quietly in their hospital bed in a semi-recumbent position. As 4 electrodes at the corner of the grid were located superior to the dura, 4 subdural electrodes in the same geometric configuration confirmed to be subdural and not located on the border of the cut dura were used for comparison. The preprocessing for the macro-ECoG signals was the same as for the micro-ECoG signals with the common average calculated from the entire ECoG array of 64 channels. Power spectral densities were calculated for the macro-ECoG contacts using the methods from the micro-ECoG experiments described above. As this recording was made with a band-pass filter (0.1-220 Hz), it was not possible to isolate the system noise floor from the hardware filters in order to determine the frequency at which the signals reached the system noise floor. While these recordings were from a single patient and made with a different recording system, they provided the unique opportunity to evaluate macro-ECoG signals from above and below the dura in awake humans and to compare the effect of the dura on ECoG recordings at different spatial scales from the micro-ECoG recordings described above and with existing literature examining of the effect of the dura on clinical ECoG recordings in an intraoperative setting (Torres Valderrama, Oostenveld et al. 2010).

4.2.3 Modeling

A finite element (FE) model of the human head was created using Comsol Multiphysics (V.3.4, Comsol, Stockholm, Sweden). The model consisted of spherical subdomains representing white matter, gray matter, CSF, dura mater, scalp and skin. The thickness and conductivity of each subdomain were assigned based on previously reported values and are summarized in Table 4.1.

Cortical source regions were modeled as radially oriented dipoles consisting of pairs of idealized current sources. A schematic of the geometric organization of the FE model is shown in Figure 4.1E. The FE model was used to solve the potential distribution at the cortical surface and the surface of the dura for dipoles placed at different depths. This information was then used to calculate the potential generated at a point electrode from unitary current sources located at different radial displacements. Dipoles placed at varying depths (0.3-1.5 mm, 0.2 mm increments) were evaluated. The FE model was solved at ~800,000 tetrahedra with a maximum element size of 400 µm in the volume closest to the dipole.

Table 4.1 Thickness and conductivity values for each explicitly represented subdomain

Subdomain	Conductivity [S/m]	Thickness (mm)
White matter	0.1428[c]	60[a]
Gray matter	0.36[b]	3.7[a]
CSF	1.70[b]	3.1[a]
Dura mater	0.065[b]	0.36[a]
Scalp	0.435[c]	5.0[a]
Skull	0.02[b]	5.0[a]

[a] *(Slutzky, Jordan et al. 2010)*[b] *(Manola, Roelofsen et al. 2005)*[c]*(Ramon, Schimpf et al. 2006)*

To evaluate the effect of different electrode diameters on recorded potentials, the potential-distance relationships generated using the methodology described above was curve fitted in Matlab (2011a) using high order sums of sine and Gaussian functions, producing a set of expressions that can be used to calculate the potential generated at any point by a dipole at an arbitrary radial displacement. The surface area of the electrodes with diameters ranging from 75 µm-10 mm was then discretized into ~800,000 points and a second set of potential-distance relationships were calculated by averaging the potentials generated across the surface area of the electrodes by dipoles at different radial displacements.

4.3 Results

Recordings from each patient demonstrated significant effects of the dura on micro-ECoG recordings. Figure 4.2 (upper plots) demonstrates exemplar epidural and subdural micro-ECoG recordings. In particular, the micro-ECoG recordings have noticeably higher amplitudes in subdural signals as compared to epidural signals. The calculated averaged power spectral densities confirm the observed differences in amplitude between epidural and subdural micro-ECoG recordings. Each patient's averaged power spectral densities for subdural and epidural micro-ECoG signals are shown in Figure 4.3. In particular, each of the 4 patients demonstrated spectral power in subdural recordings that was significantly higher ($p<0.05$) than in epidural recordings in a range up to at least 150 Hz.

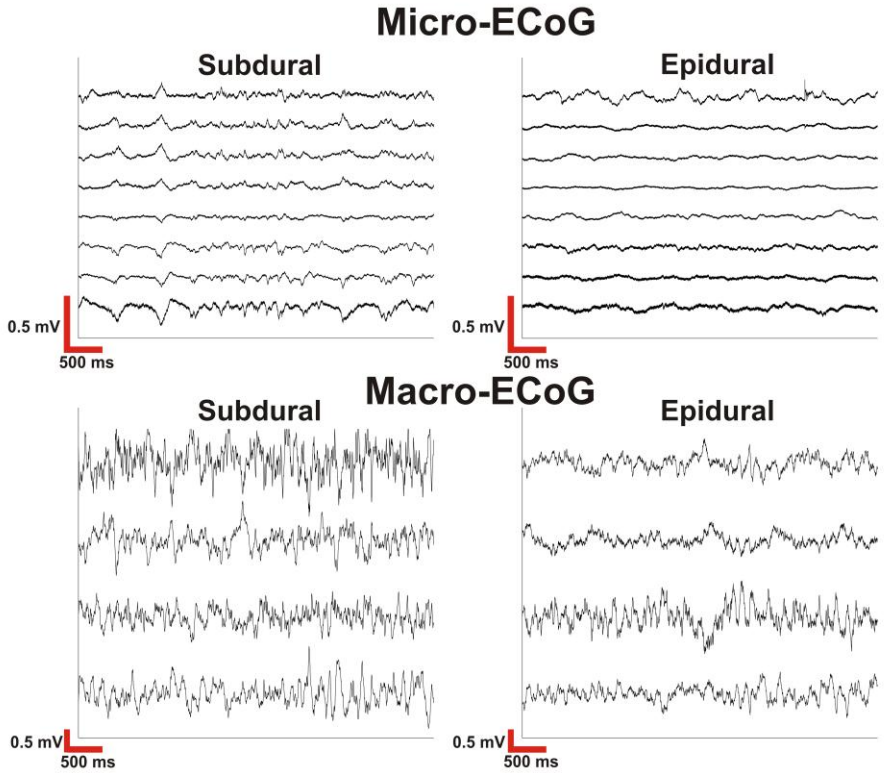

Figure 4.2 Raw electrocorticography signals
Within micro-ECoG recordings the signals were fairly correlated across channels and there was a large difference in amplitude between subdural and epidural signals. Macro-ECoG signals demonstrate smaller amplitude differences between subdural and epidural contacts. Macro-ECoG signals are also less correlated and have higher signal amplitudes than micro-ECoG signals.

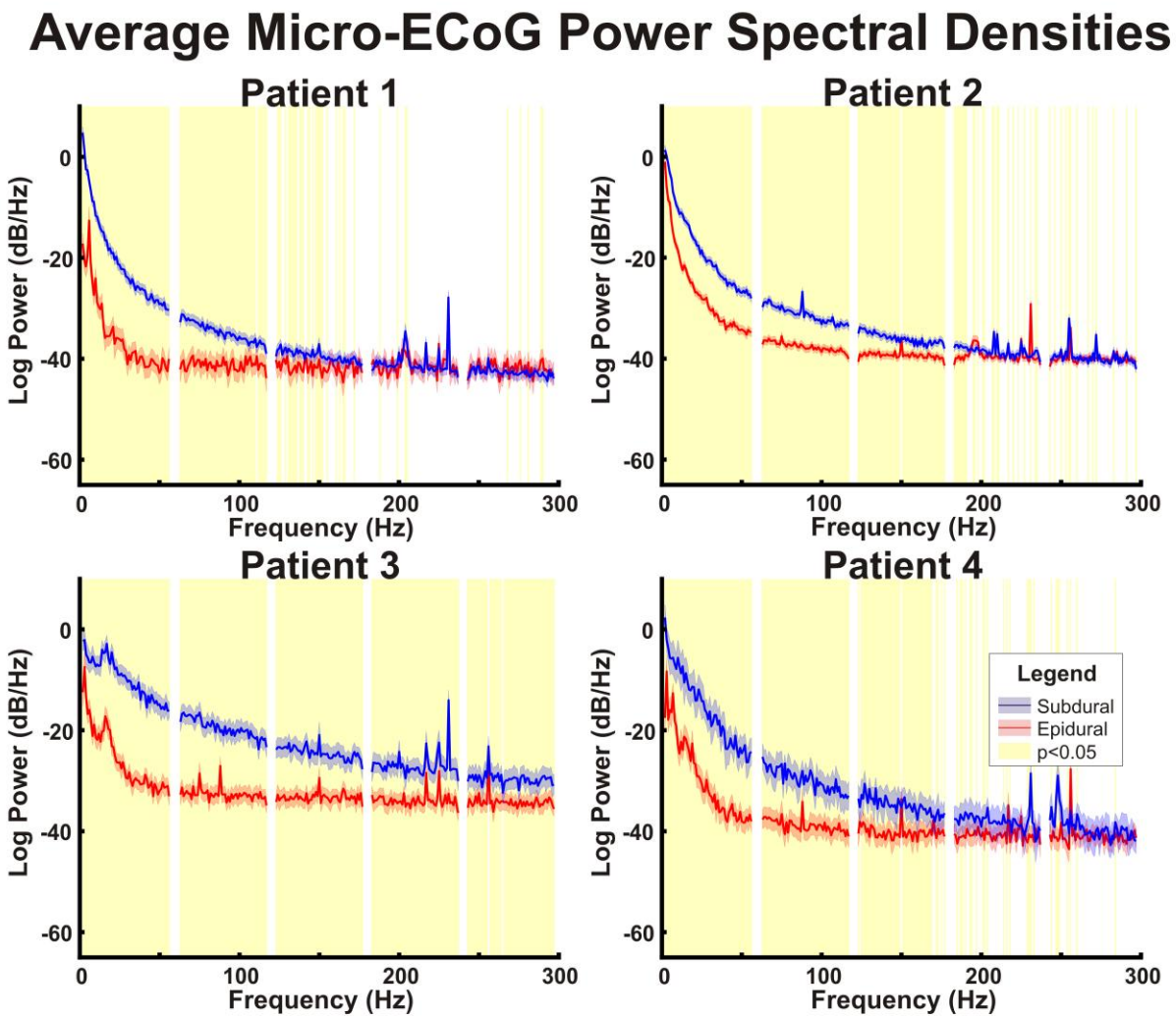

Figure 4.3 Micro-ECoG power spectral densities
Patient-specific averaged power spectral densities for epidural and subdural micro-ECoG contacts. Averaged power spectra were calculated across time windows and electrode channels. Confidence intervals represent the 95% confidence interval of the power spectral density. Areas highlighted in yellow represent frequencies with a significant ($p<0.05$) difference between power in epidural and subdural recordings corrected for multiple comparisons with false discovery rate. Power is higher in subdural recordings than epidural recordings in frequencies below 150 Hz in all patients and the 1/f decrease in amplitude is less steep in subdural recordings than epidural recordings.

While the differences in spectral amplitudes are informative, it was also important to determine the spectral frequency at which the noise floor of the ECoG signals is reached. Figure 4.4 displays the power spectral densities of micro-ECoG recordings along with the noise floor estimated using the power spectra between 550-597 Hz for the subdural and epidural grids respectively.

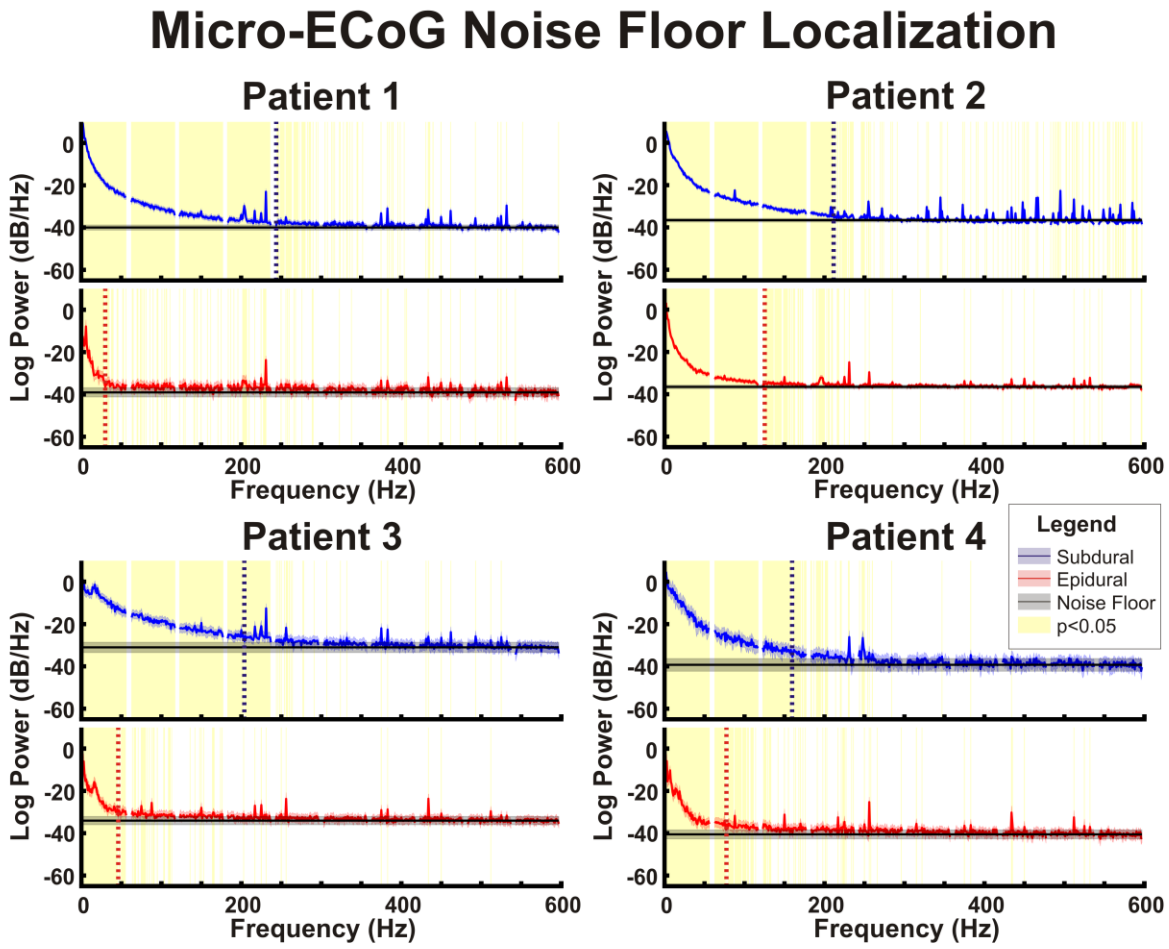

Figure 4.4 Micro-ECoG noise floor comparison
Patient-specific power spectral densities averaged across channels and time windows are shown relative to the grid-specific noise floors. Noise floors were determined based upon the power between 550-597 Hz. In all patients power spectra are flat from the frequency at which the noise floor was reached through the end of the analysis range. Vertical lines indicate the lowest frequency at which the power spectrum was not significantly different from the noise floor. This location is reached at higher frequencies for subdural recordings than epidural recordings in each patient. Confidence intervals represent the 95% confidence interval of the power spectral density and noise floor. Areas highlighted in yellow represent frequencies with a significant ($p<0.05$) difference between power in epidural and subdural recordings and their respective noise floors, corrected for multiple comparisons with false discovery rate.

As can be seen in the power spectral density plots (Figure 4.3) as well as the comparison of the power spectral density with the noise floor (Figure 4.4), micro-ECoG recordings displayed a decrease in amplitude with increasing frequency consistent with a 1/f trend. Furthermore, after flattening out, the power spectrum is flat up to the upper bound of the analysis (597 Hz), confirming that there are no other hardware filters affecting the analysis. Importantly, in micro-

ECoG recordings, the frequency where the recorded signal and the noise floor converge (i.e. the lowest frequency at which they are first not significantly differently) was at least 83 Hz lower for epidural signals than for subdural signals in all 4 patients. In particular, the epidural power spectrum was first not significantly different from the noise floor at between 30 Hz and 123 Hz, while the subdural power spectrum was first not significantly different from the noise floor at between 160 Hz and 243 Hz.

Additionally, the human dura was found to have a different effect on micro-ECoG signals when compared to macro-ECoG signals. In particular, the dura affects micro-ECoG signals much more than macro-ECoG signals. In comparing the exemplar macro- and micro-ECoG recordings (Figure 4.2), there is a large difference in amplitude between the macro- and micro-ECoG signals and the micro-ECoG traces appear more correlated to each other than the macro-ECoG traces. Both of these findings are expected due to the smaller electrode spacing and higher impedance of micro-scale electrodes. Furthermore, while less marked than the difference caused by electrode size, the macro-ECoG recordings appeared to have similar amplitudes for both subdural and epidural recordings, while there is a marked difference in amplitude between subdural and epidural micro-ECoG recordings. Additionally, the power spectra of the macro-ECoG recordings (Figure 4.5) show statistically significant differences in spectral amplitude between subdural and epidural contacts characterized by higher amplitudes in the epidural contacts in the 10-60 Hz range and higher amplitudes in the subdural contacts in the 90-240 Hz range.

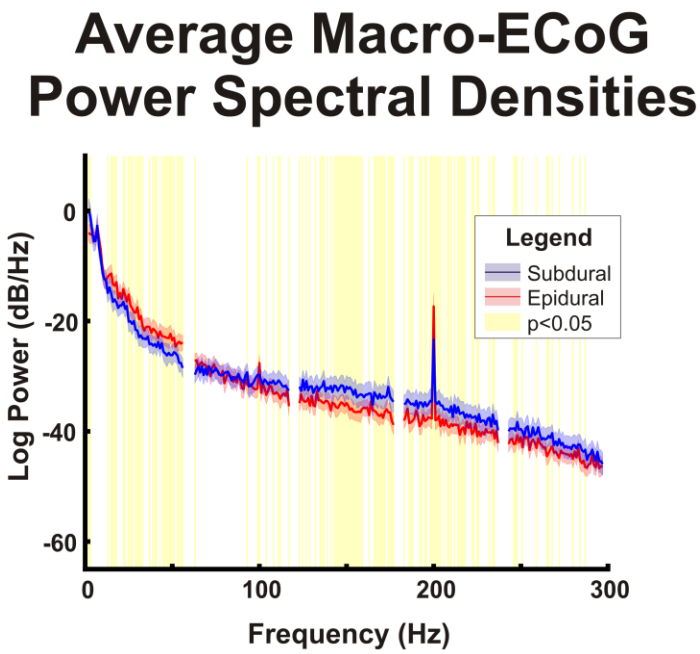

Figure 4.5 Macro-ECoG power spectral densities
Power spectral densities for epidural and subdural macro-ECoG contacts averaged across channels and time windows. Confidence intervals represent the 95% confidence intervals of the power spectral density. Areas highlighted in yellow represent frequencies with a significant ($p<0.05$) difference between power in epidural and subdural recordings corrected for multiple comparisons with false discovery rate. Although power is higher in epidural recordings at low frequencies and higher in subdural recordings in high frequencies, the 1/f decrease in power is similar in subdural and epidural recordings.

Finally, simulations from a finite element model of the human head confirm the empirical results. Figure 4.6 and 4.7 display the amplitudes for various electrode sizes placed subdurally or epidurally at various radial displacements from a dipole source with a depth of 0.9 mm. In Figure 4.6, signals are normalized to the maximum amplitude signal from any electrode size and location (a 75 μm subdural electrode placed directly over the source). In Figure 4.7, signals are normalized to the amplitude with no radial displacement. Overall, for small electrode sizes, there is a large difference in the raw amplitude between subdural and epidural contacts; for larger electrode sizes, the difference is much smaller (Figure 4.6). Furthermore, Figure 4.7 demonstrates that the differences between subdural and epidural electrodes in the decrease in signal amplitude with increasing radial displacement from the source is much greater for smaller electrode sizes than larger electrode sizes. Simulations were performed at multiple dipole depths

in addition to the depth of 0.9 mm shown in Figures 4.6 and 4.7. At other depths, a similar effect was observed with the magnitude of the differences between epidural and subdural recordings inversely related to the depth of the dipole placement.

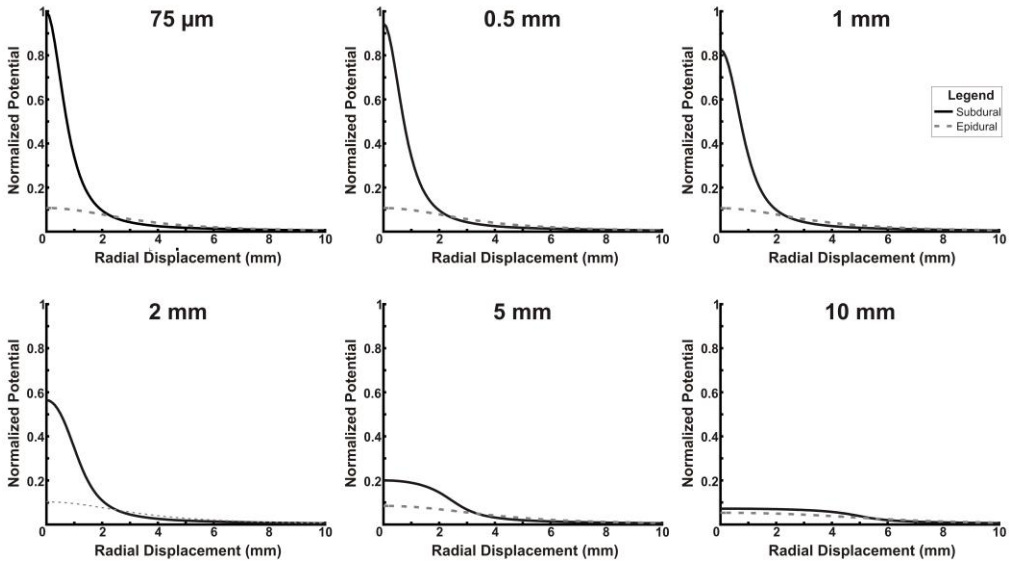

Figure 4.6 Finite element model comparison of amplitude based upon electrode Size
A finite element model was used to compare the amplitude produced by a dipole point source at electrodes with various diameters and varying radial displacements from the source. All traces are normalized to the maximum amplitude of the 75 µm subdural electrode. Small electrodes have large differences in amplitude between epidural and subdural electrodes, while at large diameters, electrodes have much smaller differences in amplitude between subdural and epidural electrodes.

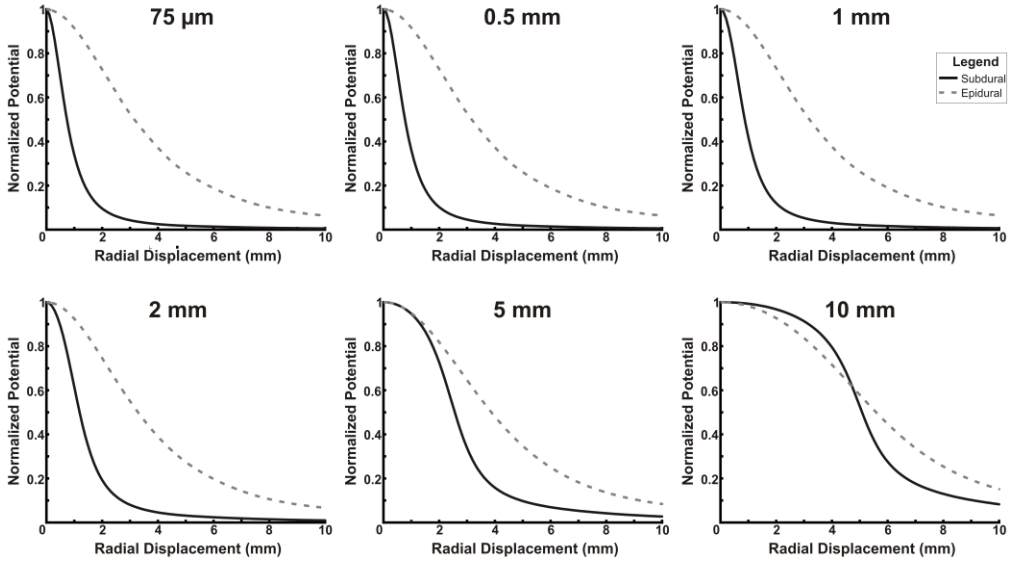

Figure 4.7 Finite element model comparison of spatial specificity based on electrode size
A finite element model was used to compare the decrease in amplitude as radial displacement from a dipole point source increases in electrodes with various diameters. All traces are normalized to the amplitude at 0 mm radial displacement. Small

electrodes have large differences in the changes in amplitude with radial displacement between epidural and subdural electrodes, while at large diameters, electrodes have much smaller differences between subdural and epidural electrodes.

4.4 Discussion

This study provides a demonstration of the effect of the human dura mater on the signal characteristics of ECoG recordings at multiple scales utilizing both electrophysiological recordings and theoretical modeling. In particular, the signal amplitude of epidural micro-ECoG recordings is significantly smaller than that of subdural micro-ECoG recordings. Furthermore, although the signal amplitude derived from epidural macro-ECoG is statistically higher than subdural macro-ECoG in low frequencies (10-60 Hz) and lower than subdural macro-ECoG at high frequencies (90-240 Hz), given the small magnitude of these differences in macro-ECoG power spectra, these differences would probably not affect the ability for either subdural or epidural macro-ECoG electrodes to be used in a BCI system. Experimentally epidural micro-ECoG signals have lower spectral amplitudes than subdural micro-ECoG signals across all frequency bands below the noise floor (which is reached at a lower frequency than for subdural micro-ECoG signals). Additionally, theoretical modeling demonstrates reduced amplitude and spread of voltage potential recorded from epidural contacts when compared to subdural contacts for micro-ECoG electrodes. However, as electrode size approaches that of currently used clinical macro-ECoG electrodes (~2 mm diameters), computer simulations suggest very little difference in signal amplitudes between subdural and epidural recordings. These findings have important implications for the development of chronic, implantable ECoG electrodes.

This study is unique in the examination of the effect of the dura mater on the electrophysiological characteristics of ECoG recordings both in that the study focuses on humans and on different scales of electrode size. While macro-scale ECoG electrodes (on the order of millimeters in diameter with an interelectrode distance on the order of 1 cm), placed below the

dura, have been utilized clinically for many years (Penfield and Jasper 1954; Engel 1996), the advent of ECoG as a potential signal platform for BCI systems (Leuthardt, Schalk et al. 2004) introduced an important question as to the effect of the dura mater on ECoG signal quality. To be applied as a control signal for a chronically utilized BCI system, ECoG signals need to be chronically stable and must balance the desire for multiple independent degrees of freedom with the desire to minimize the invasiveness of the implant. Micro-scale ECoG recordings with smaller electrode size and spacing have demonstrated an improved spatial resolution and degree of behavioral information that can be decoded from ECoG signals (Leuthardt, Freudenberg et al. 2009; Wang, Degenhart et al. 2009; Kellis, Miller et al. 2010) and could reduce the invasiveness of a chronic BCI system. Furthermore, as the outside of the dura is part of the peripheral immune system, epidural ECoG has been proposed as a method to limit the invasiveness of chronic implants and reduce the chances of an infection within the central nervous system (Tenney, Vlahov et al. 1985; Mollman and Haines 1986; Korinek 1997; Moran 2010). While implanting ECoG arrays epidurally would reduce the invasiveness of a chronic BCI system, it is important to understand the tradeoffs in terms of signal quality that would result from electrodes being further away from the brain, particularly for micro-scale electrode arrays. While a number of studies point to the ability to decode information from epidural contacts in animal models (Rouse and Moran 2009; Slutzky, Jordan et al. 2011; Flint, Lindberg et al. 2012; Shimoda, Nagasaka et al. 2012; Rouse, Williams et al. 2013), it is necessary to understand whether the different anatomy of the dura in humans would further impair epidural ECoG recordings (Shoshani, Kupsky et al. 2006; Treuting, Dintzis et al. 2012).

The results of the study clearly show that at the micro-scale, the dura has significant effects on signal amplitude. Previous ECoG BCI studies have demonstrated the importance of the high

gamma band (70-105 Hz) for BCI applications (Leuthardt, Schalk et al. 2004; Leuthardt, Miller et al. 2006; Wilson, Felton et al. 2006; Felton, Wilson et al. 2007; Schalk, Miller et al. 2008; Rouse and Moran 2009; Schalk and Leuthardt 2011). While low frequency changes in power have also been shown to be important for BCI control (Leuthardt, Schalk et al. 2004), the high frequency power changes are more anatomically focal (Miller, Leuthardt et al. 2007), indicating that the high gamma band may allow for BCI systems with higher degrees of freedom. Importantly, the results demonstrate that the amplitude of subdural micro-ECoG signals is higher than the amplitude of epidural micro-ECoG signals at all frequencies below 150 Hz (Figure 4.3), indicating that subdural micro-ECoG signals will generally have a higher SNR. While there were also significant differences in spectral amplitude between epidural and subdural macro-ECoG signals, the magnitude of the differences are small and the theoretical modeling results demonstrate smaller effects of the dura on macro-ECoG signals than for micro-ECoG signals. While we cannot compare task-based activations between epidural and subdural micro-ECoG arrays due to their different cortical locations, it is reasonable to conclude that while it may be possible to record high-gamma band activity from epidural micro-ECoG electrodes, that the differences in spectral amplitude and noise floor locations between epidural and subdural micro-ECoG arrays would lead to higher SNR in subdural electrodes during performance of a task. For all of these reasons, it appears that while the effect of the dura on micro-ECoG signals is statistically significant and would likely lead to poorer BCI performance with epidural electrodes than with subdural electrodes, that given the small magnitude of the differences between subdural and epidural macro-ECoG signals, epidural macro-ECoG contacts would likely not lead to large changes in BCI performance relative to subdural contacts.

It should also be noted that while there were several technical factors that optimized the quality of micro-ECoG recordings in this study, there are several future technical developments that could further improve the quality of the signals. The use of impedance matched, skull-facing ground and reference contacts as well as shielded connectors to connect the electrode arrays and amplifiers likely increased the SNR of the signals, allowing for recording of physiologic micro-ECoG signals. However, the high impedance of the electrode contacts due to their small size causes the amplitude of physiologic signals recorded to be low and therefore decreases the SNR. The development and use of coatings to increase the surface area of the electrode contacts would decrease the electrode impedance and increase the SNR (Venkatraman, Hendricks et al. 2011). Additionally, the development of FDA approved preamplifiers that could be located closer to the site of the electrode array could also increase the SNR of the signal. Although these developments would likely allow epidural micro-ECoG arrays to be better applied to BCI systems, they would also further improve the signal quality of subdural micro-ECoG arrays. Therefore while both epidural and subdural micro-ECoG signals could be further improved, the superiority of subdural micro-ECoG implants to epidural micro-ECoG implants would not change.

While this work represents an important evaluation of the effect of the human dura on ECoG signal quality, there are several limitations and future considerations to note. Ultimately, the best measure of ECoG signal quality in relationship to BCI applications is the ability for behavioral intentions to be predicted from neural signals. Because of the differences in subject specific anatomy and the strength and characteristics of neural activity between patients, comparison of decoding from one or more cortical regions across patients would not be meaningful in examining the effects of the human dura on electrophysiological recordings. Additionally, the

differences in relationships between cortical activity and behavior across two different locations on cortex, even within a single functional (e.g. Brodmann's) area, makes simultaneous comparison of signal quality from two grids within a single subject impossible. Because of this, we determined that the evaluation of signal characteristics during baseline activity from a single patient would provide the best possible method for evaluating the effect of the human dura on ECoG signals. There is also some concern that differences in cortical activity could affect the results, because the subdural and epidural recordings were made from different cortical areas. While it is impossible to entirely control a patient's conscious thoughts, patient behavior was visually screened to ensure that subjects were truly resting and that periods of movement were removed from the recordings. Furthermore, the results were consistent across all 4 patients with subdural and epidural micro-ECoG grid locations that were widely distributed across the brain (Figure 4.1C). Therefore, it seems reasonable to assume that the differences in signal quality were not caused by behavior but by the placement of the electrodes relative to the dura. Since the patients utilized were chronic epilepsy patients, an additional concern is that signals measured may have been affected by epileptic activity. All of the patients had focal epilepsy and care was taken to avoid areas near the epileptic foci during implantation, which was confirmed by subsequent comparison with the clinically determined epileptic foci (Figure 4.1C). All recordings were also made with a buffer period of at least one hour before or after any generalized seizure activity. Therefore, it can be reasonably assumed that the results represent normal physiologic and not epileptic activity. Additionally, while care was taken to visually verify that subdural micro-ECoG grids were not placed on blood vessels, as the epidural micro-ECoG grids were placed beyond the boundaries of the craniotomy, it was not possible to do this with the epidural arrays. While the effect of blood vessels on ECoG signals has been

demonstrated previously (Bleichner, Vansteensel et al. 2011), the consistency of the spectral differences between epidural and subdural micro-ECoG arrays across all 4 patients indicates that the results were not spuriously caused by the placement of electrodes on blood vessels. It should be noted that the macro-ECoG recordings were made from a single patient and utilized a different recording system. Additionally, there were adhesions between the cortex and the dura and a cut in the dura in the area of the recordings. While it is possible that this may account for some of the differences observed between macro- and micro-ECoG recordings, it is likely that any effect of the adhesions would be to thicken the dura and increase the effect of the dura on the ECoG signals. Furthermore, while the macro-ECoG results presented here were only derived from a single patient, they are in line with experiments demonstrating little effect of the dura on BCI performance when the gain of the dura was estimated under anesthesia intraoperatively (Torres Valderrama, Oostenveld et al. 2010). Finally, while the computational modeling results indicate a significant effect of the dura on micro-ECoG recordings with little effect on macro-ECoG recordings, it is difficult to quantitatively determine the ideal electrode size computationally. As the signal profiles are sensitive to changes in geometries, particularly the width of the CSF layer (Slutzky, Jordan et al. 2010) and dipole depth, it is difficult to predict the optimal electrode size and spacing only from a computational model.

In summary, these experimental and computational modeling results clearly demonstrate that for micro-ECoG arrays, subdural recordings have statistically significant differences from epidural recordings with magnitudes suggesting that the performance of BCI applications would suffer if epidural micro-ECoG electrodes were used, while for macro-ECoG arrays, subdural and epidural signals are similar. In particular, subdural micro-ECoG signals demonstrate increased signal amplitude, SNR, and spatial resolution. While implanting ECoG grids subdurally for chronic

BCI applications is more invasive, the advantage is that smaller, micro-scale electrodes can be used. When implanting less invasive epidural ECoG electrodes, larger scale electrodes should be used. It is a tradeoff that must be optimized to the goals of the treatment.

5 Using Ipsilateral Motor Signals in the Unaffected Cerebral Hemisphere as a Signal Platform for Brain-Computer Interfaces in Hemiplegic Stroke Survivors

Although the experiments of Chapter 3 demonstrate that neural activity can be used to decode movement trajectories of the same-sided limb in motor-intact patients, it is uncertain if stroke survivors will be able to use these signals from their unaffected hemisphere to control a brain-computer interface system. Although invasive electrodes would be required to control a system with multiple degrees of freedom, the EEG simulations in Chapter 3 along with several previous studies utilizing EEG for brain-computer interface systems indicate that it may be possible to decode movement from rest (Wolpaw, McFarland et al. 1991; Pfurtscheller, Muller et al. 2003; Pfurtscheller, Neuper et al. 2003; Wolpaw and McFarland 2004). This chapter sought to apply a neuroprosthetic system controlled from the unaffected hemisphere in chronic stroke survivors. The body of this chapter is drawn from our previously published manuscript (Bundy, Wronkiewicz et al. 2012)[2].

5.1 Introduction

Currently a challenge in the treatment of stroke survivors is the rehabilitation of chronically lost motor functions. Several studies describing hemiparesis in chronic stroke survivors demonstrate that motor recovery plateaus 3 months post-stroke (Duncan, Goldstein et al. 1992; Jorgensen, Nakayama et al. 1995; Lloyd-Jones, Adams et al. 2009). A potential novel approach for the restoration of function and improving the quality of life of these patients could be the use of a

[2] As the first author of this manuscript I collected the data, screened for and implemented the BCI control, designed and performed the posthoc data analyses, and led the writing of the manuscript.

brain computer interface (BCI). These systems use signals recorded from the central nervous system as a control signal for operating a computer or other device. Restoring function could be accomplished either through controlling an assistive device independent of the unaffected hand, or through paired BCI control and peripheral stimulation to induce functional recovery through endogenous plasticity. Thus far, substantial research has shown that information from motor cortex contralateral to an intended limb encodes useful information about motor intent and can be used to control BCI systems with multiple degrees-of-freedom using a variety of recording modalities (Taylor, Tillery et al. 2002; Leuthardt, Schalk et al. 2004; Hochberg, Serruya et al. 2006; Schalk, Miller et al. 2008; Velliste, Perel et al. 2008; Rouse and Moran 2009). While these physiologic signals are useful in controlling BCI systems designed for motor-impaired patients with intact cortices (Pfurtscheller, Guger et al. 2000; Taylor, Tillery et al. 2002; Leuthardt, Schalk et al. 2004; Kubler, Nijboer et al. 2005; Hochberg, Serruya et al. 2006), a different cortical signal would be necessary in hemiplegic stroke survivors that suffer damage to primary motor cortex contralateral to the affected limb. This is important both in a traditional BCI device (which enables brain-derived control of an assistive machine) and also in potentially encouraging functional rehabilitation (to facilitate endogenous recovery of limb function). Taken together, there is a substantive need to develop new methods for restoring function in chronic hemiplegic stroke survivors, which may be accomplished through utilizing novel cortical control signals in conjunction with a BCI system.

Recent work by Wisneski et al. has demonstrated a separable and distinct cortical physiology associated with ipsilateral hand movements (i.e. movements on the same side as the respective hemisphere) that can be distinguished from cortical signals associated with movement contralateral to a given hemisphere (2008). Electrocorticographic (ECoG) signals were recorded

while motor-intact human patients engaged in specific ipsilateral or contralateral hand motor tasks. Ipsilateral hand movements were associated with electrophysiological changes that occurred in lower frequency spectra (average 37.5Hz), at distinct anatomic locations (most notably in premotor cortex), and earlier (by 160 ms) than changes associated with contralateral hand movements. Given that these cortical changes occurred earlier and were localized preferentially in premotor cortex compared to those associated with contralateral movements, the authors postulated that ipsilateral cortex is more associated with motor planning than its execution. Furthermore, while rehabilitation from stroke has traditionally been viewed as a "perilesional awakening" of cortex (Weiller, Chollet et al. 1992; Tecchio, Zappasodi et al. 2006), recent studies in stroke survivors have shown that the potential for recovery is inversely correlated to corticospinal tract damage (Carter, Patel et al. 2011). While in general, outcome is better when perilesional activity produces a more normal pattern of contralateral activation after stroke (Ward, Brown et al. 2003a; Ward, Brown et al. 2003b), this often may not occur because of the severity of the injury to the corticospinal tract or cortex. Furthermore, ipsilateral activity has been shown to play a role in the planning of arm movements (Schaefer, Haaland et al. 2009b; Schaefer, Haaland et al. 2009a), and activity from the ipsilateral unaffected hemisphere has been shown to increase with increases in functional outcome in some patients (Cramer, Nelles et al. 1997; Tecchio, Zappasodi et al. 2006). Therefore, the unaffected hemisphere would provide an alternative pathway, allowing it to play a compensatory role in motor control in people with severe lesions. Additionally, it has been shown in hemiplegic stroke survivors that ipsilateral motor activity is independent of contralateral motor activity and that affected and unaffected limb movements can be discriminated from neural activity in a single hemisphere (Cramer, Mark et al. 2002). Taken together, these indicate that 1) there is a separable physiology associated with

actively planning and executing ipsilateral hand movements and 2) that this physiology appears to be involved in the functional reorganization of unaffected cortex and represents an alternative pathway that may facilitate some level of recovery in patients with large cortical lesions or lesions transecting the corticospinal tract.

In the past, a few case studies have demonstrated the use of BCI systems utilizing perilesional cortex contralateral to the affected limb in individual stroke survivors (Buch, Weber et al. 2008; Daly, Cheng et al. 2009; Broetz, Braun et al. 2010). This project, however, sought to develop a wholly new approach by creating a contralesional BCI in stroke survivors. In this study, we examined whether the physiology associated with ipsilateral hand movements could be used as a control signal for a BCI in hemispheric stroke patients (Figure 5.1).

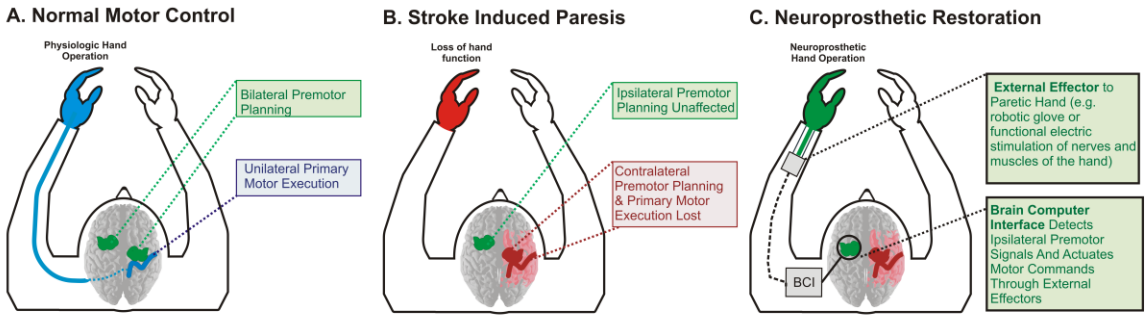

Figure 5.1 Conceptual schematic of ipsilateral BCI using the unaffected hemisphere
After a hemispheric stroke, motor-impaired stroke survivors will have damage to the contralateral primary and premotor cortices or their associated subcortical pathways. In order to implement a BCI system, we propose that an effective alternative control signal is the ipsilateral premotor planning region in the unaffected hemisphere.

Because brain signals were found to be optimal below 40 Hz and located in more prefrontal regions, we hypothesized that these signals would be accessible with electroencephalography (EEG) and provide sufficient information to control a simple device. We demonstrate for the first time that this ipsilateral cortical physiology can be effectively used to control a cursor in a one-dimensional control task. These findings support the feasibility of using brain signals from the

unaffected hemisphere as a signal platform in the setting of unilateral stroke for potential functional restoration. This approach is especially salient in dense hemiplegics for whom there is an absence of rehabilitation options or alternatives because they have minimal functional capacity to participate in current rehabilitation paradigms.

5.2 Methods

5.2.1 Patients

This study utilized four chronic first time (17-53 months post-stroke) hemispheric stroke survivors (age 48-61). Exclusion criteria included prior strokes. Additionally patients who had suffered strokes that resulted in dementia, inattention, or aphasia, which would prevent participants from performing the required cognitive tasks, were also excluded. The study was approved by the Institutional Review Board of the Human Research Protection Organization of the Washington University Medical Center. Prior to inclusion in the study, participants provided their written informed consent. Participants were enrolled from a previous study (Carter, Astafiev et al. 2010; Carter, Patel et al. 2011), which provided data on lesion localization and chronic functional evaluation. Prior to enrollment in the study, lesion locations and functional motor evaluations were considered from over 40 potential participants. The 4 patients utilized were selected considering the exclusion criteria as well as the fact that more severely impaired patients represent the population more likely to benefit from BCI applications. Before this study, patients had no prior training on the use of a BCI system. Demographic and clinical information for each of the four patients is shown in Table 5.1.

Table 5.1 Demographic and clinical information

Patient	Age	Sex	Time from stroke (mos.)	Lesion Side	Lesion Location	Chronic Motor Function Evaluation							
						ARAT Contra Scores					Contra Grip Strength	Ipsi Grip Strength	Clinical Hand Strength
						Total	Grasp	Grip	Pinch	Gross			
1	48	M	53	Right	MCA	-	-	-	-	-	-	-	4/5 Contra; 5/5 Ipsi
2	65	F	17	Right	MCA	0/65	0	0	0	0	-	-	-
3	54	F	26	Left	Scattered Lacunar	41/65	13	12	13	3	1.3 kg	19.7 kg	-
4	61	M	20	Left	MCA	30/65	18	8	2	2	4.7 kg	30.7 kg	-

5.2.2 Lesion Segmentation

Segmentation of stroke lesions was performed as described in Carter et al. using T1-weighted MP-RAGE and T2-weighted spin echo images (Carter, Astafiev et al. 2010). Voxels were categorized into air, cerebrospinal fluid (CSF), gray matter, and white matter by an unsupervised fuzzy class means-based segmentation. Expert judgment was used to determine the boundary between CSF and lesioned parenchyma. Figure 5.2 shows the location and extent of lesions in each patient.

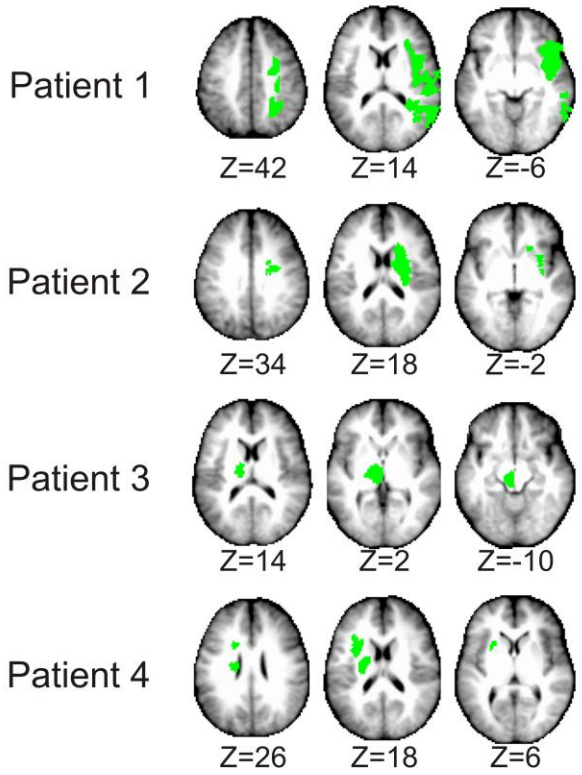

Figure 5.2 Lesion characteristics
Lesion locations segmented from T1-weighted MP-RAGE and T2-weighted spin echo images. Selected axial slices show upper, intermediate, and lower areas of the lesion (Left-on-left orientation).

5.2.3 EEG Recordings

In all patients, EEG was recorded from 33 (Patients 1 and 2) or 45 (Patients 3 and 4) scalp locations over frontal and parietal regions within the 10-20 system of electrode locations. Recording locations were channel positions AF5, AF3, AFZ, AF4, AF6, F5, F3, F1, FZ, F2, F4, F6, FC5, FC3, FC1, FCZ, FC2, FC4, FC6, C5, C3, C1, CZ, C2, C4, C6, CP5, CP3, CP1, CPZ, CP2, CP4, CP6 (all patients) and P5, P3, P1, PZ, P2, P4, P6, PO5, PO3, POZ, PO4, PO6 (Patients 3 and 4 only). Recordings were digitized using 16-channel digital amplifiers (g.USBamp, g.tec, Austria). The left and right ear lobes were used as the ground and reference respectively. Signals were spatially filtered using a bipolar derivation to enhance the spatial specificity of recordings. Recordings were sampled at 256 Hz (Patients 1 and 2) or 512 Hz

(Patients 3 and 4) and were high-pass filtered at 0.1 Hz prior to analysis. A Dell computer running the BCI2000 software platform was used to acquire, process, and store the EEG data for real-time stimulus presentation and time-locked acquisition and analysis of brain signals (Schalk, McFarland et al. 2004a).

5.2.4 Control Feature Screening

Initially, patients underwent screening to identify features of cortical activity to be used in subsequent closed-loop BCI control experiments. This procedure involved an experiment in which EEG signals were recorded while the patient performed overt or imagined self-timed, self-selected finger-tapping movements of the right or left hand in isolation from the opposite hand or rested. Cues for the rest and finger movement conditions were presented as words (‘Right’, ‘Left’) and a fixation cross (Rest) on a computer screen that was placed approximately 75cm in front of the patient. For the overt movement condition, patients with residual function in their affected hand (Patient 1) were instructed to perform overt movements of both hands, while those with less function in the affected hand were instructed to perform overt movements of the unaffected hand and intended movements of the affected hand. In a second screening task, all patients were instructed to perform imagined movements of both the affected and unaffected hands. Cues were presented in a random order with each stimulus presented for a period of 2.5 seconds. Patients were instructed to perform the specified action for the duration of the stimulus presentation. In patients with chronic hemiplegia preventing individual finger movements of the affected hand (Patients 2, 3, and 4) the patients were instructed to overtly move their unaffected hand and imagine similar movements of the affected hand during the respective stimulus periods. All patients performed the overt movement task initially while being observed for successful task performance, followed by performance of the imagined movement task.

EEG data collected during the experiment were converted from the time domain to the frequency domain using the maximum entropy method for autoregressive spectral estimation (Marple 1987a). Power spectra were estimated in 2 Hz bins ranging from 1 to 55 Hz. Candidate features were identified by calculating the signed coefficient of determination (r^2) between the 'rest' interval spectral power levels and the affected hand movement spectral power levels. EEG features in particular electrodes and frequency bands with the greatest percentage of their variance explained by the task (i.e. the highest r^2 values), were chosen as candidate control features for closed-loop BCI experiments. Selection of candidate control features was also further constrained to contain only electrodes over the unaffected hemisphere during movement or imagined movement of the affected hand. Where possible, candidate features were selected to discriminate affected hand movement from rest as well as affected hand movement from unaffected hand movement.

5.2.5 Closed-loop BCI Evaluation

After determining candidate EEG control features associated with intended movement of the affected hand using the screening procedure described previously, patients participated in closed-loop BCI control evaluation (see Figure 5.3). For this evaluation, the patient's objective was to perform intended movements of the affected hand in order to hit a target with a cursor. The target was presented on either the right or left side of a screen and the cursor moved along a single dimension. Several control scenarios were tested; (1) overt movement of the affected hand versus rest (Patient 1), (2) intended movement of the affected hand versus rest (Patients 2, 3, and 4), and (3) imagined movement of the affected hand versus imagined movement of the unaffected hand (Patients 1 and 2). The various closed-loop control conditions used depended upon the discriminability of control features as well as patient attention and fatigue.

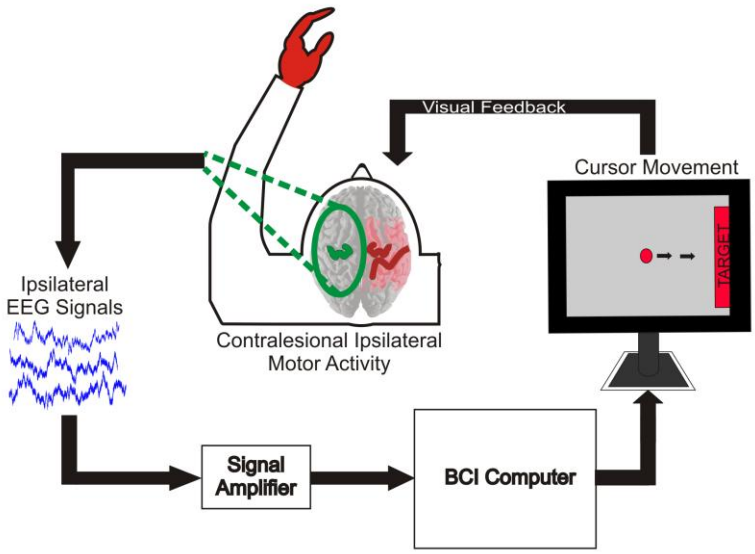

Figure 5.3 Closed-loop control with ipsilateral motor signals
Experimental setup used for the closed-loop control task. The on screen cursor moves toward target with performance of appropriate intended motor movement. Cursor movement is driven by the pre-screened control features derived from the EEG signals recorded from the patient's unaffected hemisphere.

The velocity of the cursor was calculated from the real-time EEG features through the BCI2000 software package. The change in power from baseline of the selected EEG features (i.e. the power in the selected frequency bin(s) at the selected electrode location(s) over the unaffected hemisphere) were weighted and summed to allow the patient to control the cursor. As all of the features identified for these patients were power decreases, they were weighted negatively so the task-related score increased with task-related power decreases. The feature power levels were translated into the cursor score through BCI2000 (Schalk, McFarland et al. 2004a). In order to normalize the weighted and summed power levels, the normalizer was trained using several trials in each target direction in which the patient attempted to perform the selected control task (i.e. affected hand movement, resting) in order to control the cursor. The mean of the weighted and summated features was calculated after the training period (1-2 minutes) and was used to normalize the scores to have zero mean. The normalized score was then used to control the cursor velocity. The velocity of the cursor was updated every 40 ms based upon spectra

estimated from an autoregressive method using data acquired over the previous 280 ms. Patients performed consecutive trials in which they attempted to move the cursor to the presented target. Each trial began with the presentation of a target randomly selected to be at either the right or left side of the screen. After a 1 second delay, the cursor appeared in the middle of the screen with its motion in the horizontal dimension controlled by the patient's EEG signals. The patient was instructed to begin performing the particular hand movement task or rest condition to move the cursor to the selected target as soon as the target appeared on the screen. Each trial was assessed as a success (cursor hit the selected target), or failure (cursor hit the opposite target or time ran out before success occurred, 6-10 seconds). Trials were grouped into runs of 2 minutes with rest periods of approximately 1 minute in between runs. The accuracy was assessed as the number of successful trials divided by the total number of trials at the end of each run. The development of BCI control over time was assessed by comparing the accuracy at the end of each consecutive run after training with a particular task and associated EEG control features. Because each trial did not have to result in a target being hit, chance was not necessarily 50%. As described previously by Leuthardt et al., chance performance was determined by running multiple runs of control trials using Gaussian white noise signals yielding a mean chance performance of 46.2% (2.7% SD) (Leuthardt, Gaona et al. 2011). Patients performed between 85 and 246 control trials.

5.3 Results

Each patient demonstrated cortical activations in the unaffected hemisphere associated with intended movement of the affected hand. Figure 5.4 displays that for each patient there was a cortical activation during intended movement of the affected hand within the ipsilateral cortex (within the unaffected hemisphere).

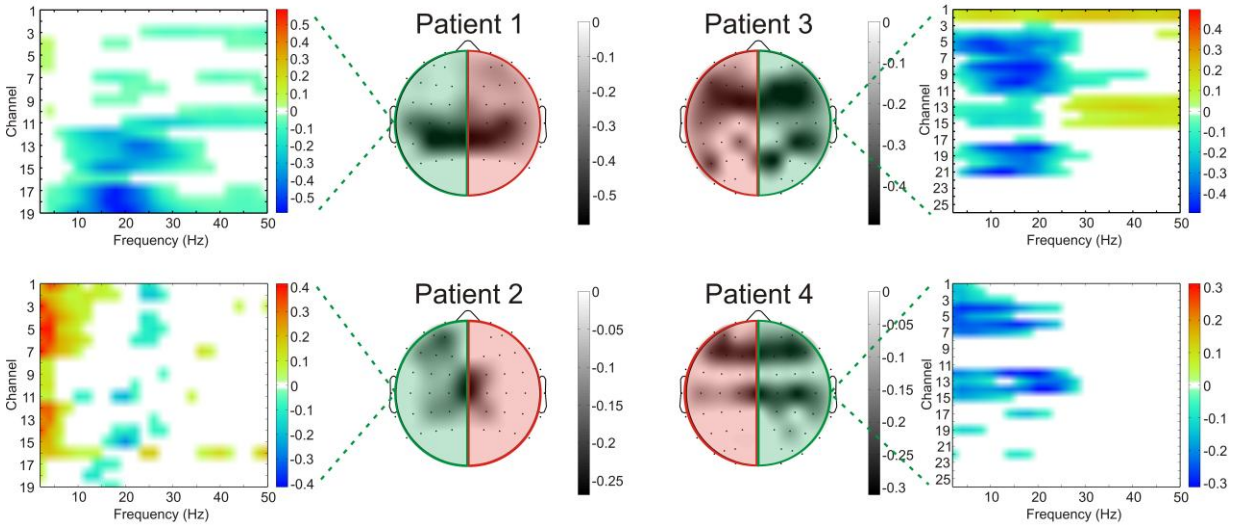

Figure 5.4 Topography of screening task activations

Topographical maps of the maximum coefficient-of-determination of significant ($p<0.05$) event-related power decreases between 0 Hz and 50 Hz for affected hand movement vs. rest conditions in each patient. As power decreases cause more negative signed r^2 values, more negative areas in the topographic activations represent increased neural activity. Green and red highlighting on the topographic plots illustrates the unaffected and affected hemisphere in each patient respectively. Feature plots demonstrate significant ipsilateral coefficient-of-determination values from the unaffected hemisphere across the frequency spectrum, illustrating that the cortical activations are observed across the frequency spectrum, but particularly in the mu (8-12 Hz) and beta (12-30 Hz) bands. Channels displayed on the feature plots correspond to electrode positions AF5, AF3, AFZ, F5, F3, F1, FZ, FC5, FC3, FC1, FCZ, C5, C3, C1, CZ, CP5, CP3, CP1, CPZ (Patients 1 and 2) and AFZ, AF4, AF6, FZ, F2, F4, F6, FCZ, FC2, FC4, FC6, CZ, C2, C4, C6, CPZ, CP2, CP4, CP6, PZ, P2, P4, P6, POZ, PO4, PO6 (Patients 3 and 4).

Notably, consistent with Wisneski el al., when these ipsilateral motor activations in the unaffected hemisphere associated with movement intentions of the affected hand were compared to cortical activations in the unaffected hemisphere associated with movement intentions of the unaffected hand (i.e. contralateral movements) there were notable differences in frequency spectra and anatomic locations (Wisneski, Anderson et al. 2008). Figure 5.5 illustrates this spectral distinction in cortical activity within a single exemplar patient (Patient 3). In this patient, the topography at 18 Hz is broad and fairly similar between ipsilateral and contralateral movement, while there are distinct differences in topography at the higher beta (26 Hz) and low gamma (>30 Hz) frequencies. Most notably there is a more extensive activation in the prefrontal region (in the left unaffected hemisphere) that demonstrates a 26 Hz power modulation with ipsilateral right hand movement that is not present with contralateral left hand movement.

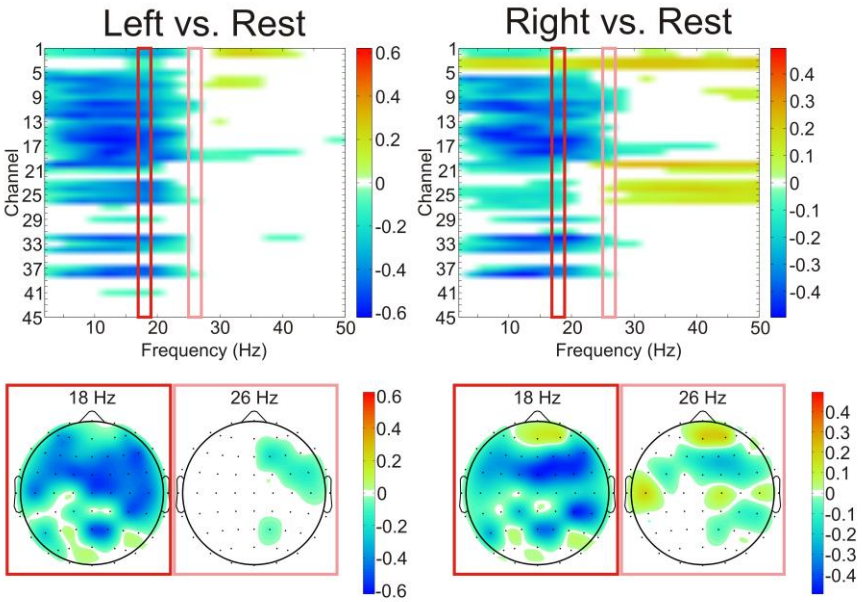

Figure 5.5 Spectral specificity of neural activity within an exemplar patient
Feature plots demonstrating the frequency specificity of movements of the affected (right) and unaffected (left) hands in an exemplar patient who had a stroke affecting the left hemisphere (Patient 3). The topography at 18 Hz is broad and fairly similar between the two conditions, while there are distinct differences in topography at the higher beta (26 Hz) frequency. Channel numbers correspond to electrode locations AF5, AF3, AFZ, AF4, AF6, F5, F3, F1, FZ, F2, F4, F6, FC5, FC3, FC1, FCZ, FC2, FC4, FC6, C5, C3, C1, CZ, C2, C4, C6, CP5, CP3, CP1, CPZ, CP2, CP4, CP6, P5, P3, P1, PZ, P2, P4, P6, PO5, PO3, POZ, PO4, PO6.

Moreover, when examining all patients, various locations and EEG frequencies separated intended affected hand movements both from rest and from unaffected hand movements (Figure 5.6). The locations that optimally separated ipsilateral from contralateral intentions in the unaffected hemisphere were located both over traditional sensorimotor regions, as well as more anterior areas associated with premotor planning. Furthermore, qualitatively it was observed that patients with more severe motor impairments demonstrate a more anterior shift in the activations within the unaffected hemisphere associated with intended movement of the ipsilateral affected hand. This shift in ipsilateral activity is similar to the anterior and ventral shift in ipsilateral activity shown by Cramer et al. with fMRI (Cramer, Finklestein et al. 1999).

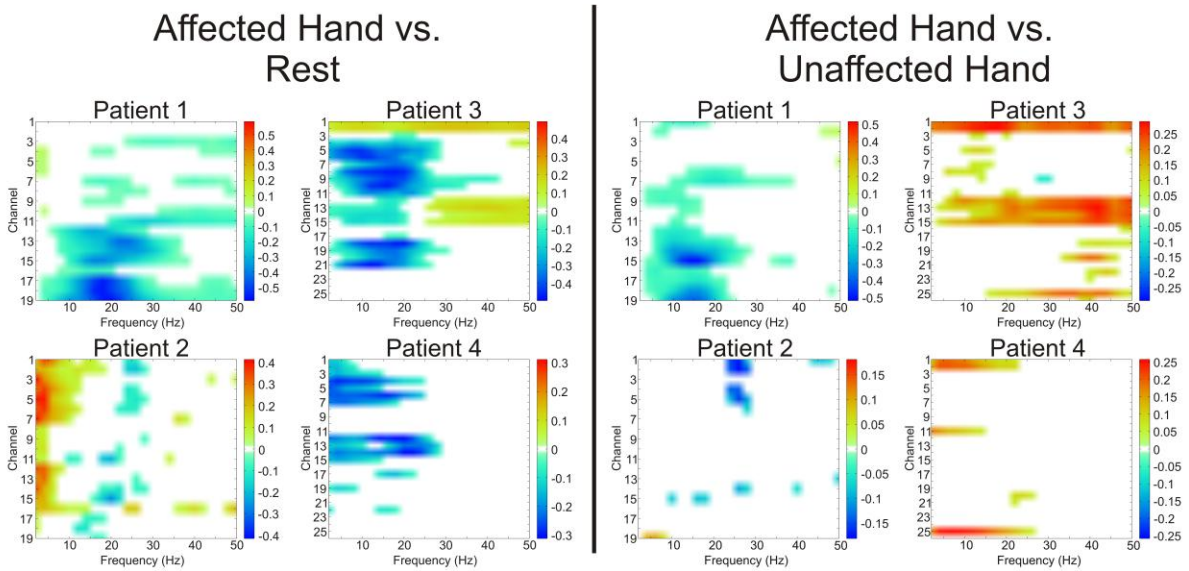

Figure 5.6 Spectral specificity differentiates movement conditions across patients
Feature plots demonstrate significant ($p<0.05$) r^2 values differentiating affected hand movements from rest (left plots) and affected hand movement from unaffected hand movements (right plots) based upon electrodes located over the unaffected hemisphere. All four patients show significant decreases in power related to intended movement of the ipsilateral, unaffected hand. Additionally, 3 of the 4 patients have unique spatial and spectral activations differentiating affected hand and unaffected hand movements within the unaffected hemisphere either through decreases in power in the alpha (9-12Hz) or Beta (12-30Hz) bands (Patients 1 and 2) or increases in gamma band (>30 Hz) power (Patient 3). Channels displayed correspond to electrode positions AF5, AF3, AFZ, F5, F3, F1, FZ, FC5, FC3, FC1, FCZ, C5, C3, C1, CZ, CP5, CP3, CP1, CPZ (Patients 1 and 2) and AFZ, AF4, AF6, FZ, F2, F4, F6, FCZ, FC2, FC4, FC6, CZ, C2, C4, C6, CPZ, CP2, CP4, CP6, PZ, P2, P4, P6, POZ, PO4, PO6 (Patients 3 and 4).

Select features were then identified for subsequent online BCI operation. Figure 5.7 illustrates the significant ($p<0.05$) activations differentiating movements of the affected hand from rest, the unaffected hand from rest, and the affected hand from the unaffected hand at frequencies utilized for subsequent BCI control by each patient.

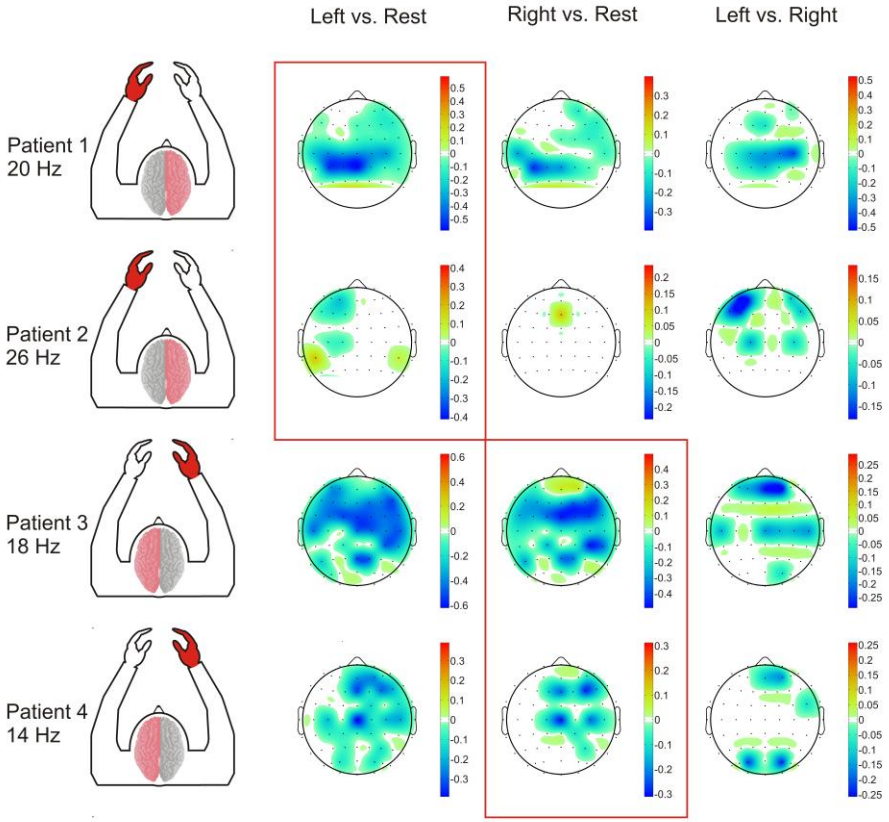

Figure 5.7 Topography of screening task activations
Topographical maps of significant ($p<0.05$) coefficient of determination values from the motor screening task are shown for all patients. The stroke injured hemisphere and affected hand area are labeled in red. Frequency bands shown correspond to those utilized in each patient's respective closed-loop BCI control experiments. All patients demonstrated significant activations related to intended movements of their affected hand in their unaffected hemisphere (highlighted within the red boxes).

The time course of each patient's performance during closed-loop BCI control is shown in Figure 5.8. Peak target accuracies for all patients were all between 62.5% and 100% and final accuracies for all patients were between 53.6% and 100% and therefore were all above chance (46.2%, 2.7% SD). This level of performance was achieved in BCI control experiments with durations ranging from 6 to 10 minutes. Table 5.2 summarizes the activities utilized for BCI control, the EEG features used, and the peak and final BCI accuracy achieved by each patient.

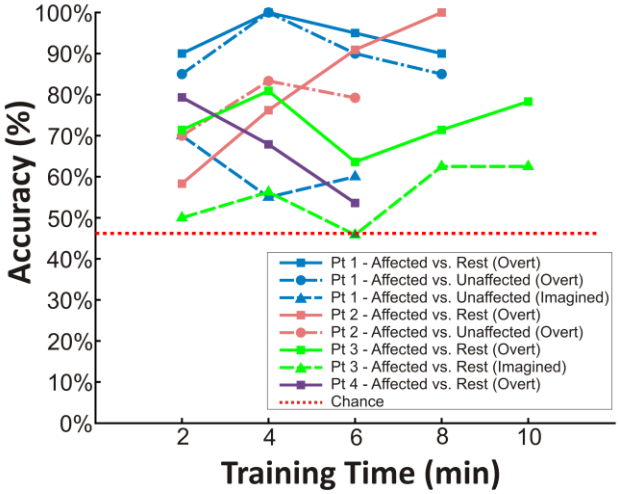

Figure 5.8 Learning curves for BCI control tasks
All patients achieved peak accuracies greater than 62.5% with only 6 to 10 minutes of training time.

Table 5.2 Closed-loop BCI performance data

Patient	Task (Direction)	EEG Channels	Frequency Used	Peak Accuracy	Final Accuracy
1	Affected Hand (Left) vs. Rest (Right) Overt	CP3, CP1	18 - 22 Hz	100%	90%
	Affected Hand (Left) vs. Unaffected Hand (Right) Overt	C1	12 - 18 Hz	100%	85%
	Affected Hand (Left) vs. Unaffected Hand (Right) Imagined	C1	12 - 18 Hz	70%	60%
2	Affected Hand (Left) vs. Rest (Right) Overt	AF5, AF3, F3, F1	24 - 28 Hz	100%	100%
	Affected Hand (Left) vs. Unaffected Hand (Right) Overt	AF5, AF3, F3, F1	24 - 28 Hz	83.30%	79%
3	Affected Hand (Right) vs. Rest (Left) Overt	FC2, FC4	16 - 18 Hz	80.90%	78.30%
	Affected Hand (Right) vs. Rest (Left) Imagined	FC2, FC4	16 - 18 Hz	62.50%	62.50%
4	Affected Hand (Right) vs. Rest (Left) Overt	CP2, F2	12 - 14 Hz	79.30%	53.60%

The EEG recordings from the closed-loop control experiments were also examined post-hoc to compare the cortical activations associated with the screening task to those associated with the closed-loop task. The activations in the selected EEG control frequency for the affected hand movement versus rest conditions are shown for both the screening and control experiments in Figure 5.9. As can be seen, there is good correspondence between the topographies of the activations during the control and screening task, indicating that the successful BCI control performance was achieved through performance of the intended motor task and not a spurious or alternative strategy. Furthermore, correlations between the topography of activations in the

selected control frequency between screening and control tasks (Patient 1: R=0.82, p<0.0001; Patient 2: R=0.6108, p=0.0002; Patient 3: R=0.7098, p<0.0001; Patient 4: R=-0.0194; P=0.8994) were highly significant in 3 of the 4 patients. The discrepancy in Patient 4 can be attributed to the patient tiring towards the end of the session, likely leading to changes to cortical activations due to decreases in attention to the task. This decrease in attention and different neural activity would also explain the fact that Patient 4 demonstrated poorer peak and final BCI control accuracies than the other 3 patients.

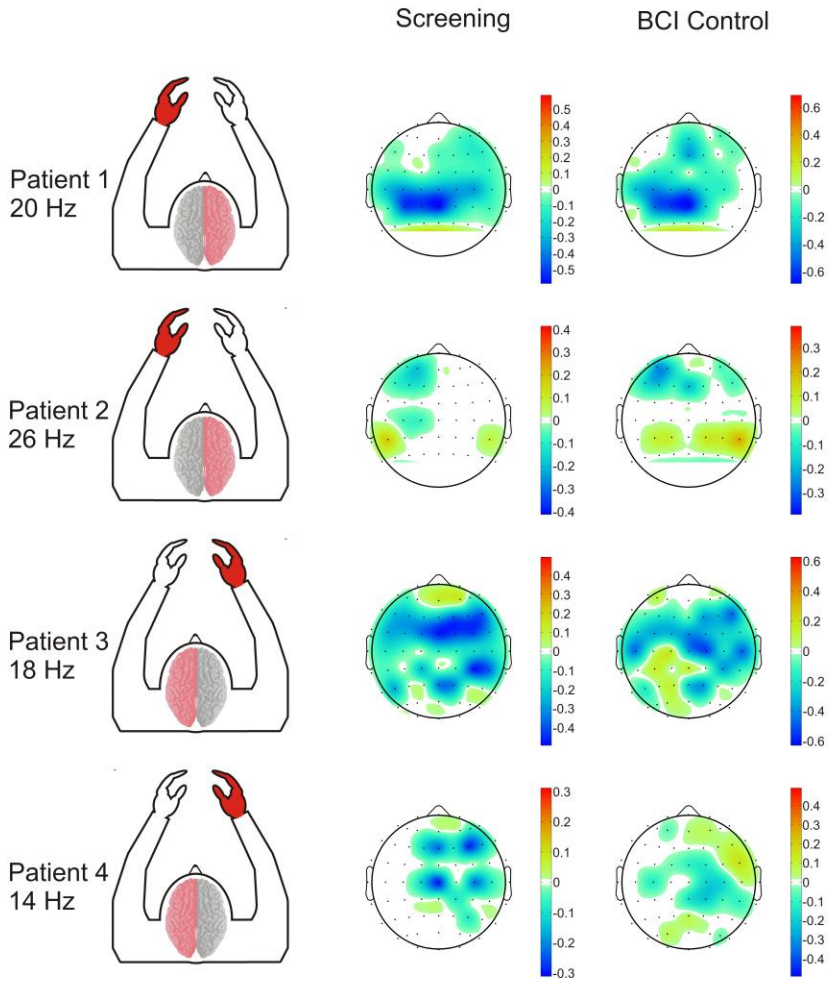

Figure 5.9 Comparison of neural activity during screening and BCI control
Significant (p<0.05) coefficient of determination values for affected hand vs. rest conditions during motor screening and control tasks. The stroke injured hemisphere and affected hand area labeled in red. Selected frequencies were utilized for overt/intended

affected hand vs. rest control in each patient. Patients exhibit similar topographies of activations, indicating that patients likely utilized the screened motor activity to achieve BCI control. Correlation values between topographies of the screening and control task were (Patient 1: R=0.82, p<0.0001; Patient 2: R=0.6108, p=0.0002; Patient 3: R=0.7098, p<0.0001; Patient 4: R=-0.0194; p=0.8994).

5.4 Discussion

This paper presents an important demonstration for the potential that hemispheric stroke survivors could use the unaffected side of their brain to potentially restore function after their unilateral motor deficit through the use of a BCI. By identifying cortical signals associated with ipsilateral hand movements, an EEG-based BCI can capture the brain's intention to move a paretic hand. This can be accomplished irrespective of their actual capacity to execute a motor movement due to their injured primary motor cortex and/or descending white matter tracts. In this study, we demonstrate that it is possible to detect in EEG over the unaffected cortex, real and imagined intentions to move the stroke affected hand and, for the first time, show that these unaffected hemisphere signals can be used for simple brain-derived control of a device. Patients achieved BCI control with peak accuracy rates between 62.5% and 100% rapidly, often with only a 30 minute screening task and less than 15 minutes of training. Importantly, these ipsilateral motor signals were distinct in anatomic location and spectral content from the cortical physiology associated with contralateral movements. This separable physiology and its ease of use for a BCI, provides an important first step towards using neuroprosthetic systems for a currently large and underserved patient population with motor disability. Given that stroke is the most common neurological disorder, affecting 795,000 patients per year in the U.S. alone (Lloyd-Jones, Adams et al. 2009), these findings can substantially extend the potential clinical impact of neuroprosthetic approaches.

This work was unique in its focus on using neural activity in the unaffected hemisphere related to intended movement of the ipsilateral limb for controlling a BCI system. While other studies have

investigated the use of control signals from perilesional cortical areas (Buch, Weber et al. 2008; Daly, Cheng et al. 2009; Broetz, Braun et al. 2010), this is the first study to focus exclusively on ipsilateral motor activity from the unaffected hemisphere after stroke. This is important because BCI systems are likely to be most clinically relevant to stroke survivors with a chronic unrecovered hemiplegic motor deficit. Because stroke survivors with any residual motor functions are likely to be candidates for current rehabilitation methodologies (Takahashi, Der-Yeghiaian et al. 2008; Wolf, Thompson et al. 2010), BCI systems are likely to be used either by the most severely motor-impaired patients who have had an absence of any function from the stroke onset (limiting their rehabilitation options), or have failed to recover function after extensive therapy. Often these patient populations are likely to have significant cortical and/or subcortical lesions that transect the corticospinal tract descending to contralateral motor pathways (Binkofski, Seitz et al. 1996; Schaechter, Perdue et al. 2008 ; Carter, Patel et al. 2011). Because of these significant lesions, these patients are likely to have atypical neural activity in the affected hemisphere during intended movement of the contralateral limb when compared with normal controls (Calford and Tweedale 1990). By using ipsilateral motor intentions in the undamaged hemisphere for a BCI control signal, the impact of the stroke with regards to the quality of the control signal will be minimized. Taken together, there are likely two ways in which this methodology could be applied, either as a chronic BCI system for long-term assistive device control, or as BCI-assisted rehabilitation tool.

As in traditional BCI systems, stroke survivors could control an artificial device to aid in daily tasks or manipulate the hemiplegic limb. Building on work by Wisneski et al., who showed that motor-intact patients could use ipsilateral motor signals for BCI control, this study extended those findings by demonstrating that stroke survivors can intentionally modulate similar

ipsilateral motor signals from their unaffected hemisphere to control a BCI system. Several of the patients in this study had fairly significant motor impairments from their strokes (Patients 2, 3, and 4). Importantly, these patients generally had shifts of the ipsilateral motor activity in their unaffected hemispheres to locations anterior to traditional sensorimotor cortices. This finding is in line with other results that have demonstrated changes in motor activity ipsilateral to the unaffected hemisphere (Cramer, Nelles et al. 1997; Green, Bialy et al. 1999; Tecchio, Zappasodi et al. 2006). It is important to note that the ipsilateral control signals were used to control a cursor on a screen as a proof of concept. This control could be easily extended to a simple one-dimensional grasping hand orthotic that could facilitate activities of daily living (Lauer, Peckham et al. 1999).

With regards to the choice of signal platform for utilizing an assistive BCI system after stroke, there are several considerations to take into account. In order to implement a traditional assistive BCI system, it will be important to scale the BCI control to a greater number of degrees of freedom. Currently, non-invasive BCI systems have produced at most 3 degrees-of-freedom in online task performance (McFarland, Sarnacki et al. 2010). This level of control required a large amount of training and utilized signals from both cortical hemispheres and midline electrodes that were related to movements of the feet and both hands. Given the broad cortical activations observed in EEG recordings, the necessity of developing BCI systems independent of the normal operation of the unaffected hand for completion of bimanual tasks, and cognitive limitations that will limit the total amount of BCI training time that some patients can undergo, it is doubtful that EEG would allow for discernment of grasping and kinematic hand movements necessary for scaling an ipsilateral BCI system to a higher number of degrees of freedom in stroke survivors. Therefore, more complex control may require more invasive approaches such as

electrocorticography (ECoG). To date, more complex movement kinematics of both hand and finger movements have been shown to be discernable using either macro-scale or micro-scale ECoG signals (Wisneski, Anderson et al. 2008; Zanos, Miller et al. 2008; Leuthardt, Freudenberg et al. 2009; Scherer, Zanos et al. 2009). Additionally, ECoG has allowed for off-line decoding of 2D joystick movements from ipsilateral cortex (Ganguly, Secundo et al. 2009; Sharma, Gaona et al. 2009). Furthermore, the results presented in Chapter 3 also show that ECoG signals can be used for off-line decoding of 3D reaching movements from ipsilateral cortex. As work continues to develop BCI systems for chronic stroke survivors, it will be important to gain a better understanding of the changes to the specific cortical dynamics associated with ipsilateral motor activity after stroke and the optimal signal platform that provides the highest benefit relative to the clinical risk of implementation.

In addition to providing a means for long-term assistive device control after stroke, BCI systems may provide a novel rehabilitation tool. The choice of motor signals from the unaffected hemisphere in this study has particular relevance to the potential for using BCI systems as a rehabilitation methodology. A number of previous studies have demonstrated changes in ipsilateral motor activity from the unaffected hemisphere after stroke. Functional imaging of chronic stroke survivors has shown increases in the ipsilateral motor activations of the unaffected hemisphere after recovery from stroke when compared to normal controls (Weiller, Chollet et al. 1992; Weiller, Ramsay et al. 1993; Cramer, Nelles et al. 1997; Nelles, Spiekramann et al. 1999; Tecchio, Zappasodi et al. 2006) as well as increases in ipsilateral, contralesional activity after constraint induced movement therapy (CIMT) (Levy, Nichols et al. 2001; Schaechter, Kraft et al. 2002). Furthermore, inhibitory transcranial magnetic stimulation in the unaffected premotor cortex slowed the reaction times for affected hand movements in stroke survivors (Johansen-

Berg, Rushworth et al. 2002). While these results seem to indicate that ipsilateral activity from the unaffected hemisphere plays a facilitating role in recovery of motor function after stroke, there are also a number of studies that have shown potentially contradictory findings regarding increases in ipsilateral, contralesional motor activity after stroke. In particular, low ipsilateral TMS thresholds were associated with poor recovery after stroke (Turton, Wroe et al. 1996; Netz, Lammers et al. 1997) and decreases in ipsilateral activity from the unaffected hemisphere correlated with longitudinal and cross-sectional studies of recovery (Ward, Brown et al. 2003a; Ward, Brown et al. 2003b). It is important to note that several of the studies described above demonstrated both perilesional changes in activity, as well as ipsilateral activity from the unaffected hemisphere after recovery, indicating that both cortical areas may lead to recovery (Green, Bialy et al. 1999; Levy, Nichols et al. 2001). Furthermore, another study revealed that patients who recover completely showed few changes to the location of their contralesional motor activity, while patients that recovered incompletely showed better recovery with increased ipsilateral activity in the unaffected hemisphere (Tecchio, Zappasodi et al. 2006). This makes sense when one considers that corticospinal tract damage is highly correlated with motor impairment after stroke (Fries, Danek et al. 1993; Carter, Patel et al. 2011). While patients with some residual motor function will most likely rehabilitate through reorganization of residual motor pathways, those for whom it is totally obliterated will likely need to develop new cortical and subcortical pathways (i.e. contralesional/ipsilateral motor pathways) for a more limited recovery. Thus, the patients that are most likely to be candidates for a BCI-based therapy are those who have substantial damage to their corticospinal tract, requiring that an alternative pathway be utilized for functional rehabilitation to take place. Because of this, the results described in this paper demonstrating that stroke survivors can utilize ipsilateral motor activity

from their unaffected hemisphere to control a BCI system represent a significant step in the development of a BCI system for encouraging rehabilitation after stroke. Moreover, in the setting of rehabilitation where the BCI is only needed transiently and the goal is to augment cortical plasticity, lower degrees of freedom for a less invasive option may be an ideal tradeoff in this clinical context.

While this work represents an exciting demonstration of the possibilities for stroke survivors to achieve increased function through controlling BCI systems with neural activity in their unaffected hemisphere, there are several limitations and future considerations. First, the work represents only a limited number of patients and while one patient (Patient 1), had some recovery, most of the patients were selected for participation because they had more significant motor impairments, making them more representative of the patient population most likely to benefit from BCI applications. Because of this it is unknown how well these results will generalize to the broader population of stroke survivors. However, the population included patients with lesions of both hemispheres as well as both cortical and subcortical infarcts (see Table 5.1), indicating that patients with various lesion types and locations can utilize BCI systems. Furthermore, because BCI systems will most likely be applied to the most significantly impaired patients, the study population does represent the intended clinical population. Second, it is impossible to ensure that the BCI control is truly achieved through the screened motor imagery task, particularly in cases in which patients have no visible motor control. In this study however, the similarity between neural activity during the screening and control tasks (see Figure 5.9) provide evidence that the patient is indeed performing the imagery task indicated. Additionally, a BCI system needs to function independently of the unaffected hand to allow for completion of bimanual tasks. Because of differences in the attentional requirements of attempting to move the

unaffected hand, it is difficult to truly assess the independence of the ipsilateral, contralesional motor signals and the traditional contralateral, contralesional motor signals during bimanual tasks, however, the ability of two patients (Patients 1 and 2) to achieve on-line control with alternating movements of the affected and unaffected hands provides evidence that ipsilateral, contralesional motor activity is independent from unaffected hand movement in this patient population. Finally, it is important to note that the observed increase in ipsilateral, contralesional activations after stroke may represent increases in the attentional requirements of attempting to move the affected hand (Johansen-Berg, Rushworth et al. 2002). Regardless of whether this represents increased attention as has been postulated from previous imaging literature or enhancements in motor planning, once this signal is identified and engaged by the user, its utilization becomes of importance to assistive technologies, or to functional reorganization of the cortex and its neural output for a novel purpose. In the future, it will be important to explicitly test the changes in neural activity in the unaffected hemisphere as stroke survivors use BCI systems for longer time periods.

In summary, these results move the applications of BCI forward to potentially benefit the large number of motor-impaired hemispheric stroke survivors. The study shows in particular that hemispheric stroke patients can volitionally control signals from the unaffected hemisphere for device operation. This specific use of the contralesional hemisphere may provide a novel neuroprosthetic approach for increasing function in the more impaired stroke populations whose rehabilitation options are currently limited.

6 Conclusion

6.1 Summary of Results

The central hypothesis underlying this dissertation is that motor signals from the unaffected hemisphere that are related to intended movements of the same-sided affected hand after stroke contain sufficient information to control a brain-computer interface (BCI) system, and furthermore, that a BCI system controlled with these signals can improve long-term function. This work has sought to advance this central hypothesis through three directions: understanding the motor physiology of the same-sided hemisphere and its relevance and feasibility for BCI applications, understanding the tradeoff between electrode invasiveness and signal quality to determine its impact on BCI implementation, and finally, demonstrating the feasibility of these systems in the patient population of interest by determining if stroke survivors can control a BCI system using ipsilateral motor signals in their unaffected hemisphere.

Chapter 3 demonstrates that electrocorticography (ECoG) signals recorded from a single cortical hemisphere can be used to decode kinematics of three-dimensional (3D) reaches of either the contralateral or the ipsilateral arm. The ability to decode kinematics of reaching movements with several degrees of freedom builds upon previous demonstrations that ECoG signals can be used to decode movement trajectories (Schalk, Kubanek et al. 2007; Pistohl, Ball et al. 2008; Sanchez, Gunduz et al. 2008; Ganguly, Secundo et al. 2009; Chao, Nagasaka et al. 2010; Shimoda, Nagasaka et al. 2012; Marathe and Taylor 2013) and is a good modality for closed-loop BCI control (Leuthardt, Schalk et al. 2004; Wilson, Felton et al. 2006; Felton, Wilson et al. 2007; Schalk, Miller et al. 2008; Rouse and Moran 2009; Rouse, Williams et al. 2013). Although a few previous studies have decoded movement trajectories from movements that were not constrained

to two dimensions (Hotson, Fifer et al. 2012; Chen, Shin et al. 2013; Hotson, Fifer et al. 2014), we believe that this is the first study to demonstrate that ECoG recordings in human patients can be used to decode movements that are independent in 3D space. Although the decoding model used neural activity both leading and lagging kinematic parameters, which would not be possible in causal on-line BCI control, the ability to use ECoG signals to decode movement kinematics underscores the degree of information that can be decoded from ECoG activity and is therefore a significant step towards the development of ECoG BCI applications for a wide variety of patient populations.

Furthermore, the ability to decode not only kinematics of contralateral arm reaches, but also to decode kinematics of ipsilateral limb movements is particularly relevant to BCI applications for stroke survivors. In particular, given that ipsilateral limb kinematics can be decoded in motor-intact patients, it is likely that similar signals from the unaffected hemisphere of stroke survivors can be used to control a BCI system. While other studies have also used ECoG signals to decode ipsilateral arm movements (Ganguly, Secundo et al. 2009; Hotson, Fifer et al. 2012; Hotson, Fifer et al. 2014), this study was unique both because we decoded kinematics of 3D arm movements and because the experiment was specifically designed to enable us to compare the ability to decode trajectories of contralateral and ipsilateral arm movements in the same patients. Specifically, we found that while the movement-related spectral power changes associated with contralateral and ipsilateral arm movements are distinct, the contralateral and ipsilateral limb decoding accuracies are very similar. Furthermore, the models used to predict contralateral and ipsilateral limb movements had the strongest prediction weights in the same cortical locations and ECoG features. Because of the similarity in the decoding models used, it is uncertain how separable the neural representations of contralateral and ipsilateral movement kinematics are.

In order to utilize the ability to decode movement kinematics to develop a BCI system, it is important to understand the relationship between signal quality and electrode invasiveness. Understanding this tradeoff will allow us to implement BCI systems using the most appropriate technical specifications to meet the necessary performance criteria. By using simulated electroencephalography (EEG) signals, we found that there is a significant decrease in the ability to decode movement kinematics with EEG signals when compared to ECoG signals. Because of this decrease in signal quality, for BCI applications requiring multiple degrees of freedom, more invasive electrodes, such as ECoG arrays, would be necessary. Because ECoG provides the signal quality needed to decode activity with multiple degrees of freedom, a further choice must be made to implant electrodes subdurally or epidurally. Chapter 4 presented the results of a study investigating the effect of the human dura on ECoG signal quality at various spatial scales. In particular, while subdural and epidural macro-ECoG signals are similar in spatial and spectral resolution, there is a significant effect of the human dura when ECoG electrodes with smaller sizes are used. It will be important to take this tradeoff between invasiveness and signal quality into consideration when designing BCI applications.

Finally, the experiments included in Chapter 5 demonstrate that stroke survivors can utilize neural activity in their unaffected hemisphere to control a simple BCI system. In particular, stroke survivors have significant movement-related spectral power changes in the unaffected hemisphere that are associated with intended movements of the affected hand. Furthermore, these signals were used to control a simple BCI system rapidly and accurately. While a number of studies have used signals from the affected hemisphere for BCI control (Buch, Weber et al. 2008; Daly, Cheng et al. 2009; Soekadar, Witkowski et al. 2011; Ramos-Murguialday, Broetz et al. 2013; Ang, Chua et al. 2014), this study provided the first demonstration that stroke survivors

can use ipsilateral motor signals from the unaffected hemisphere for BCI control (Bundy, Wronkiewicz et al. 2012). As the ability to modulate neural activity is impaired in patients with more significant lesions (Buch, Modir Shanechi et al. 2012), the unaffected hemisphere is likely an ideal control signal for BCI applications in many stroke survivors.

6.2 Future Directions

While we believe that the results of these studies are significant, there are also several future avenues of investigation that would allow us to develop a better understanding of ipsilateral motor physiology, would further the development of BCI systems in general, and would lead to further development of BCI applications for stroke survivors in particular.

6.2.1 Understanding Ipsilateral Motor Physiology

While the movement-related spectral power changes associated with contralateral and ipsilateral limb movements are distinct in both the amplitude and time course of power changes, kinematic parameters of contralateral and ipsilateral arm movements are represented at similar cortical locations and features. Several potential factors may have contributed to this similarity in speed and directional tuning. A number of task-related factors have been identified that can affect movement-related neural activity including: task complexity (Kitamura, Shibasaki et al. 1993a; Kitamura, Shibasaki et al. 1993b; Rao, Binder et al. 1993; Manganotti, Gerloff et al. 1998), perceived effort (Slobounov, Hallett et al. 2004), the specific muscles activated (Colebatch, Deiber et al. 1991; Jankelowitz and Colebatch 2002), hemispheric asymmetries (Kim, Ashe et al. 1993b), and whether unilateral or bilateral movements are performed (Donchin, Gribova et al. 1998; Kermadi, Liu et al. 2000; Steinberg, Donchin et al. 2002; Diedrichsen, Wiestler et al. 2013). Future experiments could be designed to specifically investigate the interaction between ipsilateral motor activity and any one of these parameters to increase our understanding of the

role of ipsilateral motor activations. Significantly, BCI control derived from signals in the unaffected hemisphere of stroke survivors would need to be independent from normal movements of the unaffected limb. Therefore, understanding the similarities and differences in the neural activity related to unimanual contralateral limb movements, unimanual ipsilateral limb movements, synergistic bimanual movements, and non-synergistic bimanual movements would be especially important. In particular, both electrophysiological and functional imaging studies have shown that neural activity observed during bilateral movements cannot be accounted for by a linear combination of the neural activity that occurs during each of the component unimanual movements (Tanji, Okano et al. 1988; Kermadi, Liu et al. 2000; Steinberg, Donchin et al. 2002; Diedrichsen, Wiestler et al. 2013). Because the 3D reaching task used in our study was performed with either the contralateral or ipsilateral limb separately, it is uncertain how the findings would change in a bimanual reaching task. Specifically, it would be important to determine if ECoG signals still contain representations of ipsilateral limb kinematics during bimanual movements and how the location and features underlying this representation differed for unimanual and bimanual movements.

6.2.2 Improving Kinematic Decoding

In Chapter 3, we also observed that ECoG signals from a single cortical hemisphere encode kinematics of reaching movements of either arm. We used this relationship to decode kinematics with a hierarchical partial least-squares (PLS) regression model. Furthermore, we sought not only to demonstrate that ECoG can be used to decode movement kinematics, but also to use the model weights to interpret the most significant cortical locations and features for decoding contralateral and ipsilateral arm movements. To accomplish this, we chose to use the logistic regression and PLS regression methods in part because they are both linear. Therefore, as the

ECoG features were transformed to z-score values prior to training the prediction model, we were able to easily interpret and compare the importance of each cortical location and feature through the prediction weights. Future work could seek to improve upon the decoding accuracy through a number of potential preprocessing methods or machine learning algorithms. Potential methods to improve decoding accuracy include: calculating spatial filters through unsupervised methods such as independent component analysis (Makeig, Bell et al. 1996; Kachenoura, Albera et al. 2008), calculating spatial filters designed to maximize the discriminability of behavioral conditions using supervised learning methods such as common spatial patterns (Koles, Lazar et al. 1990; Koles 1991; Ramoser, Muller-Gerking et al. 2000; Blankertz, Tomioka et al. 2008; Ince, Gupta et al. 2010; Marathe and Taylor 2013), using a model such as a kalman filter that incorporates temporal filtering into the prediction model (Wu, Black et al. 2003; Marathe and Taylor 2013), or using any of a number of alternative linear or non-linear machine learning methods for decoding kinematic time courses (Wessberg, Stambaugh et al. 2000). It should be noted that these alternative methods are not guaranteed to increase prediction accuracies as they may be poorly suited to fit the relationship between ECoG activity and movement kinematics. Additionally several of these methods may be susceptible to overfitting. For example, while we attempted to use several variations of the common spatial patterns algorithm in our ECoG dataset (Blankertz, Tomioka et al. 2008; Lotte and Guan 2011; Falzon, Camilleri et al. 2012; Samek, Vidaurre et al. 2012), each method suffered from overfitting, leading to good training set performance and poor performance on the test set.

Along with speed, velocity, and position, there are a number of alternative movement parameters that describe movement trajectories such as the component joint angles or muscle activations. One factor in choosing to begin by decoding speed, velocity, and position is their prevalence in

prior studies of single-unit motor control (Georgopoulos, Kalaska et al. 1982; Moran and Schwartz 1999b; Wang, Chan et al. 2007) and movement decoding with ECoG (Schalk, Kubanek et al. 2007; Pistohl, Ball et al. 2008; Ganguly, Secundo et al. 2009; Chao, Nagasaka et al. 2010; Marathe and Taylor 2013). While speed, position, and velocity can be decoded from ECoG recordings in human patients, it is uncertain if algorithms designed to decode alternative components of reaching movements will ultimately lead to increases in the accuracies of decoded movement trajectories.

6.2.3 Optimizing ECoG Arrays for BCI Applications

The ECoG arrays used for the analyses presented in Chapter 3 were implanted for clinical purposes. Therefore, the location, size, spacing, and extent of electrode coverage were all based upon clinical necessity. A number of previous studies have shown that ECoG electrodes with smaller sizes and spacing can be used to examine neural activity with increased spatial resolution (Leuthardt, Freudenberg et al. 2009; Wang, Degenhart et al. 2009; Kellis, Miller et al. 2010). Although smaller electrode sizes can increase the spatial specificity of recordings and will potentially decrease the invasiveness of an implant by decreasing its overall footprint, electrodes with smaller sizes have increased electrode impedances, causing a decrease in the signal-to-noise ratio of recordings. It is likely that the optimal ECoG implant for BCI applications will balance the spatial specificity and signal-to-noise ratio of recordings to allow for increased decoding performance. Along with implant specifications, studies of BCI applications can also optimize implant locations for decoding neural activity through the use of pre-operative functional imaging techniques (Wang, Collinger et al. 2013). Finally, in characterizing the effect of the human dura on ECoG recordings in Chapter 4, two extremes of electrode size were examined. In between these extremes, the computer modeling that was performed showed that the effect of the

dura on signal quality varies with electrode size. As the optimal ECoG specifications for BCI applications are identified, it will be important to use computer models such as this one and additional experimental recordings to specifically characterize the effect of the dura at the intermediate electrode sizes that are ultimately used.

6.2.4 Transitioning from Movement Decoding to BCI Control

The optimal method to evaluate the accuracy of a BCI system is ultimately through closed-loop experiments. While open-loop decoding of motor activity allows us to assess the feasibility of a BCI application, to compare the decoding performance of different signal modalities, and to test a variety of decoding methods with limited data sets, there are a number of important differences between open-loop and closed-loop methods. In particular, closed-loop BCI control provides feedback to the user, allowing them to learn to adapt their neural activity to improve the accuracy of the BCI system. This increase in accuracy due to on-line adaptation has been demonstrated not only for BCI systems driven by single unit recordings (Taylor, Tillery et al. 2002; Jarosiewicz, Chase et al. 2008), but also BCI systems using ECoG recordings in non-human primates (Rouse and Moran 2009; Rouse, Williams et al. 2013). Additionally, co-adaptively modifying the decoding model in conjunction with the subject's ability to learn has led to further improvements in on-line BCI control (Williams 2013). The increase in accuracy with adaptation indicates that the open-loop accuracies demonstrated in this work could be further improved upon during closed-loop BCI control.

Because decoding accuracy can improve though closed-loop adaptation, BCI systems should be designed to enhance the ability of the BCI user to learn and adapt. This additional constraint on BCI system design is illustrated by the fact that during control of a prosthetic simulator, although open-loop decoding accuracies were maximized through algorithms with slow temporal update

times, closed-loop decoding accuracies were maximized with fast temporal updates allowing for easier learning and adaptation (Cunningham, Nuyujukian et al. 2011). Therefore, it will be important for future studies to “close the loop” in order to ensure that algorithms that increase the accuracy of off-line kinematic decoding will also have corresponding increases in BCI control performance. Based upon this consideration and the results of Chapter 3, a further question is how valuable the local motor potential (LMP) will be for closed-loop control. In line with previous studies (Schalk, Kubanek et al. 2007; Pistohl, Ball et al. 2008; Hotson, Fifer et al. 2014), we found that the LMP amplitude had a significant contribution to the decoding of kinematics. Although the LMP signal is clearly important for movement decoding, very few studies have used time domain signals of local field potentials for BCI control (Kennedy, Andreasen et al. 2004; Kennedy, Kirby et al. 2004). Because the LMP is derived from applying a low-pass smoothing filter to ECoG signals, it changes on a relatively slow time scale. This slow time scale may make it difficult for patients to adapt their LMP signals during BCI control. Future studies seeking to use LMP signals within closed-loop BCI control tasks with several degrees of freedom will be important to understand the advantages and disadvantages of the LMP signal within BCI systems.

6.2.5 BCI Systems for Stroke

Finally, the study described in Chapter 5 was the first demonstration that stroke survivors can control a BCI system using ipsilateral motor activity from the unaffected hemisphere. We envision that a BCI system using the unaffected hemisphere after stroke can be used to improve function in stroke survivors either through long-term control of an assistive device or through encouraging functional rehabilitation by encouraging neuroplasticity with paired BCI control and

external stimulation. Each of these clinical end-points has its own requirements and future work needed to translate them from our demonstration of feasibility into clinically significant devices.

For meaningful long-term device control, BCI systems need to enable stable and long-term control of devices with multiple degrees of freedom and high levels of accuracy. Although this study provides evidence that ECoG signals can be used to decode 3D movements, the patients had an intact motor system. After a stroke, movement-related neural activity is altered in a variety of ways (Pfurtscheller, Ladurner et al. 1984; Honda, Nagamine et al. 1997; Green, Bialy et al. 1999; Buch, Modir Shanechi et al. 2012). Therefore, prior to implementing a BCI system, we will need to gain a better understanding of how the movement-related neural activity in stroke patients differs from motor-intact patients based upon the location and extent of the lesion. Understanding the changes in movement-related neural activity after stroke would inform the choices made in the implementation of BCI systems including the location, features, and type of electrodes used in each individual patient.

Designing a BCI system as a rehabilitation tool requires us to answer a number of other questions. Because remodeling of perilesional areas has been associated with improved function after stroke (Nudo, Wise et al. 1996; Turton, Wroe et al. 1996; Netz, Lammers et al. 1997; Ward, Brown et al. 2003a; Ward, Brown et al. 2003b), previous BCI applications for rehabilitation after stroke have focused on areas in the affected hemisphere for BCI control (Buch, Weber et al. 2008; Daly, Cheng et al. 2009; Ramos-Murguialday, Broetz et al. 2013). A number of studies have also shown that there are increases in ipsilateral motor activity in the contralesional hemisphere after recovery from stroke (Weiller, Chollet et al. 1992; Weiller, Ramsay et al. 1993; Cramer, Nelles et al. 1997; Green, Bialy et al. 1999; Levy, Nichols et al. 2001; Schaechter, Kraft

et al. 2002). A trial is currently underway to determine whether training with a BCI-controlled hand orthosis that is driven by ipsilateral motor signals in the unaffected hemisphere can lead to functional rehabilitation in chronic stroke survivors. Although demonstrations of increased function after BCI training are exciting it is imperative that larger clinical trials are conducted to determine the optimal strategies for BCI rehabilitation systems. In particular, it will be important to understand the complex interactions between rehabilitation and a number of factors including: the location of lesions, the residual motor function at trial onset, whether BCI feedback is given through electrical or mechanical stimulation, the latency between neural activity and external stimulation, the type of neural activity used for BCI control, the duration and volume of BCI training, and the combination of BCI training with additional therapies to enhance plasticity. Through well-designed and well-implemented studies to determine the roles of these factors, it will be possible to further develop and translate BCI systems into tools to improve patients' lives.

6.3 Final Thoughts

Over the last several decades, there have been tremendous advancements that have brought BCI systems from the pages of science fiction novels to real-world systems that have been demonstrated to be feasible both in animal models and in individual human patients. Collectively this dissertation has advanced the development of BCI applications in general by demonstrating the feasibility of ECoG for decoding movement kinematics with multiple degrees of freedom and by further developing our understanding of the tradeoff between signal quality and electrode invasiveness. Furthermore, this body of work showed that ECoG signals could be used to decode kinematics of the ipsilateral limb, demonstrating the feasibility of BCI systems that would use these signals in stroke survivors. Finally, we found that these ipsilateral motor signals, recorded

from the unaffected hemisphere of stroke survivors, can be modulated to enable control of a computer cursor. In light of the recent progress towards developing BCI systems, the future is very bright. In particular, it will be exciting to go beyond demonstrations of feasibility and optimize the techniques for implementation and translation of BCI systems into patient populations. Finally, with the potential to use BCI systems not only for device control, but also to encourage neuroplasticity, it is clear that we have only just begun to explore the range of possible ways to apply BCI technology to aid a wide range of patient populations.

References

Aizawa, H., H. Mushiake, M. Inase and J. Tanji (1990). "An output zone of the monkey primary motor cortex specialized for bilateral hand movement." Exp Brain Res **82**(1): 219-221.

Allison, T., G. McCarthy, A. Nobre, A. Puce and A. Belger (1994). "Human extrastriate visual cortex and the perception of faces, words, numbers, and colors." Cereb Cortex **4**(5): 544-554.

Anderson, N. R., T. Blakely, G. Schalk, E. C. Leuthardt and D. W. Moran (2012). "Electrocorticographic (ECoG) correlates of human arm movements." Exp Brain Res **223**(1): 1-10.

Ang, K. K., K. S. Chua, K. S. Phua, C. Wang, Z. Y. Chin, C. W. Kuah, W. Low and C. Guan (2014). "A Randomized Controlled Trial of EEG-Based Motor Imagery Brain-Computer Interface Robotic Rehabilitation for Stroke." Clin EEG Neurosci.

Arroyo, S., R. P. Lesser, B. Gordon, S. Uematsu, D. Jackson and R. Webber (1993). "Functional significance of the mu rhythm of human cortex: an electrophysiologic study with subdural electrodes." Electroencephalogr Clin Neurophysiol **87**(3): 76-87.

Barnes, S. (1901). "Degenerations in hemiplegia: with special reference to a ventro-lateral pyramidal tract, the accessory fillet and Pick's bundle." Brain **24**(3): 463-501.

Bashir, S., M. Kaeser, A. Wyss, A. Hamadjida, Y. Liu, J. Bloch, J. F. Brunet, A. Belhaj-Saif and E. M. Rouiller (2012). "Short-term effects of unilateral lesion of the primary motor cortex (M1) on ipsilesional hand dexterity in adult macaque monkeys." Brain Struct Funct **217**(1): 63-79.

Baskett, J. J., H. J. Marshall, J. B. Broad, P. H. Owen and G. Green (1996). "The good side after stroke: ipsilateral sensory-motor function needs careful assessment." Age Ageing **25**(3): 239-244.

Benjamini, Y. and Y. Hochberg (1995). "Controlling the False Discovery Rate - a Practical and Powerful Approach to Multiple Testing." Journal of the Royal Statistical Society Series B-Methodological **57**(1): 289-300.

Benjamini, Y. and D. Yekutieli (2001). "The control of the false discovery rate in multiple testing under dependency." Annals of Statistics **29**(4): 1165-1188.

Berger, H. (1969). "On the electroencephalogram of man." Electroencephalogr Clin Neurophysiol: Suppl 28:37+.

Binkofski, F., R. J. Seitz, S. Arnold, J. Classen, R. Benecke and H. J. Freund (1996). "Thalamic metbolism and corticospinal tract integrity determine motor recovery in stroke." Ann Neurol **39**(4): 460-470.

Bjornsson, C. S., S. J. Oh, Y. A. Al-Kofahi, Y. J. Lim, K. L. Smith, J. N. Turner, S. De, B. Roysam, W. Shain and S. J. Kim (2006). "Effects of insertion conditions on tissue strain and vascular damage during neuroprosthetic device insertion." J Neural Eng **3**(3): 196-207.

Blankertz, B., R. Tomioka, S. Lemm, M. Kawanabe and K.-R. Muller (2008). "Optimizing spatial filters for robust EEG single-trial analysis." Signal Processing Magazine, IEEE **25**(1): 41-56.

Bleichner, M. G., M. J. Vansteensel, G. M. Huiskamp, D. Hermes, E. J. Aarnoutse, C. H. Ferrier and N. F. Ramsey (2011). "The effects of blood vessels on electrocorticography." J Neural Eng **8**(4): 044002.

Bradberry, T. J., R. J. Gentili and J. L. Contreras-Vidal (2010). "Reconstructing three-dimensional hand movements from noninvasive electroencephalographic signals." J Neurosci **30**(9): 3432-3437.

Breshears, J. D., J. L. Roland, M. Sharma, C. M. Gaona, Z. V. Freudenburg, R. Tempelhoff, M. S. Avidan and E. C. Leuthardt (2010). "Stable and dynamic cortical electrophysiology of induction and emergence with propofol anesthesia." Proc Natl Acad Sci U S A **107**(49): 21170-21175.

Brindley, G. S. and M. D. Craggs (1972). "The electrical activity in the motor cortex that accompanies voluntary movement." J Physiol **223**(1): 28P-29P.

Broetz, D., C. Braun, C. Weber, S. R. Soekadar, A. Caria and N. Birbaumer (2010). "Combination of brain-computer interface training and goal-directed physical therapy in chronic stroke: a case report." Neurorehabil Neural Repair **24**(7): 674-679.

Brus-Ramer, M., J. B. Carmel and J. H. Martin (2009). "Motor cortex bilateral motor representation depends on subcortical and interhemispheric interactions." J Neurosci **29**(19): 6196-6206.

Buch, E., C. Weber, L. G. Cohen, C. Braun, M. A. Dimyan, T. Ard, J. Mellinger, A. Caria, S. Soekadar, A. Fourkas and N. Birbaumer (2008). "Think to move: a neuromagnetic brain-computer interface (BCI) system for chronic stroke." Stroke **39**(3): 910-917.

Buch, E. R., A. Modir Shanechi, A. D. Fourkas, C. Weber, N. Birbaumer and L. G. Cohen (2012). "Parietofrontal integrity determines neural modulation associated with grasping imagery after stroke." Brain **135**(Pt 2): 596-614.

Bucy, P. C. (1933). "Representation of Ipsilateral-Extremities in the Cerebral Cortex." Science **78**(2027): 418.

Bucy, P. C. and J. F. Fulton (1933). "IPSILATERAL REPRESENTATION IN THE MOTOR AND PREMOTOR CORTEX OP MONKEYS." Brain **56**(3): 318-342.

Bundy, D. T., M. Wronkiewicz, M. Sharma, D. W. Moran, M. Corbetta and E. C. Leuthardt (2012). "Using ipsilateral motor signals in the unaffected cerebral hemisphere as a signal platform for brain-computer interfaces in hemiplegic stroke survivors." J Neural Eng **9**(3): 036011.

Bundy, D. T., E. Zellmer, C. M. Gaona, M. Sharma, N. Szrama, C. Hacker, Z. V. Freudenburg, A. Daitch, D. W. Moran and E. C. Leuthardt (2014). "Characterization of the effects of the human dura on macro- and micro-electrocorticographic recordings." J Neural Eng **11**(1): 016006.

Calford, M. B. and R. Tweedale (1990). "Interhemispheric transfer of plasticity in the cerebral cortex." Science **249**(4970): 805-807.

Caminiti, R., P. B. Johnson, C. Galli, S. Ferraina and Y. Burnod (1991). "Making arm movements within different parts of space: the premotor and motor cortical representation of a coordinate system for reaching to visual targets." J Neurosci **11**(5): 1182-1197.

Carmena, J. M., M. A. Lebedev, R. E. Crist, J. E. O'Doherty, D. M. Santucci, D. F. Dimitrov, P. G. Patil, C. S. Henriquez and M. A. Nicolelis (2003). "Learning to control a brain-machine interface for reaching and grasping by primates." PLoS Biol **1**(2): E42.

Carter, A. R., S. V. Astafiev, C. E. Lang, L. T. Connor, J. Rengachary, M. J. Strube, D. L. Pope, G. L. Shulman and M. Corbetta (2010). "Resting interhemispheric functional magnetic resonance imaging connectivity predicts performance after stroke." Ann Neurol **67**(3): 365-375.

Carter, A. R., K. R. Patel, S. V. Astafiev, A. Z. Snyder, J. Rengachary, M. J. Strube, A. Pope, J. S. Shimony, C. E. Lang, G. L. Shulman and M. Corbetta (2011). "Upstream Dysfunction of Somatomotor Functional Connectivity After Corticospinal Damage in Stroke." Neurorehabil Neural Repair.

Carter, A. R., K. R. Patel, S. V. Astafiev, A. Z. Snyder, J. Rengachary, M. J. Strube, A. Pope, J. S. Shimony, C. E. Lang, G. L. Shulman and M. Corbetta (2012). "Upstream dysfunction of somatomotor functional connectivity after corticospinal damage in stroke." Neurorehabil Neural Repair **26**(1): 7-19.

Chao, Z. C., Y. Nagasaka and N. Fujii (2010). "Long-term asynchronous decoding of arm motion using electrocorticographic signals in monkeys." Front Neuroeng **3**: 3.

Chen, C., D. Shin, H. Watanabe, Y. Nakanishi, H. Kambara, N. Yoshimura, A. Nambu, T. Isa, Y. Nishimura and Y. Koike (2013). "Prediction of hand trajectory from electrocorticography signals in primary motor cortex." PLoS One **8**(12): e83534.

Cheney, P. D. and E. E. Fetz (1980). "Functional classes of primate corticomotoneuronal cells and their relation to active force." J Neurophysiol **44**(4): 773-791.

Chestek, C. A., V. Gilja, C. H. Blabe, B. L. Foster, K. V. Shenoy, J. Parvizi and J. M. Henderson (2013). "Hand posture classification using electrocorticography signals in the gamma band over human sensorimotor brain areas." J Neural Eng **10**(2): 026002.

Cisek, P., D. J. Crammond and J. F. Kalaska (2003). "Neural activity in primary motor and dorsal premotor cortex in reaching tasks with the contralateral versus ipsilateral arm." J Neurophysiol **89**(2): 922-942.

Colebatch, J. G., M. P. Deiber, R. E. Passingham, K. J. Friston and R. S. Frackowiak (1991). "Regional cerebral blood flow during voluntary arm and hand movements in human subjects." J Neurophysiol **65**(6): 1392-1401.

Cooper, R., A. L. Winter, H. J. Crow and W. G. Walter (1965). "Comparison of Subcortical, Cortical and Scalp Activity Using Chronically Indwelling Electrodes in Man." Electroencephalogr Clin Neurophysiol **18**: 217-228.

Coupar, F., A. Pollock, P. Rowe, C. Weir and P. Langhorne (2012). "Predictors of upper limb recovery after stroke: a systematic review and meta-analysis." Clin Rehabil **26**(4): 291-313.

Craggs, M. D. (1975). "Cortical control of motor prostheses: using the cord-transected baboon as the primate model for human paraplegia." Adv Neurol **10**: 91-101.

Cramer, S. C. (2004). "Functional imaging in stroke recovery." Stroke **35**(11 Suppl 1): 2695-2698.

Cramer, S. C., S. P. Finklestein, J. D. Schaechter, G. Bush and B. R. Rosen (1999). "Activation of distinct motor cortex regions during ipsilateral and contralateral finger movements." J Neurophysiol **81**(1): 383-387.

Cramer, S. C., A. Mark, K. Barquist, H. Nhan, K. C. Stegbauer, R. Price, K. Bell, I. R. Odderson, P. Esselman and K. R. Maravilla (2002). "Motor cortex activation is preserved in patients with chronic hemiplegic stroke." Ann Neurol **52**(5): 607-616.

Cramer, S. C., G. Nelles, R. R. Benson, J. D. Kaplan, R. A. Parker, K. K. Kwong, D. N. Kennedy, S. P. Finklestein and B. R. Rosen (1997). "A functional MRI study of subjects recovered from hemiparetic stroke." Stroke **28**(12): 2518-2527.

Crone, N. E., D. L. Miglioretti, B. Gordon and R. P. Lesser (1998a). "Functional mapping of human sensorimotor cortex with electrocorticographic spectral analysis. II. Event-related synchronization in the gamma band." Brain **121 (Pt 12)**: 2301-2315.

Crone, N. E., D. L. Miglioretti, B. Gordon, J. M. Sieracki, M. T. Wilson, S. Uematsu and R. P. Lesser (1998b). "Functional mapping of human sensorimotor cortex with electrocorticographic spectral analysis. I. Alpha and beta event-related desynchronization." Brain **121 (Pt 12)**: 2271-2299.

Cunningham, J. P., P. Nuyujukian, V. Gilja, C. A. Chestek, S. I. Ryu and K. V. Shenoy (2011). "A closed-loop human simulator for investigating the role of feedback control in brain-machine interfaces." J Neurophysiol **105**(4): 1932-1949.

Daly, J. J., R. Cheng, J. Rogers, K. Litinas, K. Hrovat and M. Dohring (2009). "Feasibility of a New Application of Noninvasive Brain Computer Interface (BCI): A Case Study of Training for Recovery of Volitional Motor Control After Stroke." J Neurol Phys Ther **33**(4): 203-211.

Dandy, W. E. (1928). "Removal of right cerebral hemisphere for certain tumors with hemiplegia: preliminary report." Journal of the American Medical Association **90**(11): 823-825.

Deecke, L. and H. H. Kornhuber (1978). "An electrical sign of participation of the mesial 'supplementary' motor cortex in human voluntary finger movement." Brain Res **159**(2): 473-476.

Deecke, L., P. Scheid and H. H. Kornhuber (1969). "Distribution of readiness potential, pre-motion positivity, and motor potential of the human cerebral cortex preceding voluntary finger movements." Exp Brain Res **7**(2): 158-168.

der-Yeghiaian, L., K. Sharp, J. See, N. Abidi, K. Mai, V. Le and S. C. Cramer (2009). "Robotic therapy after stroke and the influence of baseline motor status." International Stroke Conference: e169.

Di Lazzaro, V., A. Oliviero, P. Profice, A. Insola, P. Mazzone, P. Tonali and J. C. Rothwell (1999). "Direct demonstration of interhemispheric inhibition of the human motor cortex produced by transcranial magnetic stimulation." Exp Brain Res **124**(4): 520-524.

Diedrichsen, J., T. Wiestler and J. W. Krakauer (2013). "Two distinct ipsilateral cortical representations for individuated finger movements." Cereb Cortex **23**(6): 1362-1377.

Donchin, O., A. Gribova, O. Steinberg, H. Bergman and E. Vaadia (1998). "Primary motor cortex is involved in bimanual coordination." Nature **395**(6699): 274-278.

Dum, R. P. and P. L. Strick (1991). "The origin of corticospinal projections from the premotor areas in the frontal lobe." J Neurosci **11**(3): 667-689.

Duncan, P. W., L. B. Goldstein, D. Matchar, G. W. Divine and J. Feussner (1992). "Measurement of motor recovery after stroke. Outcome assessment and sample size requirements." Stroke **23**(8): 1084-1089.

Engel, J., Jr. (1996). "Surgery for seizures." N Engl J Med **334**(10): 647-652.

Evarts, E. V. (1966). "Pyramidal tract activity associated with a conditioned hand movement in the monkey." J Neurophysiol **29**(6): 1011-1027.

Falzon, O., K. P. Camilleri and J. Muscat (2012). "The analytic common spatial patterns method for EEG-based BCI data." J Neural Eng **9**(4): 045009.

Felton, E. A., J. A. Wilson, J. C. Williams and P. C. Garell (2007). "Electrocorticographically controlled brain-computer interfaces using motor and sensory imagery in patients with temporary subdural electrode implants. Report of four cases." J Neurosurg **106**(3): 495-500.

Ferbert, A., A. Priori, J. C. Rothwell, B. L. Day, J. G. Colebatch and C. D. Marsden (1992). "Interhemispheric inhibition of the human motor cortex." J Physiol **453**: 525-546.

Filimon, F. (2010). "Human cortical control of hand movements: parietofrontal networks for reaching, grasping, and pointing." Neuroscientist **16**(4): 388-407.

Flamary, R. and A. Rakotomamonjy (2012). "Decoding Finger Movements from ECoG Signals Using Switching Linear Models." Front Neurosci **6**: 29.

Flint, R. D., E. W. Lindberg, L. R. Jordan, L. E. Miller and M. W. Slutzky (2012). "Accurate decoding of reaching movements from field potentials in the absence of spikes." J Neural Eng **9**(4): 046006.

Fox, P. T. and M. E. Raichle (1986). "Focal physiological uncoupling of cerebral blood flow and oxidative metabolism during somatosensory stimulation in human subjects." Proc Natl Acad Sci U S A **83**(4): 1140-1144.

Francisco, G., J. Chae, H. Chawla, S. Kirshblum, R. Zorowitz, G. Lewis and S. Pang (1998). "Electromyogram-triggered neuromuscular stimulation for improving the arm function of acute stroke survivors: a randomized pilot study." Arch Phys Med Rehabil **79**(5): 570-575.

Freudenburg, Z. V., C. M. Gaona, M. Sharma, D. T. Bundy, J. D. Breshears, R. B. Pless and E. C. Leuthardt (2014). "Fast-scale network dynamics in human cortex have specific spectral covariance patterns." Proc Natl Acad Sci U S A **111**(12): 4602-4607.

Fried, I., G. A. Ojemann and E. E. Fetz (1981). "Language-related potentials specific to human language cortex." Science **212**(4492): 353-356.

Fries, W., A. Danek, K. Scheidtmann and C. Hamburger (1993). "Motor recovery following capsular stroke. Role of descending pathways from multiple motor areas." Brain **116 (Pt 2)**: 369-382.

Frostig, R. D., E. E. Lieke, D. Y. Ts'o and A. Grinvald (1990). "Cortical functional architecture and local coupling between neuronal activity and the microcirculation revealed by in vivo high-resolution optical imaging of intrinsic signals." Proc Natl Acad Sci U S A **87**(16): 6082-6086.

Gallivan, J. P., D. A. McLean, J. R. Flanagan and J. C. Culham (2013). "Where one hand meets the other: limb-specific and action-dependent movement plans decoded from preparatory signals in single human frontoparietal brain areas." J Neurosci **33**(5): 1991-2008.

Ganguly, K., L. Secundo, G. Ranade, A. Orsborn, E. F. Chang, D. F. Dimitrov, J. D. Wallis, N. M. Barbaro, R. T. Knight and J. M. Carmena (2009). "Cortical representation of ipsilateral arm movements in monkey and man." J Neurosci **29**(41): 12948-12956.

Gaona, C. M., M. Sharma, Z. V. Freudenburg, J. D. Breshears, D. T. Bundy, J. Roland, D. L. Barbour, G. Schalk and E. C. Leuthardt (2011). "Nonuniform high-gamma (60-500 Hz) power changes dissociate cognitive task and anatomy in human cortex." J Neurosci **31**(6): 2091-2100.

Gardner, W. J. (1933). "Removal of the right cerebral hemisphere for infiltrating glioma: report of a case." Journal of the American Medical Association **101**(11): 823-826.

Georgopoulos, A. P., R. Caminiti and J. F. Kalaska (1984). "Static spatial effects in motor cortex and area 5: quantitative relations in a two-dimensional space." Exp Brain Res **54**(3): 446-454.

Georgopoulos, A. P., J. F. Kalaska, R. Caminiti and J. T. Massey (1982). "On the relations between the direction of two-dimensional arm movements and cell discharge in primate motor cortex." J Neurosci **2**(11): 1527-1537.

Georgopoulos, A. P., R. E. Kettner and A. B. Schwartz (1988). "Primate motor cortex and free arm movements to visual targets in three-dimensional space. II. Coding of the direction of movement by a neuronal population." J Neurosci **8**(8): 2928-2937.

Georgopoulos, A. P., A. B. Schwartz and R. E. Kettner (1986). "Neuronal population coding of movement direction." Science **233**(4771): 1416-1419.

Gilden, L., H. G. Vaughan, Jr. and L. D. Costa (1966). "Summated human EEG potentials with voluntary movement." Electroencephalogr Clin Neurophysiol **20**(5): 433-438.

Glees, P. and J. Cole (1952). "Ipsilateral representation in the cerebral cortex; its significance in relation to motor function." Lancet **1**(6720): 1191-1192.

Go, A. S., D. Mozaffarian, V. L. Roger, E. J. Benjamin, J. D. Berry, M. J. Blaha, S. Dai, E. S. Ford, C. S. Fox, S. Franco, H. J. Fullerton, C. Gillespie, S. M. Hailpern, J. A. Heit, V. J. Howard, M. D. Huffman, S. E. Judd, B. M. Kissela, S. J. Kittner, D. T. Lackland, J. H. Lichtman, L. D. Lisabeth, R. H. Mackey, D. J. Magid, G. M. Marcus, A. Marelli, D. B. Matchar, D. K. McGuire, E. R. Mohler, 3rd, C. S. Moy, M. E. Mussolino, R. W. Neumar, G. Nichol, D. K. Pandey, N. P. Paynter, M. J. Reeves, P. D. Sorlie, J. Stein, A. Towfighi, T. N. Turan, S. S. Virani, N. D. Wong, D. Woo and M. B. Turner (2014). "Heart disease and stroke statistics--2014 update: a report from the American Heart Association." Circulation **129**(3): e28-e292.

Goble, D. J. and S. H. Brown (2007). "Task-dependent asymmetries in the utilization of proprioceptive feedback for goal-directed movement." Exp Brain Res **180**(4): 693-704.

Goble, D. J. and S. H. Brown (2008). "The biological and behavioral basis of upper limb asymmetries in sensorimotor performance." Neurosci Biobehav Rev **32**(3): 598-610.

Goldring, S. and R. Ratcheson (1972). "Human motor cortex: sensory input data from single neuron recordings." Science **175**(4029): 1493-1495.

Grafton, S. T., J. C. Mazziotta, S. Presty, K. J. Friston, R. S. Frackowiak and M. E. Phelps (1992). "Functional anatomy of human procedural learning determined with regional cerebral blood flow and PET." J Neurosci **12**(7): 2542-2548.

Green, J. B., Y. Bialy, E. Sora and A. Ricamato (1999). "High-resolution EEG in poststroke hemiparesis can identify ipsilateral generators during motor tasks." Stroke **30**(12): 2659-2665.

Haaland, K. Y., J. L. Prestopnik, R. T. Knight and R. R. Lee (2004). "Hemispheric asymmetries for kinematic and positional aspects of reaching." Brain **127**(Pt 5): 1145-1158.

Haaland, K. Y., S. Y. Schaefer, R. T. Knight, J. Adair, A. Magalhaes, J. Sadek and R. L. Sainburg (2009). "Ipsilesional trajectory control is related to contralesional arm paralysis after left hemisphere damage." Exp Brain Res **196**(2): 195-204.

Heldman, D. A., W. Wang, S. S. Chan and D. W. Moran (2006). "Local field potential spectral tuning in motor cortex during reaching." IEEE Trans Neural Syst Rehabil Eng **14**(2): 180-183.

Hochberg, L. R., M. D. Serruya, G. M. Friehs, J. A. Mukand, M. Saleh, A. H. Caplan, A. Branner, D. Chen, R. D. Penn and J. P. Donoghue (2006). "Neuronal ensemble control of prosthetic devices by a human with tetraplegia." Nature **442**(7099): 164-171.

Honda, M., T. Nagamine, H. Fukuyama, Y. Yonekura, J. Kimura and H. Shibasaki (1997). "Movement-related cortical potentials and regional cerebral blood flow change in patients with stroke after motor recovery." J Neurol Sci **146**(2): 117-126.

Hotson, G., M. S. Fifer, S. Acharya, W. S. Anderson, N. V. Thakor and N. E. Crone (2012). "Electrocorticographic decoding of ipsilateral reach in the setting of contralateral arm weakness from a cortical lesion." Conf Proc IEEE Eng Med Biol Soc **2012**: 4104-4107.

Hotson, G., M. S. Fifer, S. Acharya, H. L. Benz, W. S. Anderson, N. V. Thakor and N. E. Crone (2014). "Coarse electrocorticographic decoding of ipsilateral reach in patients with brain lesions." PLoS One **9**(12): e115236.

Ince, N. F., R. Gupta, S. Arica, A. H. Tewfik, J. Ashe and G. Pellizzer (2010). "High accuracy decoding of movement target direction in non-human primates based on common spatial patterns of local field potentials." PLoS One **5**(12): e14384.

Jankelowitz, S. K. and J. G. Colebatch (2002). "Movement-related potentials associated with self-paced, cued and imagined arm movements." Exp Brain Res **147**(1): 98-107.

Jarosiewicz, B., S. M. Chase, G. W. Fraser, M. Velliste, R. E. Kass and A. B. Schwartz (2008). "Functional network reorganization during learning in a brain-computer interface paradigm." Proc Natl Acad Sci U S A **105**(49): 19486-19491.

Jasper, H. and W. Penfield (1949). "Electrocorticograms in man: effect of voluntary movement upon the electrical activity of the precentral gyrus." Archiv für Psychiatrie und Nervenkrankheiten **183**(1-2): 163-174.

Jasper, H. H. and H. L. Andrews (1938). "Electro-encephalography: III. Normal differentiation of occipital and precentral regions in man." Archives of Neurology & Psychiatry **39**(1): 96-115.

Jerbi, K., T. Ossandon, C. M. Hamame, S. Senova, S. S. Dalal, J. Jung, L. Minotti, O. Bertrand, A. Berthoz, P. Kahane and J. P. Lachaux (2009). "Task-related gamma-band dynamics from an intracerebral perspective: review and implications for surface EEG and MEG." Hum Brain Mapp **30**(6): 1758-1771.

Johansen-Berg, H., M. F. Rushworth, M. D. Bogdanovic, U. Kischka, S. Wimalaratna and P. M. Matthews (2002). "The role of ipsilateral premotor cortex in hand movement after stroke." Proc Natl Acad Sci U S A **99**(22): 14518-14523.

Jorgensen, H. S., H. Nakayama, H. O. Raaschou, J. Vive-Larsen, M. Stoier and T. S. Olsen (1995). "Outcome and time course of recovery in stroke. Part II: Time course of recovery. The Copenhagen Stroke Study." Arch Phys Med Rehabil **76**(5): 406-412.

Kaas, J. H. (1995). The organization of callosal connections in primates. Epilepsy and the corpus callosum 2, Springer**:** 15-27.

Kachenoura, A., L. Albera, L. Senhadji and P. Comon (2008). "ICA: a potential tool for BCI systems." Signal Processing Magazine, IEEE **25**(1): 57-68.

Kakei, S., D. S. Hoffman and P. L. Strick (1999). "Muscle and movement representations in the primary motor cortex." Science **285**(5436): 2136-2139.

Karni, A., G. Meyer, P. Jezzard, M. M. Adams, R. Turner and L. G. Ungerleider (1995). "Functional MRI evidence for adult motor cortex plasticity during motor skill learning." Nature **377**(6545): 155-158.

Kawashima, R., P. E. Roland and B. T. O'Sullivan (1994). "Activity in the human primary motor cortex related to ipsilateral hand movements." Brain Res **663**(2): 251-256.

Kawashima, R., K. Yamada, S. Kinomura, T. Yamaguchi, H. Matsui, S. Yoshioka and H. Fukuda (1993). "Regional cerebral blood flow changes of cortical motor areas and prefrontal areas in humans related to ipsilateral and contralateral hand movement." Brain Res **623**(1): 33-40.

Kellis, S., K. Miller, K. Thomson, R. Brown, P. House and B. Greger (2010). "Decoding spoken words using local field potentials recorded from the cortical surface." J Neural Eng **7**(5): 056007.

Kennedy, P., D. Andreasen, P. Ehirim, B. King, T. Kirby, H. Mao and M. Moore (2004). "Using human extra-cortical local field potentials to control a switch." J Neural Eng **1**(2): 72-77.

Kennedy, P. R. and R. A. Bakay (1998). "Restoration of neural output from a paralyzed patient by a direct brain connection." Neuroreport **9**(8): 1707-1711.

Kennedy, P. R., M. T. Kirby, M. M. Moore, B. King and A. Mallory (2004). "Computer control using human intracortical local field potentials." IEEE Trans Neural Syst Rehabil Eng **12**(3): 339-344.

Kermadi, I., Y. Liu and E. M. Rouiller (2000). "Do bimanual motor actions involve the dorsal premotor (PMd), cingulate (CMA) and posterior parietal (PPC) cortices? Comparison with primary and supplementary motor cortical areas." Somatosens Mot Res **17**(3): 255-271.

Kim, S. G., J. Ashe, A. P. Georgopoulos, H. Merkle, J. M. Ellermann, R. S. Menon, S. Ogawa and K. Ugurbil (1993a). "Functional imaging of human motor cortex at high magnetic field." J Neurophysiol **69**(1): 297-302.

Kim, S. G., J. Ashe, K. Hendrich, J. M. Ellermann, H. Merkle, K. Ugurbil and A. P. Georgopoulos (1993b). "Functional magnetic resonance imaging of motor cortex: hemispheric asymmetry and handedness." Science **261**(5121): 615-617.

Kim, S. P., J. D. Simeral, L. R. Hochberg, J. P. Donoghue and M. J. Black (2008). "Neural control of computer cursor velocity by decoding motor cortical spiking activity in humans with tetraplegia." J Neural Eng **5**(4): 455-476.

Kitamura, J., H. Shibasaki and T. Kondo (1993a). "A cortical slow potential is larger before an isolated movement of a single finger than simultaneous movement of two fingers." Electroencephalogr Clin Neurophysiol **86**(4): 252-258.

Kitamura, J., H. Shibasaki, A. Takagi, H. Nabeshima and A. Yamaguchi (1993b). "Enhanced negative slope of cortical potentials before sequential as compared with simultaneous extensions of two fingers." Electroencephalogr Clin Neurophysiol **86**(3): 176-182.

Koles, Z. J. (1991). "The quantitative extraction and topographic mapping of the abnormal components in the clinical EEG." Electroencephalogr Clin Neurophysiol **79**(6): 440-447.

Koles, Z. J., M. S. Lazar and S. Z. Zhou (1990). "Spatial patterns underlying population differences in the background EEG." Brain Topogr **2**(4): 275-284.

Korinek, A. M. (1997). "Risk factors for neurosurgical site infections after craniotomy: a prospective multicenter study of 2944 patients. The French Study Group of Neurosurgical Infections, the SEHP, and the C-CLIN Paris-Nord. Service Epidemiologie Hygiene et Prevention." Neurosurgery **41**(5): 1073-1079; discussion 1079-1081.

Kornhuber, H. H. and L. Deecke (1965). "[Changes in the Brain Potential in Voluntary Movements and Passive Movements in Man: Readiness Potential and Reafferent Potentials]." Pflugers Arch Gesamte Physiol Menschen Tiere **284**: 1-17.

Kubler, A., F. Nijboer, J. Mellinger, T. M. Vaughan, H. Pawelzik, G. Schalk, D. J. McFarland, N. Birbaumer and J. R. Wolpaw (2005). "Patients with ALS can use sensorimotor rhythms to operate a brain-computer interface." Neurology **64**(10): 1775-1777.

Kwakkel, G., B. J. Kollen, J. van der Grond and A. J. Prevo (2003). "Probability of regaining dexterity in the flaccid upper limb: impact of severity of paresis and time since onset in acute stroke." Stroke **34**(9): 2181-2186.

Lauer, R. T., P. H. Peckham and K. L. Kilgore (1999). "EEG-based control of a hand grasp neuroprosthesis." Neuroreport **10**(8): 1767-1771.

Leuthardt, E. C., Z. Freudenberg, D. Bundy and J. Roland (2009). "Microscale recording from human motor cortex: implications for minimally invasive electrocorticographic brain-computer interfaces." Neurosurg Focus **27**(1): E10.

Leuthardt, E. C., C. Gaona, M. Sharma, N. Szrama, J. Roland, Z. Freudenberg, J. Solis, J. Breshears and G. Schalk (2011). "Using the electrocorticographic speech network to control a brain-computer interface in humans." J Neural Eng **8**(3): 036004.

Leuthardt, E. C., K. J. Miller, G. Schalk, R. P. Rao and J. G. Ojemann (2006). "Electrocorticography-based brain computer interface--the Seattle experience." IEEE Trans Neural Syst Rehabil Eng **14**(2): 194-198.

Leuthardt, E. C., G. Schalk, J. Roland, A. Rouse and D. W. Moran (2009). "Evolution of brain-computer interfaces: going beyond classic motor physiology." Neurosurg Focus **27**(1): E4.

Leuthardt, E. C., G. Schalk, J. R. Wolpaw, J. G. Ojemann and D. W. Moran (2004). "A brain-computer interface using electrocorticographic signals in humans." J Neural Eng **1**(2): 63-71.

Levy, C. E., D. S. Nichols, P. M. Schmalbrock, P. Keller and D. W. Chakeres (2001). "Functional MRI evidence of cortical reorganization in upper-limb stroke hemiplegia treated with constraint-induced movement therapy." Am J Phys Med Rehabil **80**(1): 4-12.

Liepert, J., H. Bauder, H. R. Wolfgang, W. H. Miltner, E. Taub and C. Weiller (2000). "Treatment-induced cortical reorganization after stroke in humans." Stroke **31**(6): 1210-1216.

Liepert, J., W. H. Miltner, H. Bauder, M. Sommer, C. Dettmers, E. Taub and C. Weiller (1998). "Motor cortex plasticity during constraint-induced movement therapy in stroke patients." Neurosci Lett **250**(1): 5-8.

Lloyd-Jones, D., R. Adams, M. Carnethon, G. De Simone, T. B. Ferguson, K. Flegal, E. Ford, K. Furie, A. Go, K. Greenlund, N. Haase, S. Hailpern, M. Ho, V. Howard, B. Kissela, S. Kittner, D. Lackland, L. Lisabeth, A. Marelli, M. McDermott, J. Meigs, D. Mozaffarian, G. Nichol, C. O'Donnell, V. Roger, W. Rosamond, R. Sacco, P. Sorlie, R. Stafford, J. Steinberger, T. Thom, S. Wasserthiel-Smoller, N. Wong, J. Wylie-Rosett and Y. Hong (2009). "Heart disease and stroke statistics--2009 update: a report from the American Heart Association Statistics Committee and Stroke Statistics Subcommittee." Circulation **119**(3): e21-181.

Lotte, F. and C. Guan (2011). "Regularizing common spatial patterns to improve BCI designs: unified theory and new algorithms." IEEE Trans Biomed Eng **58**(2): 355-362.

Lotze, M., J. Markert, P. Sauseng, J. Hoppe, C. Plewnia and C. Gerloff (2006). "The role of multiple contralesional motor areas for complex hand movements after internal capsular lesion." J Neurosci **26**(22): 6096-6102.

Mackay, J., G. A. Mensah, S. Mendis, K. Greenlund and World Health Organization. (2004). The atlas of heart disease and stroke. Geneva, World Health Organization.

Makeig, S., A. J. Bell, T.-P. Jung and T. J. Sejnowski (1996). "Independent component analysis of electroencephalographic data." Advances in neural information processing systems: 145-151.

Manganotti, P., C. Gerloff, C. Toro, H. Katsuta, N. Sadato, P. Zhuang, L. Leocani and M. Hallett (1998). "Task-related coherence and task-related spectral power changes during sequential finger movements." Electroencephalogr Clin Neurophysiol **109**(1): 50-62.

Manola, L., B. H. Roelofsen, J. Holsheimer, E. Marani and J. Geelen (2005). "Modelling motor cortex stimulation for chronic pain control: electrical potential field, activating functions and responses of simple nerve fibre models." Med Biol Eng Comput **43**(3): 335-343.

Marathe, A. R. and D. M. Taylor (2013). "Decoding continuous limb movements from high-density epidural electrode arrays using custom spatial filters." J Neural Eng **10**(3): 036015.

Marple, L. (1987a). Digital spectral analysis with applications. Upper Saddle River, NJ, Prentice-Hall.

Marple, S. L. (1987b). Digital spectral analysis : with applications. Englewood Cliffs, N.J., Prentice-Hall.

Marshall, R. S., G. M. Perera, R. M. Lazar, J. W. Krakauer, R. C. Constantine and R. L. DeLaPaz (2000). "Evolution of cortical activation during recovery from corticospinal tract infarction." Stroke **31**(3): 656-661.

McFarland, D. J., W. A. Sarnacki and J. R. Wolpaw (2010). "Electroencephalographic (EEG) control of three-dimensional movement." J Neural Eng **7**(3): 036007.

Miller, K. J., E. C. Leuthardt, G. Schalk, R. P. Rao, N. R. Anderson, D. W. Moran, J. W. Miller and J. G. Ojemann (2007). "Spectral changes in cortical surface potentials during motor movement." J Neurosci **27**(9): 2424-2432.

Miller, K. J., S. Makeig, A. O. Hebb, R. P. Rao, M. denNijs and J. G. Ojemann (2007). "Cortical electrode localization from X-rays and simple mapping for electrocorticographic research: The "Location on Cortex" (LOC) package for MATLAB." J Neurosci Methods **162**(1-2): 303-308.

Miller, K. J., L. B. Sorensen, J. G. Ojemann and M. den Nijs (2009). "Power-law scaling in the brain surface electric potential." Plos Computational Biology **5**(12): e1000609.

Miller, K. J., S. Zanos, E. E. Fetz, M. den Nijs and J. G. Ojemann (2009). "Decoupling the cortical power spectrum reveals real-time representation of individual finger movements in humans." J Neurosci **29**(10): 3132-3137.

Mollman, H. D. and S. J. Haines (1986). "Risk factors for postoperative neurosurgical wound infection. A case-control study." J Neurosurg **64**(6): 902-906.

Moran, D. (2010). "Evolution of brain-computer interface: action potentials, local field potentials and electrocorticograms." Curr Opin Neurobiol **20**(6): 741-745.

Moran, D. W. and A. B. Schwartz (1999a). "Motor cortical activity during drawing movements: population representation during spiral tracing." J Neurophysiol **82**(5): 2693-2704.

Moran, D. W. and A. B. Schwartz (1999b). "Motor cortical representation of speed and direction during reaching." J Neurophysiol **82**(5): 2676-2692.

Mukaino, M., T. Ono, K. Shindo, T. Fujiwara, T. Ota, A. Kimura, M. Liu and J. Ushiba (2014). "Efficacy of brain-computer interface-driven neuromuscular electrical stimulation for chronic paresis after stroke." J Rehabil Med **46**(4): 378-382.

Murase, N., J. Duque, R. Mazzocchio and L. G. Cohen (2004). "Influence of interhemispheric interactions on motor function in chronic stroke." Ann Neurol **55**(3): 400-409.

Nakanishi, Y., T. Yanagisawa, D. Shin, R. Fukuma, C. Chen, H. Kambara, N. Yoshimura, M. Hirata, T. Yoshimine and Y. Koike (2013). "Prediction of three-dimensional arm

trajectories based on ECoG signals recorded from human sensorimotor cortex." PLoS One **8**(8): e72085.
Nelles, G., G. Spiekramann, M. Jueptner, G. Leonhardt, S. Muller, H. Gerhard and H. C. Diener (1999). "Evolution of functional reorganization in hemiplegic stroke: a serial positron emission tomographic activation study." Ann Neurol **46**(6): 901-909.
Netz, J., T. Lammers and V. Homberg (1997). "Reorganization of motor output in the non-affected hemisphere after stroke." Brain **120 (Pt 9)**: 1579-1586.
Nudo, R. J., B. M. Wise, F. SiFuentes and G. W. Milliken (1996). "Neural substrates for the effects of rehabilitative training on motor recovery after ischemic infarct." Science **272**(5269): 1791-1794.
Nyberg-Hansen, R. and A. Brodal (1963). "Sites of termination of corticospinal fibers in the cat. An experimental study with silver impregnation methods." J Comp Neurol **120**: 369-391.
Nyberg-Hansen, R. and E. Rinvik (1963). "Some comments on the pyramidal tract, with special reference to its individual variations in man." Acta Neurologica Scandinavica **39**(1): 1-30.
Penfield, W. and E. Boldrey (1937). "Somatic motor and sensory representation in the cerebral cortex of man as studied by electrical stimulation." Brain: A journal of neurology.
Penfield, W. and H. H. Jasper (1954). Epilepsy and the functional anatomy of the human brain. Boston,, Little.
Penfield, W. and T. Rasmussen (1950). The cerebral cortex of man; a clinical study of localization of function. New York,, Macmillan.
Pfurtscheller, G. (1992). "Event-related synchronization (ERS): an electrophysiological correlate of cortical areas at rest." Electroencephalogr Clin Neurophysiol **83**(1): 62-69.
Pfurtscheller, G. and A. Aranibar (1979). "Evaluation of event-related desynchronization (ERD) preceding and following voluntary self-paced movement." Electroencephalogr Clin Neurophysiol **46**(2): 138-146.
Pfurtscheller, G. and A. Berghold (1989). "Patterns of cortical activation during planning of voluntary movement." Electroencephalogr Clin Neurophysiol **72**(3): 250-258.
Pfurtscheller, G. and R. Cooper (1975). "Frequency dependence of the transmission of the EEG from cortex to scalp." Electroencephalogr Clin Neurophysiol **38**(1): 93-96.
Pfurtscheller, G., C. Guger, G. Muller, G. Krausz and C. Neuper (2000). "Brain oscillations control hand orthosis in a tetraplegic." Neurosci Lett **292**(3): 211-214.
Pfurtscheller, G., G. Ladurner, H. Maresch and R. Vollmer (1984). "Brain electrical activity mapping in normal and ischemic brain." Prog Brain Res **62**: 287-302.
Pfurtscheller, G. and F. H. Lopes da Silva (1999). "Event-related EEG/MEG synchronization and desynchronization: basic principles." Clin Neurophysiol **110**(11): 1842-1857.
Pfurtscheller, G., G. R. Muller, J. Pfurtscheller, H. J. Gerner and R. Rupp (2003). "'Thought'--control of functional electrical stimulation to restore hand grasp in a patient with tetraplegia." Neurosci Lett **351**(1): 33-36.
Pfurtscheller, G. and C. Neuper (1997). "Motor imagery activates primary sensorimotor area in humans." Neurosci Lett **239**(2-3): 65-68.
Pfurtscheller, G., C. Neuper and G. Krausz (2000). "Functional dissociation of lower and upper frequency mu rhythms in relation to voluntary limb movement." Clin Neurophysiol **111**(10): 1873-1879.

Pfurtscheller, G., C. Neuper, G. R. Muller, B. Obermaier, G. Krausz, A. Schlogl, R. Scherer, B. Graimann, C. Keinrath, D. Skliris, M. Wortz, G. Supp and C. Schrank (2003). "Graz-BCI: state of the art and clinical applications." IEEE Trans Neural Syst Rehabil Eng **11**(2): 177-180.

Pfurtscheller, G., A. Stancak, Jr. and G. Edlinger (1997). "On the existence of different types of central beta rhythms below 30 Hz." Electroencephalogr Clin Neurophysiol **102**(4): 316-325.

Pistohl, T., T. Ball, A. Schulze-Bonhage, A. Aertsen and C. Mehring (2008). "Prediction of arm movement trajectories from ECoG-recordings in humans." J Neurosci Methods **167**(1): 105-114.

Ramon, C., P. H. Schimpf and J. Haueisen (2006). "Influence of head models on EEG simulations and inverse source localizations." Biomed Eng Online **5**: 10.

Ramos-Murguialday, A., D. Broetz, M. Rea, L. Laer, O. Yilmaz, F. L. Brasil, G. Liberati, M. R. Curado, E. Garcia-Cossio, A. Vyziotis, W. Cho, M. Agostini, E. Soares, S. Soekadar, A. Caria, L. G. Cohen and N. Birbaumer (2013). "Brain-machine interface in chronic stroke rehabilitation: a controlled study." Ann Neurol **74**(1): 100-108.

Ramoser, H., J. Muller-Gerking and G. Pfurtscheller (2000). "Optimal spatial filtering of single trial EEG during imagined hand movement." IEEE Trans Rehabil Eng **8**(4): 441-446.

Rao, S. M., J. R. Binder, P. A. Bandettini, T. A. Hammeke, F. Z. Yetkin, A. Jesmanowicz, L. M. Lisk, G. L. Morris, W. M. Mueller, L. D. Estkowski and et al. (1993). "Functional magnetic resonance imaging of complex human movements." Neurology **43**(11): 2311-2318.

Rau, C., C. Plewnia, F. Hummel and C. Gerloff (2003). "Event-related desynchronization and excitability of the ipsilateral motor cortex during simple self-paced finger movements." Clin Neurophysiol **114**(10): 1819-1826.

Reddy, C. G., G. G. Reddy, H. Kawasaki, H. Oya, L. E. Miller and M. A. Howard, 3rd (2009). "Decoding movement-related cortical potentials from electrocorticography." Neurosurg Focus **27**(1): E11.

Rickert, J., S. C. Oliveira, E. Vaadia, A. Aertsen, S. Rotter and C. Mehring (2005). "Encoding of movement direction in different frequency ranges of motor cortical local field potentials." J Neurosci **25**(39): 8815-8824.

Roland, P. E. (1985). "Cortical organization of voluntary behavior in man." Hum Neurobiol **4**(3): 155-167.

Roland, P. E., B. Larsen, N. A. Lassen and E. Skinhoj (1980). "Supplementary motor area and other cortical areas in organization of voluntary movements in man." J Neurophysiol **43**(1): 118-136.

Roland, P. E., E. Meyer, T. Shibasaki, Y. L. Yamamoto and C. J. Thompson (1982). "Regional cerebral blood flow changes in cortex and basal ganglia during voluntary movements in normal human volunteers." J Neurophysiol **48**(2): 467-480.

Rossiter, H. E., C. Eaves, E. Davis, M. H. Boudrias, C. H. Park, S. Farmer, G. Barnes, V. Litvak and N. S. Ward (2012). "Changes in the location of cortico-muscular coherence following stroke." Neuroimage Clin **2**: 50-55.

Rouse, A. G. and D. W. Moran (2009). "Neural adaptation of epidural electrocorticographic (EECoG) signals during closed-loop brain computer interface (BCI) tasks." Conf Proc IEEE Eng Med Biol Soc **2009**: 5514-5517.

Rouse, A. G., A. T. Roussin and M. H. Schieber (2014). Location then object representations sequentially predominate in the widely distributed activation of the primary motor cortex during reach to grasp. 2014 Neuroscience Meeting Planner. P. N. 437.23. Washington, DC, Society for Neuroscience. **Online**.

Rouse, A. G., S. R. Stanslaski, P. Cong, R. M. Jensen, P. Afshar, D. Ullestad, R. Gupta, G. F. Molnar, D. W. Moran and T. J. Denison (2011). "A chronic generalized bi-directional brain-machine interface." J Neural Eng **8**(3): 036018.

Rouse, A. G., J. J. Williams, J. J. Wheeler and D. W. Moran (2013). "Cortical adaptation to a chronic micro-electrocorticographic brain computer interface." J Neurosci **33**(4): 1326-1330.

Sainburg, R. L. and D. Kalakanis (2000). "Differences in control of limb dynamics during dominant and nondominant arm reaching." J Neurophysiol **83**(5): 2661-2675.

Sainburg, R. L. and S. Y. Schaefer (2004). "Interlimb differences in control of movement extent." J Neurophysiol **92**(3): 1374-1383.

Salmelin, R. and R. Hari (1994). "Spatiotemporal characteristics of sensorimotor neuromagnetic rhythms related to thumb movement." Neuroscience **60**(2): 537-550.

Samek, W., C. Vidaurre, K. R. Muller and M. Kawanabe (2012). "Stationary common spatial patterns for brain-computer interfacing." J Neural Eng **9**(2): 026013.

Sanchez, J. C., A. Gunduz, P. R. Carney and J. C. Principe (2008). "Extraction and localization of mesoscopic motor control signals for human ECoG neuroprosthetics." J Neurosci Methods **167**(1): 63-81.

Schaechter, J. D., E. Kraft, T. S. Hilliard, R. M. Dijkhuizen, T. Benner, S. P. Finklestein, B. R. Rosen and S. C. Cramer (2002). "Motor recovery and cortical reorganization after constraint-induced movement therapy in stroke patients: a preliminary study." Neurorehabil Neural Repair **16**(4): 326-338.

Schaechter, J. D., K. L. Perdue and R. Wang (2008). "Structural damage to the corticospinal tract correlates with bilateral sensorimotor cortex reorganization in stroke patients." Neuroimage **39**(3): 1370-1382.

Schaefer, S. Y., K. Y. Haaland and R. L. Sainburg (2007). "Ipsilesional motor deficits following stroke reflect hemispheric specializations for movement control." Brain **130**(Pt 8): 2146-2158.

Schaefer, S. Y., K. Y. Haaland and R. L. Sainburg (2009a). "Dissociation of initial trajectory and final position errors during visuomotor adaptation following unilateral stroke." Brain Res **1298**: 78-91.

Schaefer, S. Y., K. Y. Haaland and R. L. Sainburg (2009b). "Hemispheric specialization and functional impact of ipsilesional deficits in movement coordination and accuracy." Neuropsychologia **47**(13): 2953-2966.

Schaefer, S. Y., P. K. Mutha, K. Y. Haaland and R. L. Sainburg (2012). "Hemispheric specialization for movement control produces dissociable differences in online corrections after stroke." Cereb Cortex **22**(6): 1407-1419.

Schalk, G., J. Kubanek, K. J. Miller, N. R. Anderson, E. C. Leuthardt, J. G. Ojemann, D. Limbrick, D. Moran, L. A. Gerhardt and J. R. Wolpaw (2007). "Decoding two-dimensional movement trajectories using electrocorticographic signals in humans." J Neural Eng **4**(3): 264-275.

Schalk, G. and E. C. Leuthardt (2011). "Brain-computer interfaces using electrocorticographic signals." IEEE Rev Biomed Eng **4**: 140-154.

Schalk, G., D. J. McFarland, T. Hinterberger, N. Birbaumer and J. R. Wolpaw (2004a). "BCI2000: a general-purpose brain-computer interface (BCI) system." IEEE Trans Biomed Eng **51**(6): 1034-1043.

Schalk, G., D. J. McFarland, T. Hinterberger, N. Birbaumer and J. R. Wolpaw (2004b). "BCI2000: A general-purpose, brain-computer interface (BCI) system." Ieee Transactions on Biomedical Engineering **51**(6): 1034-1043.

Schalk, G., K. J. Miller, N. R. Anderson, J. A. Wilson, M. D. Smyth, J. G. Ojemann, D. W. Moran, J. R. Wolpaw and E. C. Leuthardt (2008). "Two-dimensional movement control using electrocorticographic signals in humans." J Neural Eng **5**(1): 75-84.

Scherer, R., S. P. Zanos, K. J. Miller, R. P. Rao and J. G. Ojemann (2009). "Classification of contralateral and ipsilateral finger movements for electrocorticographic brain-computer interfaces." Neurosurg Focus **27**(1): E12.

Schwartz, A. B. and D. W. Moran (1999). "Motor cortical activity during drawing movements: population representation during lemniscate tracing." J Neurophysiol **82**(5): 2705-2718.

Serruya, M. D., N. G. Hatsopoulos, L. Paninski, M. R. Fellows and J. P. Donoghue (2002). "Instant neural control of a movement signal." Nature **416**(6877): 141-142.

Sharma, M., C. Gaona, J. Roland, N. Anderson, Z. Freudenberg and E. C. Leuthardt (2009). "Ipsilateral directional encoding of joystick movements in human cortex." Conf Proc IEEE Eng Med Biol Soc **2009**: 5502-5505.

Shibasaki, H. and M. Hallett (2006). "What is the Bereitschaftspotential?" Clin Neurophysiol **117**(11): 2341-2356.

Shimoda, K., Y. Nagasaka, Z. C. Chao and N. Fujii (2012). "Decoding continuous three-dimensional hand trajectories from epidural electrocorticographic signals in Japanese macaques." J Neural Eng **9**(3): 036015.

Shoshani, J., W. J. Kupsky and G. H. Marchant (2006). "Elephant brain. Part I: gross morphology, functions, comparative anatomy, and evolution." Brain Res Bull **70**(2): 124-157.

Slobounov, S., M. Hallett and K. M. Newell (2004). "Perceived effort in force production as reflected in motor-related cortical potentials." Clin Neurophysiol **115**(10): 2391-2402.

Slutzky, M. W., L. R. Jordan, T. Krieg, M. Chen, D. J. Mogul and L. E. Miller (2010). "Optimal spacing of surface electrode arrays for brain-machine interface applications." J Neural Eng **7**(2): 26004.

Slutzky, M. W., L. R. Jordan, E. W. Lindberg, K. E. Lindsay and L. E. Miller (2011). "Decoding the rat forelimb movement direction from epidural and intracortical field potentials." J Neural Eng **8**(3): 036013.

Soekadar, S. R., S. Silvoni, L. G. Cohen and N. Birbaumer (2015). Brain–Machine Interfaces in Stroke Neurorehabilitation. Clinical Systems Neuroscience, Springer**:** 3-14.

Soekadar, S. R., M. Witkowski, J. Mellinger, A. Ramos, N. Birbaumer and L. G. Cohen (2011). "ERD-based online brain-machine interfaces (BMI) in the context of neurorehabilitation: optimizing BMI learning and performance." IEEE Trans Neural Syst Rehabil Eng **19**(5): 542-549.

Steinberg, O., O. Donchin, A. Gribova, S. Cardosa de Oliveira, H. Bergman and E. Vaadia (2002). "Neuronal populations in primary motor cortex encode bimanual arm movements." Eur J Neurosci **15**(8): 1371-1380.

Sunderland, A. (2000). "Recovery of ipsilateral dexterity after stroke." Stroke **31**(2): 430-433.

Takahashi, C. D., L. Der-Yeghiaian, V. Le, R. R. Motiwala and S. C. Cramer (2008). "Robot-based hand motor therapy after stroke." Brain **131**(Pt 2): 425-437.
Tanji, J., K. Okano and K. C. Sato (1987). "Relation of neurons in the nonprimary motor cortex to bilateral hand movement." Nature **327**(6123): 618-620.
Tanji, J., K. Okano and K. C. Sato (1988). "Neuronal activity in cortical motor areas related to ipsilateral, contralateral, and bilateral digit movements of the monkey." J Neurophysiol **60**(1): 325-343.
Taylor, D. M., S. I. Tillery and A. B. Schwartz (2002). "Direct cortical control of 3D neuroprosthetic devices." Science **296**(5574): 1829-1832.
Tecchio, F., F. Zappasodi, M. Tombini, A. Oliviero, P. Pasqualetti, F. Vernieri, M. Ercolani, V. Pizzella and P. M. Rossini (2006). "Brain plasticity in recovery from stroke: an MEG assessment." Neuroimage **32**(3): 1326-1334.
Tenney, J. H., D. Vlahov, M. Salcman and T. B. Ducker (1985). "Wide variation in risk of wound infection following clean neurosurgery. Implications for perioperative antibiotic prophylaxis." J Neurosurg **62**(2): 243-247.
Toro, C., G. Deuschl, R. Thatcher, S. Sato, C. Kufta and M. Hallett (1994). "Event-related desynchronization and movement-related cortical potentials on the ECoG and EEG." Electroencephalogr Clin Neurophysiol **93**(5): 380-389.
Torres Valderrama, A., R. Oostenveld, M. J. Vansteensel, G. M. Huiskamp and N. F. Ramsey (2010). "Gain of the human dura in vivo and its effects on invasive brain signal feature detection." J Neurosci Methods **187**(2): 270-279.
Treuting, P. M., S. M. Dintzis, C. W. Frevert, H. D. Liggitt and K. S. Montine (2012). Comparative anatomy and histology : a mouse and human atlas. Amsterdam ; Boston, Elsevier/Academic Press.
Tung, S. W., C. Guan, K. K. Ang, K. S. Phua, C. Wang, L. Zhao, W. P. Teo and E. Chew (2013). "Motor imagery BCI for upper limb stroke rehabilitation: An evaluation of the EEG recordings using coherence analysis." Conf Proc IEEE Eng Med Biol Soc **2013**: 261-264.
Turton, A., S. Wroe, N. Trepte, C. Fraser and R. N. Lemon (1996). "Contralateral and ipsilateral EMG responses to transcranial magnetic stimulation during recovery of arm and hand function after stroke." Electroencephalogr Clin Neurophysiol **101**(4): 316-328.
Velliste, M., S. Perel, M. C. Spalding, A. S. Whitford and A. B. Schwartz (2008). "Cortical control of a prosthetic arm for self-feeding." Nature **453**(7198): 1098-1101.
Venkatraman, S., J. Hendricks, Z. A. King, A. J. Sereno, S. Richardson-Burns, D. Martin and J. M. Carmena (2011). "In vitro and in vivo evaluation of PEDOT microelectrodes for neural stimulation and recording." IEEE Trans Neural Syst Rehabil Eng **19**(3): 307-316.
Verstynen, T. and R. B. Ivry (2011). "Network dynamics mediating ipsilateral motor cortex activity during unimanual actions." J Cogn Neurosci **23**(9): 2468-2480.
Wang, W., S. S. Chan, D. A. Heldman and D. W. Moran (2007). "Motor cortical representation of position and velocity during reaching." J Neurophysiol **97**(6): 4258-4270.
Wang, W., S. S. Chan, D. A. Heldman and D. W. Moran (2010). "Motor cortical representation of hand translation and rotation during reaching." J Neurosci **30**(3): 958-962.
Wang, W., J. L. Collinger, A. D. Degenhart, E. C. Tyler-Kabara, A. B. Schwartz, D. W. Moran, D. J. Weber, B. Wodlinger, R. K. Vinjamuri, R. C. Ashmore, J. W. Kelly and M. L. Boninger (2013). "An electrocorticographic brain interface in an individual with tetraplegia." PLoS One **8**(2): e55344.

Wang, W., A. D. Degenhart, J. L. Collinger, R. Vinjamuri, G. P. Sudre, P. D. Adelson, D. L. Holder, E. C. Leuthardt, D. W. Moran, M. L. Boninger, A. B. Schwartz, D. J. Crammond, E. C. Tyler-Kabara and D. J. Weber (2009). "Human motor cortical activity recorded with Micro-ECoG electrodes, during individual finger movements." Conf Proc IEEE Eng Med Biol Soc **2009**: 586-589.

Wang, Z., A. Gunduz, P. Brunner, A. L. Ritaccio, Q. Ji and G. Schalk (2012). "Decoding onset and direction of movements using Electrocorticographic (ECoG) signals in humans." Front Neuroeng **5**: 15.

Ward, N. S., M. M. Brown, A. J. Thompson and R. S. Frackowiak (2003a). "Neural correlates of motor recovery after stroke: a longitudinal fMRI study." Brain **126**(Pt 11): 2476-2496.

Ward, N. S., M. M. Brown, A. J. Thompson and R. S. Frackowiak (2003b). "Neural correlates of outcome after stroke: a cross-sectional fMRI study." Brain **126**(Pt 6): 1430-1448.

Weiller, C., F. Chollet, K. J. Friston, R. J. Wise and R. S. Frackowiak (1992). "Functional reorganization of the brain in recovery from striatocapsular infarction in man." Ann Neurol **31**(5): 463-472.

Weiller, C., S. C. Ramsay, R. J. Wise, K. J. Friston and R. S. Frackowiak (1993). "Individual patterns of functional reorganization in the human cerebral cortex after capsular infarction." Ann Neurol **33**(2): 181-189.

Wessberg, J., C. R. Stambaugh, J. D. Kralik, P. D. Beck, M. Laubach, J. K. Chapin, J. Kim, S. J. Biggs, M. A. Srinivasan and M. A. Nicolelis (2000). "Real-time prediction of hand trajectory by ensembles of cortical neurons in primates." Nature **408**(6810): 361-365.

Williams, J. (2013). ECoG correlates of visuomotor transformation, neural plasticity, and application to a force-based brain computer interface. St. Louis, Washington University. **PhD**.

Williams, J. C., J. A. Hippensteel, J. Dilgen, W. Shain and D. R. Kipke (2007). "Complex impedance spectroscopy for monitoring tissue responses to inserted neural implants." J Neural Eng **4**(4): 410-423.

Wilson, J. A., E. A. Felton, P. C. Garell, G. Schalk and J. C. Williams (2006). "ECoG factors underlying multimodal control of a brain-computer interface." IEEE Trans Neural Syst Rehabil Eng **14**(2): 246-250.

Wisneski, K. J., N. Anderson, G. Schalk, M. Smyth, D. Moran and E. C. Leuthardt (2008). "Unique cortical physiology associated with ipsilateral hand movements and neuroprosthetic implications." Stroke **39**(12): 3351-3359.

Wold, S., A. Ruhe, H. Wold and W. J. Dunn (1984). "The Collinearity Problem in Linear-Regression - the Partial Least-Squares (Pls) Approach to Generalized Inverses." Siam Journal on Scientific and Statistical Computing **5**(3): 735-743.

Wolf, S. L., P. A. Thompson, C. J. Winstein, J. P. Miller, S. R. Blanton, D. S. Nichols-Larsen, D. M. Morris, G. Uswatte, E. Taub, K. E. Light and L. Sawaki (2010). "The EXCITE stroke trial: comparing early and delayed constraint-induced movement therapy." Stroke **41**(10): 2309-2315.

Wolpaw, J. R. and D. J. McFarland (2004). "Control of a two-dimensional movement signal by a noninvasive brain-computer interface in humans." Proc Natl Acad Sci U S A **101**(51): 17849-17854.

Wolpaw, J. R., D. J. McFarland, G. W. Neat and C. A. Forneris (1991). "An EEG-based brain-computer interface for cursor control." Electroencephalogr Clin Neurophysiol **78**(3): 252-259.

Wolpaw, J. R., D. J. McFarland, T. M. Vaughan and G. Schalk (2003). "The Wadsworth Center brain-computer interface (BCI) research and development program." IEEE Trans Neural Syst Rehabil Eng **11**(2): 204-207.

Wu, W., M. J. Black, Y. Gao, E. Bienenstock, M. Serruya, A. Shaikhouni and J. P. Donoghue (2003). "Neural decoding of cursor motion using a Kalman filter." Advances in neural information processing systems: 133-140.

Wyss, O. A. (1938). "On an ipsilateral motor effect from cortical stimulation in the Macaque monkey." Journal of Neurophysiology **1**(2): 125-126.

Yakovlev, P. and P. Rakic (1966). "Patterns of decussation of bulbar pyramids and distribution of pyramidal tracts on two sides of the spinal cord." Trans Am Neurol Assoc **91**: 366-367.

Yarosh, C. A., D. S. Hoffman and P. L. Strick (2004). "Deficits in movements of the wrist ipsilateral to a stroke in hemiparetic subjects." J Neurophysiol **92**(6): 3276-3285.

Yelnik, A., I. Bonan, M. Debray, E. Lo, F. Gelbert and B. Bussel (1996). "Changes in the execution of a complex manual task after ipsilateral ischemic cerebral hemispheric stroke." Arch Phys Med Rehabil **77**(8): 806-810.

Yoshii, F., M. D. Ginsberg, R. E. Kelley, J. Y. Chang, W. W. Barker, G. Ingenito, A. M. Apicella, M. Y. Globus, R. Duara and T. E. Boothe (1989). "Asymmetric somatosensory activation with right- vs left-hand stimulation: a positron emission tomographic study." Brain Res **483**(2): 355-360.

Zanos, S., K. J. Miller and J. G. Ojemann (2008). "Electrocorticographic spectral changes associated with ipsilateral individual finger and whole hand movement." Conf Proc IEEE Eng Med Biol Soc **2008**: 5939-5942.

Appendix: Surrogate Models Used to Evaluate ECoG Predictions of Movements

To examine whether the predictions of kinematic parameters were significantly different from chance, the prediction accuracy expected by chance was evaluated using two surrogate prediction methods to ensure that the results were not affected by any systematic bias. First, a surrogate kinematic dataset was created by randomly reordering training set trials, randomly choosing a time point within each trial as the beginning of the trial, and constructing a new kinematic time course of the same length for the trial by wrapping the kinematic data from the beginning of the trial onto the end of the trial. A surrogate prediction model was trained using the original ECoG data and the surrogate training kinematic data. The surrogate model accuracy was calculated using the original testing set. An example of the original and surrogate kinematic data from a single training fold is shown in Figure A.1. This method was used as it randomized the relationship between ECoG activity and kinematic parameters, while maintaining the autocorrelation structure of real movement kinematics. Figure A.2 shows the autocorrelation of the original kinematics and surrogate kinematic sets for all patients. For all patients, the shape of the autocorrelation is indeed similar between the original and temporal surrogates.

For the second surrogate method, after training prediction models, the ECoG channels and features were shuffled by reordering the prediction weights. The surrogate model accuracy was calculated by using these reshuffled prediction weights with the original ECoG data to calculate predicted kinematics. Both surrogate methods were used to calculate the statistical significance of the logistic regression model predicting movement state as well as the PLS model predicting movement kinematics.

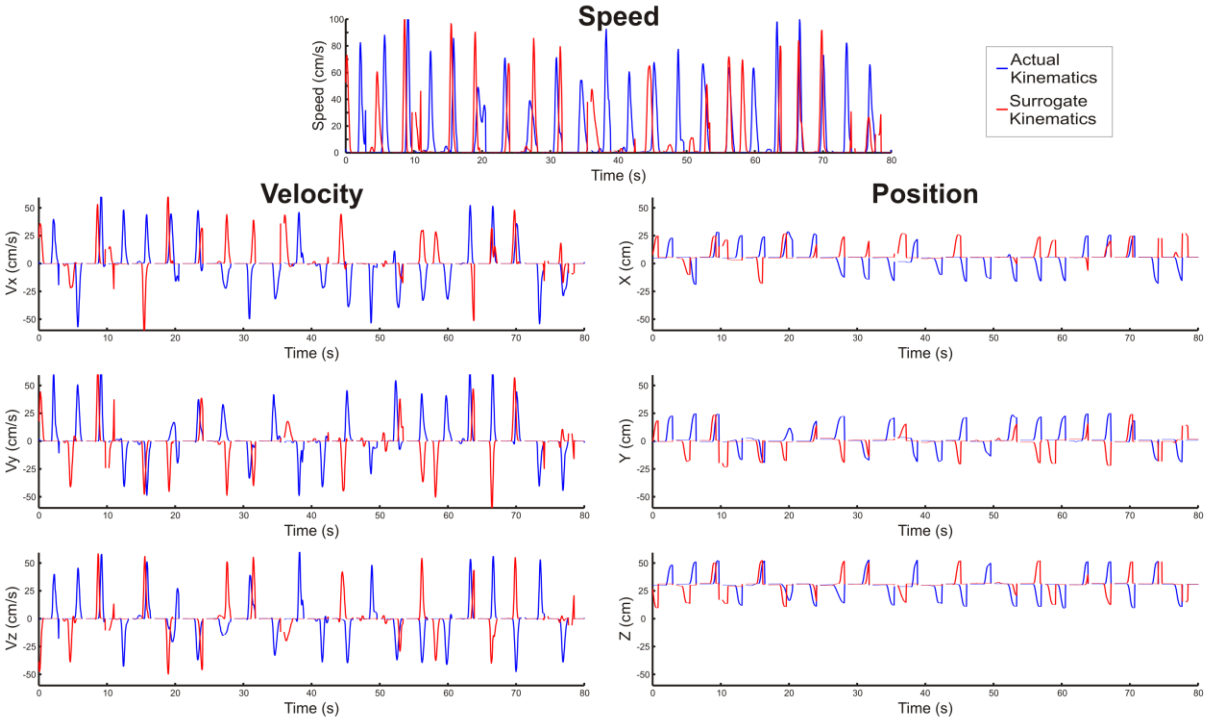

Figure A. 1 Exemplar original and surrogate kinematic training data
The first method for establishing the prediction accuracy expected by chance involved calculating surrogate kinematic training data. The original kinematic training data (blue traces) and surrogate kinematic data (red traces) are shown for a single training fold for speed, velocity, and position. The surrogate data has a new and random relationship between kinematics and ECoG activity as seen by the different movement times and directions, but maintained the smooth temporal structure of the original kinematics.

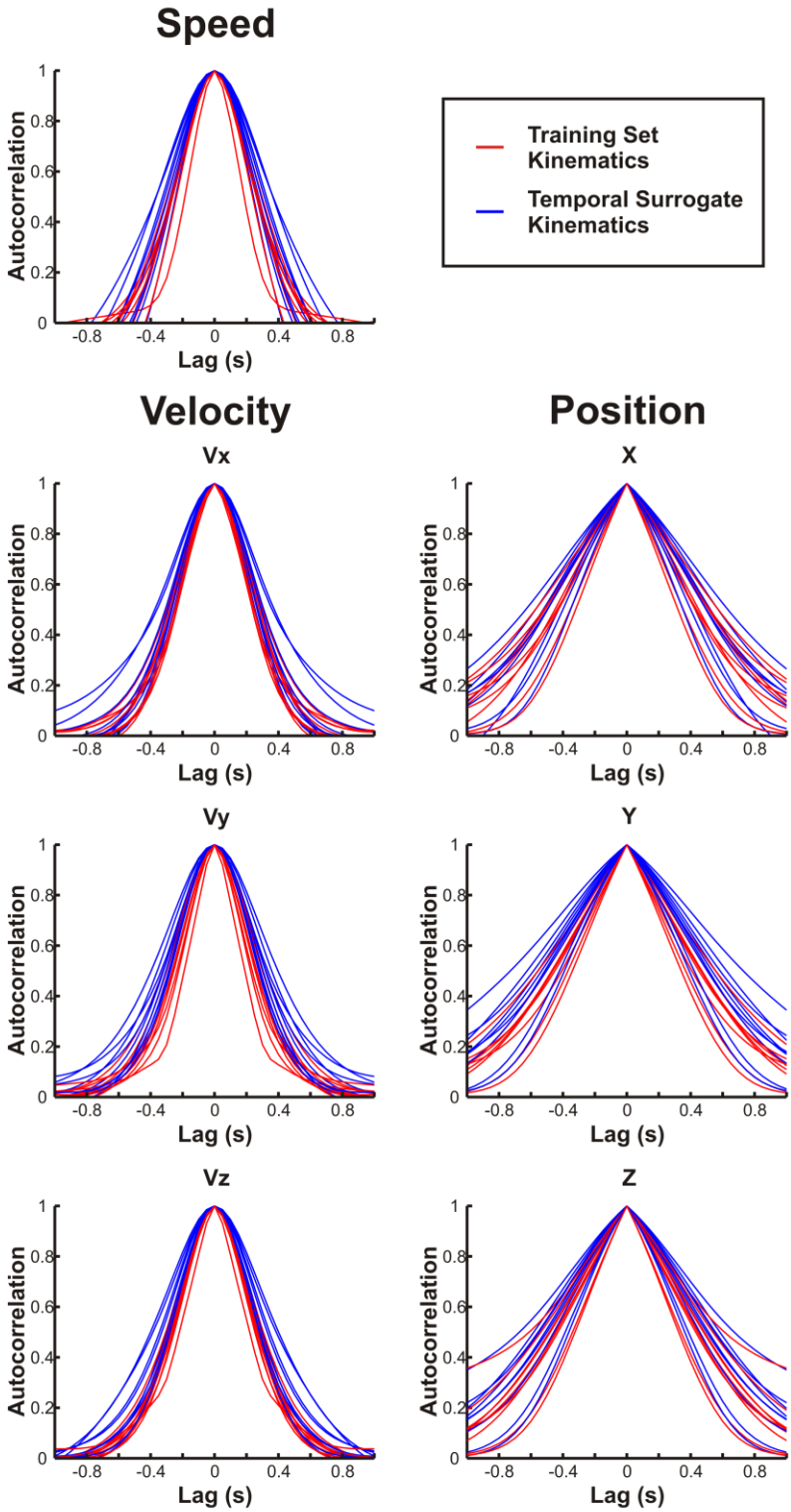

Figure A.2 Autocorrelations of original and temporal surrogate kinematic data
The temporal reshuffling strategy was designed to randomize the relationship between movement kinematics and ECoG activity while maintaining the autocorrelation structure between the two datasets. The plots show the average autocorrelation of each

kinematic parameter for each of the patients. In each of the kinematics, the shape of the autocorrelation is similar for both the original and surrogate data, demonstrating that the surrogates did indeed maintain the temporal structure inherent in the kinematic data.

Figure A.3 Shows exemplar movement class predictions using the original model, a surrogate prediction from a model trained with temporally shuffled kinematics, and a surrogate prediction using reshuffled features. Figure A.4 Shows exemplar PLS predictions made using the original model as well as both of the surrogate methods. The accuracies for predictions made using both surrogate methods are worse than the original model, confirming the group results presented in the main text.

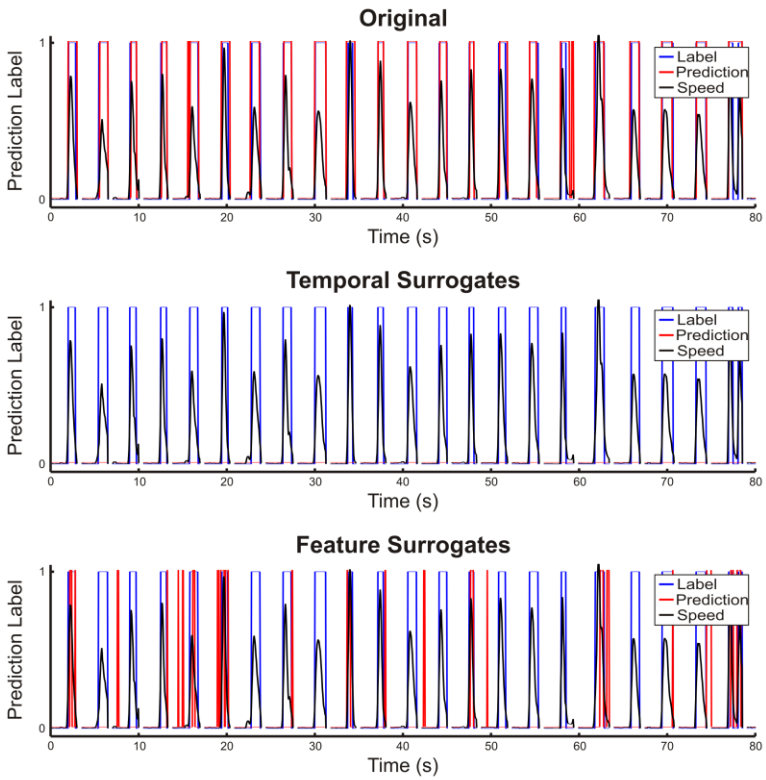

Figure A.3 Exemplar Original and Surrogate Movement Class Predictions
The original and surrogate predictions of movement class are shown for a testing set from a single exemplar patient. Both the surrogate predictions made using the temporal and feature surrogates fail to accurate classify movement from rest.

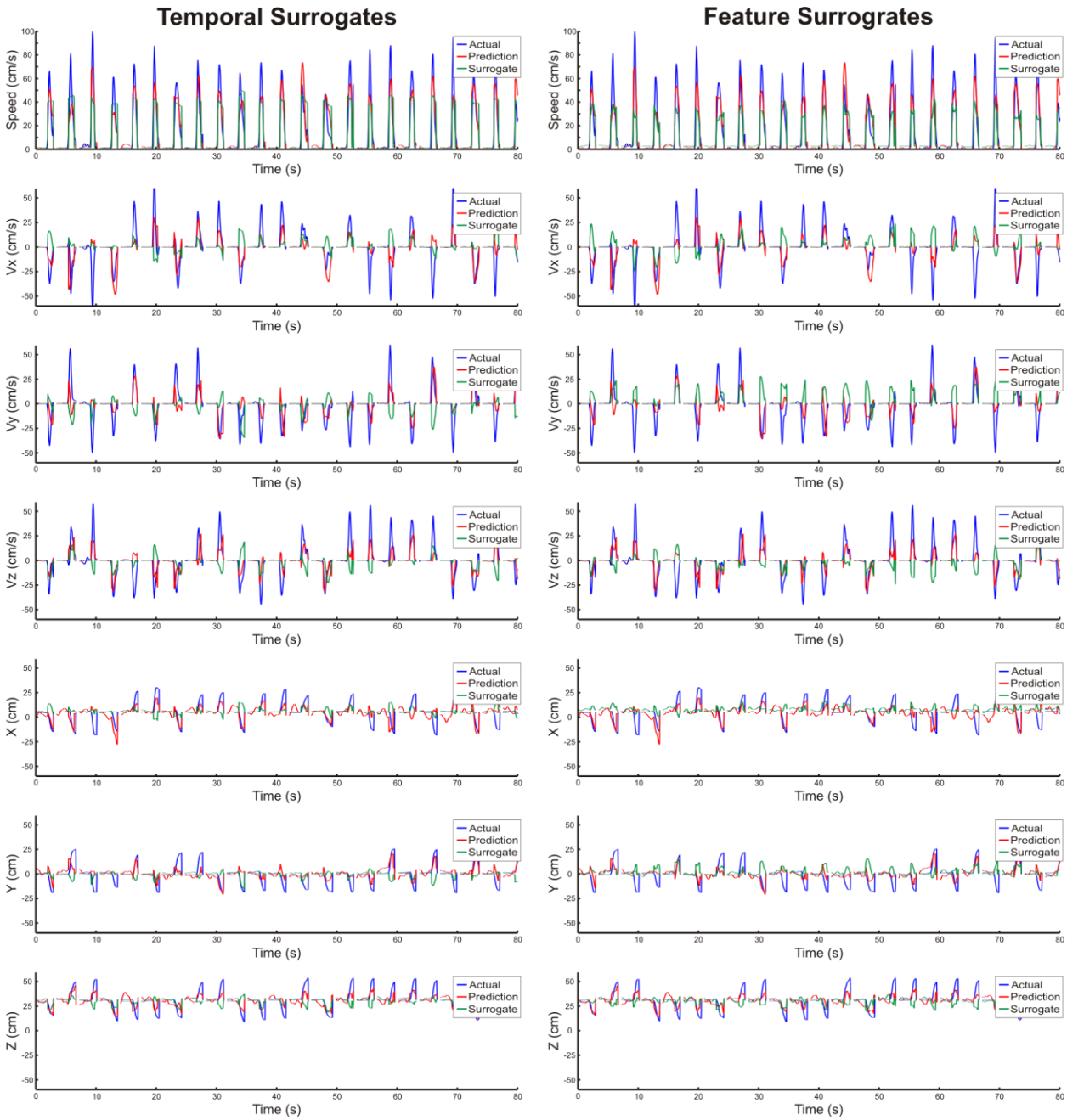

Figure A.4 Exemplar Original and Surrogate Kinematic Predictions

The original and surrogate predictions of movement kinematics are shown for a testing set from a single exemplar patient. Surrogate predictions made with the models trained using the temporally reordered surrogate kinematics are shown on the left. Surrogate predictions generated from reshuffling the features and channels within the model are shown on the left. Original and surrogate predictions were generated by using the actual movement class labels to switch between the PLS regression models for the rest and movement classes. While surrogate predictions for speed are correlated with the actual speed, the surrogate predictions cluster around the average speed during rest and movement classes and do not fit the time course of speed as well as the original model predictions. For directional kinematics, both of the surrogate predictions are directed towards the incorrect direction much more frequently than the original model predictions.

Curriculum Vitae

David T. Bundy

EDUCATION

Ph.D. Biomedical Engineering, May 2015
Washington University, St. Louis, MO USA
Dissertation Title: Human Ipsilateral Motor Physiology and Neuroprosthetic Applications in Chronic Stroke
Advisor: Eric C. Leuthardt, MD

M.S. Clinical Investigation, May 2015
Washington University, St. Louis, MO USA
Advisor: Eric C. Leuthardt, MD

B.S. Biomedical Engineering, Suma Cum Laude, May 2008
Texas A&M University, College Station, TX
Minor: Mathematics

RESEARCH EXPERIENCE

Washington University Saint Louis, MO
Graduate Research Assistant
Advisor: Dr. Eric Leuthardt

- Designed, programmed, and built hardware for a 3D center-out reaching experimental paradigm to examine the neural activity related to motor movements of the contralateral and ipsilateral limbs.
- Collected neural data from research subjects using EEG and ECoG in normal controls and clinical populations.
- Utilized neural signal processing and machine learning algorithms to demonstrate the relationship of ECoG and EEG recordings to kinematics of reaching movements and used this relationship to decode kinematics of motor movements.
- Demonstrated the feasibility of brain-computer interface control utilizing the unaffected hemisphere in chronic stroke survivors.
- Evaluated the effect of the human dura on electrophysiologic characteristics of micro- and macro-scale ECoG recordings

National Institutes of Health Bethesda, MD

Bioengineering Summer Internship Program – Magnetoencephalography Core Facility (June 2007 - August 2007)

Advisor: Dr. Richard Coppola

- Analyzed magnetoencephalography data collected during the working memory and motor control behavioral tasks
- Collected magnetoencephalography data during subject performance of behavioral research paradigms as part of a schizophrenia sibling study.

Texas A&M Biomedical Engineering Department College Station, TX

Independent Study Research Project – Nanomaterials and Biophotonics Laboratory (August 2007 – May 2008)

Advisor: Dr. Kennith Meissner

- Programmed a control system for a digitizer and microscope stage for use during two-photon microscopy experiments

Texas A&M Biomedical Engineering Department College Station, TX

Undergraduate Summer Research Grant Program Participant – Cellular Biomechanics Laboratory (June 2006 – August 2006)

Advisor: Dr. Roland Kaunas

- Studied the effect of fluid shear stress and circumferential tensile stress on vascular cells
- Prepared sterile poly(ethylene)-glycol hydrogels for culture of vascular endothelial cells
- Assisted with microscopy experiments investigating cellular mechanics

PROFESSIONAL EXPERIENCE

Neurolutions Inc. St. Louis, MO

Technical Consultant

April 2013-Present

- Contributed towards the development of the IpsiHand non-invasive brain-computer interface system for stroke rehabilitation as part of an interdisciplinary team.
- Collected and analyzed EEG signals during the design and testing of the device as well as in a clinical trial demonstrating the feasibility of the IpsiHand device.

TEACHING EXPERIENCE

Washington University St. Louis, MO

Graduate Teaching Assistant, Quantitative Physiology

August 2009 – December 2009

- Led students in performance of physiology laboratory experiments
- Assisted in leading weekly office hours and student help sessions

Texas A&M Math Department College Station, TX

Math Department Grader

January 2006 – May 2007

- Graded weekly quizzes, homework, and test problems
- Graded for Linear Algebra (Spring 2006) and Differential Equations (Fall 2006 & Spring 2007)

HONORS/AFFILIATIONS

Society for Neuroscience, member

Tau Beta Pi, Engineering Honor Society

Alpha Eta Mu Beta, Biomedical Engineering Honor Society

Cognitive, Computational Systems Neuroscience IGERT Traineeship, 2009-2011

Washington University Institute for Clinical and Translational Sciences, Clinical Research Training Center: TL1 Traineeship, 2011-2014

PUBLICATIONS

1. **D.T. Bundy**, E. Zellmer, C.M. Gaona, M. Sharma, N. Szrama, C. Hacker, Z.V. Freudenburg, A. Daitch, D.W. Moran, E.C. Leuthardt. Characterization of the effects of the human dura on macro- and micro-electrocorticographic recordings. *Journal of Neural Engineering*. 11(1):016006, February 2014.
2. **D.T. Bundy**, M. Wronkiewicz, M. Sharma, D.W. Moran, M. Corbetta, E.C. Leuthardt. Using ipsilateral motor signals in the unaffected cerebral hemisphere as a signal platform for brain-computer interfaces in hemiplegic stroke survivors. *Journal of Neural Engineering.* 9(3):036011, May 2012.
3. S.K. Bandt, **D.T. Bundy**, A.H. Hawasli, K.W. Ayoub, M. Sharma, C.D. Hacker, M. Pahwa, E.C. Leuthardt. The role of resting state networks in focal neocortical seizures. *PLOS One*. 9(9): e107401, September 2014.
4. Z.V. Freudenburg, C.M. Gaona, M. Sharma, **D.T. Bundy**, J.D. Breshears, R.B. Pless, E.C. Leuthardt. Fast-scale network dynamics in human cortex have specific spectral covariance patterns. *Proc Natl Acad Sci USA*. 111(12): 4602-4607, March 2014.
5. T.J. Mitchell, C.D. Hacker, J.D. Breshears, N.P. Szrama, M. Sharma, **D.T. Bundy**, M. Pahwa, M. Corbetta, A.Z. Snyder, J.S. Shimony, E.C. Leuthardt. A novel data-driven approach to preoperative mapping of functional cortex using resting-state functional magnetic resonance imaging. *Neurosurgery*.73(6): 969-983, December 2013.
6. A.L. Daitch, M. Sharma, J.L. Roland, S.V. Astafiev, **D.T. Bundy**, C.M. Gaona, A.Z. Snyder, G.L. Shulman, E.C. Leuthardt, M. Corbetta. Frequency-specific mechanism links human brain networks for spatial attention. *Proc Natl Acad Sci USA*.110 (48):19585-19590, November 2013.
7. J.D. Breshears, C.M. Gaona, J.L. Roland, M. Sharma, **D.T. Bundy**, J.S. Shimony, S. Rashid, L.N. Eisenman, R.E. Hogan, A.Z. Snyder, E.C. Leuthardt. Mapping sensorimotor cortex with

slow cortical potential resting-state networks while awake and under anesthesia. *Neurosurgery*. 71(2):305-16, Aug. 2012.

8. J.D. Breshears, C.M. Gaona, J.L. Roland, M. Sharma, N.R. Anderson, **D.T. Bundy**, Z.V. Freudenburg, M.D. Smyth, J. Zempel, D.D. Limbrick, W.D. Smart, E.C. Leuthardt. Decoding motor signals from the pediatric cortex: implications for brain-computer interfaces in children. *Pediatrics*. 128(1):e160-e168, July 2011.
9. C.M. Gaona, M. Sharma, Z.V. Freudenburg, J.D. Breshears, **D.T. Bundy**, J. Roland, D.L. Barbour, G. Schalk, E.C. Leuthardt. Nonuniform high-gamma (60-500 Hz) power changes dissociate cognitive task and anatomy in human cortex. *Journal of Neuroscience*. 31(6):2091-2100, Feb. 2011.
10. E.C. Leuthardt, Z. Freudenburg, **D. Bundy**, J. Roland. Microscale recording from human motor cortex: implications for minimally invasive electrocorticographic brain-computer interfaces. *Neurosurgical Focus*. 27(1):E10, July 2009.

ABSTRACTS

1. **D. Bundy**, M. Sharma, N.Szrama, M. Pahwa, E. Leuthardt. Prediction of 3D kinematics during contralateral and ipsilateral reaching movements using electrocorticography. Poster presentation, *Translational Science*, April 9-11, 2014, Washington, DC.
2. **D.T. Bundy**, M. Sharma, N. Szrama, M. Pahwa, C. Hacker, A. Daitch, T. Mitchell, E.C. Leuthardt. Human electrocorticographic correlates of contralateral and ipsilateral 3D reaching movements. Poster presentation, *Society for Neuroscience Abstracts*, November 9-13, 2013, San Diego, CA.
3. **D.T. Bundy**, M. Sharma, N. Szrama, M. Pahwa, C. Hacker, A. Daitch, T. Mitchell, E.C. Leuthardt. Towards neuroprosthetic applications in chronic stroke: electrocorticographic correlates of contralateral and ipsilater reaching movements. Poster presentation, National Clinical and Translational Sciences Predoctoral Programs Meeting, May 5-7, 2013, Rochester, MN.
4. **D.T. Bundy**, M. Wronkiewicz, M. Sharma, N. Szrama, D.M. Moran, M. Corbetta, E.C. Leuthardt. Brain-Computer Interface applications utilizing the unaffected hemisphere after stroke. Poster presentation. *Society for Neuroscience Abstracts*, October 13-17, 2012, New Orleans, LA.
5. **D.T. Bundy**, M. Wronkiewicz, M. Sharma, D.M. Moran, M. Corbetta, E.C. Leuthardt. Brain-Computer Interface applications utilizing the unaffected hemisphere after stroke. Podium presentation, National Clinical and Translational Sciences Predoctoral Programs Meeting, May 6-8, 2012, Rochester, MN.
6. **D.T. Bundy**, C.M. Gaona, Z.V. Freudenburg, M. Sharma, J.D. Breshears, N. Szrama, C. Hacker, A. Daitch, J. Solis, D. Moran, E.C. Leuthardt. Comparison of signal characteristics of subdural and epidural microscale electrocorticographic recordings. Poster presentation. *Society for Neuroscience Abstracts*, November 12-16, 2011, Washington, D.C.
7. **D.T. Bundy**, P. Brunner, G. Schalk, E.C. Leuthardt. Using a Gaussian mixture model (SIGFRIED) for seizure detiction. Poster presentation. *Society for Neuroscience Abstracts*, October 17-21, 2009, Chicago, IL.